Long-term variability of the primary production and export production in the Madeira Basin

Kumulative Dissertation

zur
Erlangung des akademischen Grades
doctor rerum naturalium (Dr. rer. nat.)
der Mathematisch-Naturwissenschaftlichen Fakultät
der Universität Rostock

vorgelegt von

Birte Fründt
geb. am 05.03.1986 in Nordhorn
aus Rostock

Rostock, den 27. Juni 2014

urn:nbn:de:gbv:28-diss2015-0130-3

Gutachter:

- PD Dr. habil. Joanna J. Waniek
  Leibniz-Institut für Ostseeforschung Warnemünde
- Prof. Dr. Andreas Oschlies
  GEOMAR Helmholtz-Zentrum für Ozeanforschung Kiel

Datum der öffentlichen Verteidigung: 10.04.2015

Contents

Abstract

Long-term variability of the oceanic primary and export production plays a major role in the global climate system: On the one hand, climate changes influence the temperature of the ocean, the depth of the mixed layer and the import of nutrients into the euphotic zone which has an effect on the primary production. On the other hand, primary production reacts upon the global climate by exporting carbon dioxide from the atmosphere into the ocean due to photosynthesis. The sinking organic matter, the export production, acts as a long-term sink for this greenhouse gas.

The present work analyses the long-term and interannual variability of both primary and export production in the north eastern part of the North Atlantic Subtropical Gyre. In the study area, the Madeira Basin, the Azores Front forms the boundary between the oligotrophic subtropical ocean and the colder and nutrient enriched North Atlantic. Oceanic fronts are areas of enhanced primary productivity and, therefore, particularly important for the carbon export into the deep oceans. To analyse the variability of export production in the area of the Azores Front, mass flux data from sediment traps in 2000 m depth at the mooring Kiel 276 (33°N, 22°W) were used from 1993 until 2007. Additionally, the position of the Azores Front was examined from 1966 until 2008 applying a modeled temperature field. The long-term variability of the front's propagation is forced by the North Atlantic Oscillation which induces changes in the wind field and its associated Ekman transport. In the time period from 1966 to 2008, a northward displacement of the Azores Front was determined enlarging the oligotrophic area of the North Atlantic. The strong interannual variability of the export production is caused by the propagation of the front: a deeper mixed layer is found at the southern edge of the front compared to the northern edge enhancing the nutrient supply and hence the primary- and export production. According to the position of the front relative to the mooring, intensified or reduced export production subsequently follows the bloom and is then sampled by the sediment trap.

Due to a lack of *in-situ* chlorophyll *a* measurements, as an indicator for primary pro-

duction, the analysis of the long-term variability of primary production is not possible without modeled data sets. Therefore, a new method was developed to calculate a past chlorophyll *a* field over several decades based on *in-situ* measured temperature, nitrate, and chlorophyll *a*. A modeled temperature field functions as basis on which the correlation between temperature and nitrate is applied resulting in a nitrate field. The relation between chlorophyll *a*, temperature, and nitrate as well as the temperature and calculated nitrate fields are used to gain the chlorophyll *a* field which mirrors the seasonal to interannual variability. Due to its high depth resolution, especially the deep chlorophyll maximum is well reproduced. The method is validated via satellite measurements of chlorophyll *a*.

To analyse the long-term variability of primary production in the Madeira Basin, this method was applied on a modeled temperature field from 1871 until 2008 resulting in a chlorophyll *a* field of 138 years. The vertical chlorophyll *a* pattern is dominated by the deep chlorophyll maximum with a distinct multidecadal variability: the chlorophyll *a* concentration increases until the 1930s followed by a strong decrease until the 1970s. As forcing mechanisms, the North Atlantic Oscillation as well as the strength of the solar irradiation were identified. Over the entire time period, the depth integrated chlorophyll *a* content decreased by 3 % in the Madeira Basin. An estimation over all subtropical gyres shows a decline of the global carbon uptake by the oceans by about 1.5 % between 1871 and 2008. Thus, the ocean's capacity to absorb and store carbon dioxide in the deep ocean and sediments decreased in the last hundred years.

Future application of the newly developed method on further oceanic regions, as well as a linkage with the particle flux, will contribute to a more profound understanding of the interaction between climate changes and primary production providing more reliable projections of the global climate evolution.

Zusammenfassung

Im Rahmen des globalen Klimageschehens spielen langzeitliche Variabilitäten der Primär- und Exportproduktion der Ozeane eine große Rolle: Zum Einen wirken Veränderungen des Klimas auf die Meerestemperatur, die Durchmischungstiefe und den Zufluss an Nährstoffen und beeinflussen somit die Produktion. Zum Anderen wirkt die Produktion gleichzeitig auf das Klima ein, indem bei der Photosynthese Kohlenstoffdioxid aus der Atmosphäre entfernt wird, und das Absinken des Materials – die Exportproduktion – für dieses Treibhausgas als eine langzeitliche Senke im tiefen Ozean agiert.

Die vorliegende Arbeit untersucht die langzeitliche und zwischenjährliche Variabilität sowohl der Primärproduktion als auch der Exportproduktion im nordöstlichen Teil des Nordatlantischen Subtropischen Wirbels. In dem Untersuchungsgebiet, dem Madeira Becken, bildet die Azorenfront die Grenze zwischen dem oligotrophen Subtropischen Wirbel und dem kälteren und nährstoffreicheren Nordatlantik. Ozeanische Fronten gelten als Gebiete erhöhter Primärproduktion und sind deshalb von großer Bedeutung für den Kohlenstoffexport in die tiefen Schichten der Ozeane. Zur Analyse der Variabilität der Exportproduktion wurden Sinkstofffallendaten aus 2000 m Tiefe von der Verankerungsstation Kiel 276 (33°N, 22°W) im Gebiet der Azorenfront über den Zeitraum 1993 bis 2007 herangezogen. Zusätzlich wurde mit Hilfe eines modellierten Temperaturfeldes die Position der Azorenfront von 1966 bis 2008 untersucht. Deren Propagation wird langfristig durch die Nordatlantische Oszillation bestimmt, die Veränderungen im Windfeld und im assoziierten Ekmantransport bewirkt. Über den Zeitraum 1966 bis 2008 konnte eine nördliche Verlagerung der Front festgestellt werden, die somit den produktionsarmen Bereich im Nordatlantik vergrößert. Die starke zwischenjährliche Variabilität in der Exportproduktion wird durch die Bewegung der Front bestimmt. An der südlichen Flanke der Front findet sich eine tiefere durchmischte Schicht, die die Nährstoffzufuhr und damit die Primärproduktion im Vergleich zur nördlichen Flanke erhöht. Je nach Lage der Front im Verhältnis zur Verankerungsstation führt dies zu

einer verstärkten oder verminderten Exportproduktion im Anschluss an die Blüte im Oberflächenwasser.

Da aufgrund eines Mangels an ausreichenden *in-situ* Chlorophyll *a*-Messungen, als Indikator der Primärproduktion, die Untersuchung der langzeitlichen Variabilität der Primärproduktion ohne künstlich hergestellte Daten nicht möglich ist, wurde eine neue Methode entwickelt, die anhand von *in-situ* Messungen der Temperatur, des Nitrats und des Chlorophylls die Chlorophyllverteilung über mehrere Jahrzehnte zurück berechnet. Als Basis dient ein modelliertes Temperaturfeld, auf dem die Beziehung zwischen Temperatur- und Nitratmessungen angewandt wird, um ein Nitratfeld zu erhalten. Der Zusammenhang zwischen Chlorophyll *a*, Temperatur und Nitrat wird genutzt, um mit Hilfe der Temperatur- und Nitratfelder ein Chlorophyllfeld zu berechnen, welches sowohl die saisonale als auch zwischenjährliche Variabilität widerspiegelt. Dieses weist eine hohe Tiefenauflösung auf, sodass insbesondere das Tiefenchlorophyllmaximum gut wiedergegeben wird. Die Validierung dieser Methode erfolgte mit Satellitenmessungen des Chlorophylls.

Zur Untersuchung der langzeitlichen Variabilität der Primärproduktion wurde diese Methode auf ein modelliertes Temperaturfeld im Madeira Becken von 1871 bis 2008 angewandt, sodass sich ein Chlorophyll *a*-Feld gleicher Länge ergab. Das im Chlorophyllmuster dominierende Tiefenchlorophyllmaximum zeigte eine starke multidekadische Variabilität mit einem Anstieg der Chlorophyllkonzentration bis in die 1930er Jahre und einem starken Abfall bis in die 1970er. Als Antriebsfaktoren konnten sowohl die Nordatlantische Oszillation als auch die Stärke der solaren Einstrahlung ermittelt werden. Über den gesamten Zeitraum hinweg nahm der über die Tiefe integrierte Chlorophyllgehalt im Madeira Becken um 3 % ab. Bei einer Abschätzung über alle subtropischen Wirbel bedeutete dies eine Abnahme der globalen Kohlenstoffaufnahme der Ozeane um 1.5 %. Die Kapazität der Ozeane, anthropogenes CO_2 aufzunehmen und langfristig in den tiefen Schichten und Sedimenten zu speichern, ist dementsprechend in den letzten hundert Jahren zurückgegangen.

Eine zukünftige Anwendung der neu entwickelten Methode auf weitere ozeanische Gebiete sowie eine Kopplung mit dem Partikelfluss wird dazu beitragen, die Wechselwirkungen zwischen Klimaveränderungen und Primärproduktion besser zu verstehen und damit zuverlässigere Vorhersagen für die künftige Klimaentwicklung zu liefern.

Preface

The present thesis "*Long-term variability of the primary production and export production in the Madeira Basin*" was completed in the framework of the project "*Dekadische Variabilität der Primärproduktion und Exportproduktion im Madeira Becken*" funded by the Deutsche Forschungsgemeinschaft (DFG).

Primary production is the conversion of inorganic material, such as nitrate or phosphate, into organic compounds by photosynthesis. In the pelagic regions of the oceans, it is mainly processed by phytoplankton [*Lalli and Parsons*, 1993]. As an indicator for primary production, the dominant pigment specific to photosynthesis, chlorophyll *a*, is most established [*Lalli and Parsons*, 1993; *Chavez et al.*, 2011].

Export production means the flux of the biogenic material out of the euphotic zone into the ocean's deeper levels [e.g. *Eppley and Peterson*, 1979].

The export production of this study is measured by a deep-moored sediment trap in the Madeira Basin in the subtropical Northeast Atlantic and analysed regarding the high interannual variability. The time series of the primary production arises from a self-developed model which recalculates the chlorophyll *a* distribution of the last decades. The analysis focusses on long-term changes related to low-frequency climate variability.

This doctoral thesis comprises three main chapters in which the results of the analyses are presented in form of three manuscripts. One of the chapters has already been published in a peer-reviewed journal (*Central European Journal of Geosciences*, Chapter 3). Two of the chapters are published to the peer-reviewed *Journal of Geophysical Research: Biogeosciences* (Chapter 4 and 5) in 2015. Therefore, short contentwise overlaps of the three chapters, e.g. for the study area, are inevitable. All references are listed in a section at the end of the thesis.

In **chapter 1**, an introduction gives an scientific framework in relation to the global climate change of the last century and its correlation to the presented study with an outline of the main scientific questions.

Chapter 2 specifies the study area, the data, and the methods used in this thesis.

Predominantly, the mathematical background of methods as well as a short elucidation of different climate indices are outlined which are nearby mentioned in the manuscripts.

The analysis of the interannual variability of the export production in the Madeira Basin is given in **chapter 3**. At first, the propagation of the Azores Front and its driving mechanisms are determined. Secondly, this propagation is correlated to the particle flux regarding the different growth conditions for phytoplankton north and south of the Azores Front.

A new method to recalculate a past chlorophyll *a* field with high time and depth resolution based on *in-situ* measurements is described in **chapter 4**. This method was implemented to the Madeira Basin and first results and their analysis are shown.

In **chapter 5**, the new method, introduced in chapter 4, is applied to the Madeira Basin resulting in a chlorophyll *a* field from 1871 to 2008. The analysis focusses on the relation of the chlorophyll *a* evolution with long-term climate variability and an estimation of the change of carbon uptake by the oceans due to photosynthesis in the euphotic layer of the subtropical oceans.

Chapter 6 summarizes the results of the three manuscripts with respect to the scientific questions in chapter 1 and outlines further questions and perspectives of the thesis.

1 Introduction

1.1 Global scientific framework

The theme of the increasing global temperatures has been studied in several scientific and socioeconomic works and it still leaves much to be discussed. Current estimates of the Intergovernmental Panel on Climate Change *IPCC* [2013], for example, report an increase of global temperature ranging between 0.3 and 4.8 °C at the end of the 21st century in comparison to its beginning. This result has and especially will have a massive impact on both marine and terrestrial ecosystems. It also has and will have a massive influence on human population. One of the reasons are the changing weather conditions which cause extreme events of precipitation, storminess or droughts more often. Furthermore, we already have a rising sea level, caused by melting of the Greenland and Antarctic ice sheets as well as an increasing ocean volume, caused by higher ocean temperatures. These changes even could banish human societies from a wide variety of coastal areas [*IPCC*, 2013]. Additionally, a change of the global temperature correlates with a change in marine and terrestrial biodiversity which will not only influence human's diet but will promote or counteract the trends in climate.

The current period of global warming started at the beginning of the 20th century following the Little Ice Age between 1570 and 1730 [*Bradley and Jonest*, 1993]. Since the beginning of the Industrial Revolution in Great Britain in the 18th century and on the European continent in the 19th century, the usage of fossil fuels has been raising the atmospheric content of CO_2 and other green house gases [*Osterhammel*, 2011; *Neftel et al.*, 1985]. Continuous measurements of atmospheric CO_2 taking place on Hawaii since 1959 [*Keeling et al.*, 1976] clearly demonstrate an increase of about 40 % to preindustrial levels [*IPCC*, 2013] with a concentration of approximately 397 ppm in 2014 [*Ciais et al.*, 2013; *Dlugokencky and Tans*, 2014]. The correlation between global mean temperatures and the atmospheric level of CO_2 has already been proved by analysing

past climate changes using ice cores [*Sigman and Boyle*, 2000]. The recent temperature rise is therefore mostly related to the increase of this anthropogenic CO_2. Nevertheless, the degree of influence of natural climate variability on global warming has not yet been determined.

Besides the atmosphere, lithosphere and the terrestrial biosphere, the world's ocean, covering 71 % of the planet's surface [*Lalli and Parsons*, 1993], and the marine population play a major role in affecting the global climate system by energy and material transformation on time scales of several to billions of years [*Pielke Sr*, 2008]. Parallel to the temperature increase of the earth's surface in the last century [*Jones et al.*, 1986, 1999] warming has especially been observed in the upper 700 m of the global oceans since 1971. The most noticeable increase was measured in the North Atlantic with 0.409 °C between 1969 and 2008 in comparison to the global increase of 0.168 °C in the same time period [*Levitus et al.*, 2009]. By comparing data back to the Challenger expedition (1872–1876), *Roemmich et al.* [2012] assume that the increase of the temperatures even began earlier than in the 1970s. The oceans contribute to a large extent to the storage of heat so that in the last 50 years about 93 % of the excess heat energy of the earth has been absorbed by the oceans [*Levitus et al.*, 2012; *Church et al.*, 2011]. The outcome of this is an increase of the water temperature of about 0.11 °C per decade in the upper 75 m and 0.015 °C per decade even in depths of 700 m, though these global mean values can be exceeded to a large extent by individual long-term *in-situ* measurements. *Fründt et al.* [2013] reported temperature gradients of 0.48 °C per decade in 240 m and 0.38 °C per decade in 500 m in the northeastern part of the subtropical Atlantic from 1980 to 2008.

Due to a lack of *in-situ* measurements, the extent of warming in the deeper ocean levels in the last decades can not be determined reliably [*Rhein et al.*, 2013]. Estimates by *Levitus et al.* [2012] gave rise to the assumption that the heat content trend between 700 m and 2000 m may amount to 30 % of the trend from surface to 700 m depth. Statements of ocean warming in depths deeper than 2000 m are still very speculative.

As a direct consequence of rising global temperatures, sea surface height is ascending mostly due to extension of the less dense, warmer water body of the ocean and melting of continental ice sheets. In the 20th century, the sea level increased globally by 1.5 – 2.0 mm yr^{-1} [*Miller and Douglas*, 2004; *Church et al.*, 2004; *Church and White*, 2006] whereas this trend rose up to 3.1 $\pm$ 0.7 mm yr^{-1} between 1993 and 2003

[*Cazenave and Nerem*, 2004; *Leuliette et al.*, 2004]. The consequence of uninhabitability of wide coastal areas will impact both the economic and social life not only of aggrieved nations.

Higher temperatures not just lead to an increase of the sea surface height but may also influence global ocean current systems [*Bryden et al.*, 2012]. Warming of the upper ocean effects changes in water mass properties in the ocean's interior like freshening of the intermediate waters [*Rhein et al.*, 2013]. Coupled climate models predict a weakening of the Atlantic Meridional Overturning Circulation (AMOC) due to freshwater input by melting of the continental ice sheets. The AMOC is responsible for the meridional poleward heat transport and its attenuation would impact the global climate – cooling of the Northern Hemisphere and modification of the distribution of winds and precipitation [*Vellinga and Wood*, 2002; *Kirtman et al.*, 2013].

In addition to the effects on global weather and climate as well as hydrographic conditions of the oceans, the biogeochemical cycles in the oceans are highly influenced and their possible modifications will react upon the global climate. The ocean's surface interacts with the atmospheric CO_2 reservoir through gas exchange driven by the partial pressure difference of CO_2 between air and sea [*Ciais et al.*, 2013]. The ocean stores a 50 times larger amount of carbon than the atmosphere [*Sabine et al.*, 2004], its main component as dissolved inorganic carbon, i.e. carbonic acid, bicarbonate and carbonate ions. Only a small fraction of approximately 2 % is fixed in the pool of dissolved organic carbon [*Hansell et al.*, 2009; *Ciais et al.*, 2013]. The amount of organic carbon in marine biota is negligibly small. Due to their capability to store atmospheric CO_2, the oceans can act as sink for anthropogenic CO_2 and therefore contribute to a large extent to future global climate conditions. The transportation route of carbon within the oceans is characterised by three mechanisms: the physiochemical solubility pump controls the transport of dissolved inorganic carbon from the surface to the ocean's interior. Because the solubility of CO_2 increases with decreasing water temperature, this pump is driven by the temperature difference of warm surface and cold deep water [*Volk and Hoffert*, 1985]. The marine carbonate pump counteracts the removal of CO_2 from the atmosphere. During formation of calcareous shells by microorganisms, such as coccolithophores, foraminifera and pteropods, dissolved CO_2 emerges in the euphotic zone, increasing the partial pressure of CO_2 in surface waters. By sinking of the dead organisms, the carbonate bound in the shells is removed and the dissociation equilibrium of

the carbonate system is shifted to higher CO_2 concentrations in the upper ocean, reducing the uptake of CO_2 from the atmosphere. In the deep ocean, the material is then remineralised to dissolved inorganic carbon and calcium ions [*James*, 2005; *Ciais et al.*, 2013]. The biological pump describes the fixation of CO_2 in organic material by phytoplankton during photosynthesis in the surface waters and its export by sinking of dead phytoplankton in deeper levels with the potential of a long-term sink for anthropogenic CO_2 [*Eppley and Peterson*, 1979; *Goes et al.*, 2000]. The dominant role of global carbon export is thought to be played by diatoms [*Goldman*, 1993; *Ragueneau et al.*, 2006]. However, *Francois et al.* [2002] and *Klaas and Archer* [2002] imply that the proportion of carbon export by calcifying organisms is strongly underestimated.

Caused by consumption and microbial respiration, approximately 15 % of the organic matter reaches depths below the thermocline as export production, and approximately 0.1 % the seafloor where it is embedded in the sediments and removed from interaction with the atmosphere for geological time scales [*Falkowski and Oliver*, 2007]. Due to its fixation of atmospheric CO_2, oceanic primary production is an important contribution to the global climate system [*Falkowski*, 2000; *Schwab et al.*, 2012] and strongly influences both climate processes [*Murtugudde et al.*, 2002] and the biogeochemical cycles [*Sabine et al.*, 2004].

Nearly half of the global primary production takes place in the ocean [*Field et al.*, 1998; *Boyce et al.*, 2010]. Under the influence of increasing global sea surface temperatures, primary productivity decreased in the last century [*Antoine et al.*, 2005; *Behrenfeld et al.*, 2006; *Martinez et al.*, 2009; *Boyce et al.*, 2010]. Modeling studies also predict that new production will abate on long time scales [*Bopp et al.*, 2001; *Boyd and Doney*, 2002; *Sarmiento et al.*, 2004; *Riebesell et al.*, 2009]. Accompanied by higher temperatures, increasing stratification of the upper water column is thought to hinder mixing processes that are responsible for the supply of nutrients into the euphotic zone from depths below resulting in reduced primary productivity especially in the mid- to low latitudes [*Doney et al.*, 2012]. An increase of the globally averaged temperature difference between surface and 200 m depth by about 0.25 °C is reported between 1971 and 2009 [*Levitus et al.*, 2009] indicating higher stratification. At the end of the 21st century, a reduction of global primary productivity between 2 % and 20 % is likely [*Steinacher et al.*, 2010]. Furthermore, the fraction of the small phytoplankton is predicted to increase in warmer waters [*Daufresne et al.*, 2009] which diminishes the flux of energy

to higher trophic levels [*Morán et al.*, 2010]. A change in species composition in wide oceanic regions is caused by migration of species to higher altitudes and latitudes influencing the predators-prey-relationship [*Daufresne et al.*, 2009]. Socioeconomic impacts on fishery and related industries are the consequence [*IPCC*, 2013].

Due to the rising partial pressure of CO_2 in the atmosphere, more CO_2 is dissolved in the ocean where it forms the weak carbon acid influencing the pH value. Compared to the preindustrial era, the pH of the surface ocean is reduced by about 0.1 [*Orr et al.*, 2005; *Feely et al.*, 2009; *Rhein et al.*, 2013] with impacts especially on calcifying organisms like corals [*Gattuso et al.*, 1998; *Kleypas et al.*, 1999], foraminifera [*Barker and Elderfield*, 2002; *Moy et al.*, 2009], and coccolithophores [*Riebesell et al.*, 2000; *Beaufort et al.*, 2011] which build one of the dominant species of phytoplankton in the tropical to temperate oceans [*Schwab et al.*, 2012] and account for a large part of the carbon export by the oceans [*Michaels and Silver*, 1988; *Brzezinski et al.*, 1998; *Henson et al.*, 2010].

As the largest part of the global oceans, the subtropical gyres add up to 40 % of the planetary surface [*Polovina et al.*, 2008]. In these regions, shallow mixed layer depths and a deep and stable permanent thermo- and nutricline dominate [*Chavez et al.*, 2011]. Because these areas are mainly oligotrophic, resulting in low primary productivity, they are often considered as "ocean deserts" (Fig. 1.1, *Emerson et al.* [1997]; *Oschlies* [2002]). Primary production in the subtropical gyres is characterised by a bloom near the surface in winter and early spring after nutrient enrichment of surface waters by wind mixing processes in winter [*Longhurst*, 1998]. To a lower extent, import of nutrients into the euphotic zone occurs by mesoscale eddies, nitrogen fixation and diffusion processes across the nutricline [*Lewis et al.*, 1994; *McGillicuddy et al.*, 1998; *Mahaffey et al.*, 2003]. When the nutrients are depleted at the surface, primary production moves to the lower edge of the euphotic zone where nutrient concentrations are higher, to form the deep chlorophyll maximum as a consistent feature of the subtropical oceans [*Pérez et al.*, 2006]. Caused by the large extent and proceeding primary productivity all year in the deep chlorophyll maximum, these "ocean deserts" (Fig. 1.1) contribute to a quarter of global primary production [*Longhurst et al.*, 1995] and a half of the global ocean carbon export by export production [*Emerson et al.*, 1997].

The subtropical gyres are bordered to the north in the northern oceans and to the south in the southern oceans by so-called "subtropical fronts" (Fig. 1.1). Oceanic fronts

are characterised as narrow zones of strong vertical as well as horizontal temperature, salinity and density gradients inducing intensified mixing and advection [*Lalli and Parsons*, 1993; *Pérez et al.*, 2003] and build the boundary between different water masses or different vertical structure [*Belkin et al.*, 2009]. The formation of oceanic fronts is caused by a variety of physical processes leading to different types of fronts, e.g. the tidal mixing fronts, upwelling fronts especially in coastal and equatorial regions, western and eastern boundary current fronts and the subtropical convergence fronts [*Belkin et al.*, 2009]. These convergence fronts are formed between approximately 20° and 45° north and south of the equator where the Trade Winds and the Westerlies build a zone of enhanced Ekman transport convergence in the ocean [*James et al.*, 2002]. Whereas the climate change of the last century needed several years to decades to change ocean water properties such as temperature, salinity or nutrient concentration, the frontal zones are areas to study the influence of these changes on the local marine population on short time and length scales. The position of the subtropical convergence fronts in the ocean are not static, but they propagate in meridional direction and build meanders due to high eddy abundance [*Olson et al.*, 1994] leading to fast changes of water masses to which the biocoenosis has to adapt. This can cause a relative isolation of the frontal ecosystems [*Belkin et al.*, 2009]. Exactly these special living conditions make fronts to a region of enhanced primary productivity and associated increased export production [*Fasham et al.*, 1985; *Pak et al.*, 1988; *Olson et al.*, 1994; *Longhurst*, 1998]. This influences not only the higher trophic levels from zooplankton [*Boyd et al.*, 1978; *Olson et al.*, 1994] to the distribution of tuna and sword fishes [*Nakamura*, 1969; *Palko et al.*, 1981] but increases the export production with impacts on the carbon export from the surface waters to the deep ocean levels [*Belkin et al.*, 2009].

1.2 Scientific questions

The interannual to interdecadal variability of primary and export production in the subtropical gyres, on which this thesis focusses, is a debatable issue because, in case of primary production, no long-term *in-situ* measurements are available, and in case of export production, these measurements are very scarce and do not span time periods of several decades.

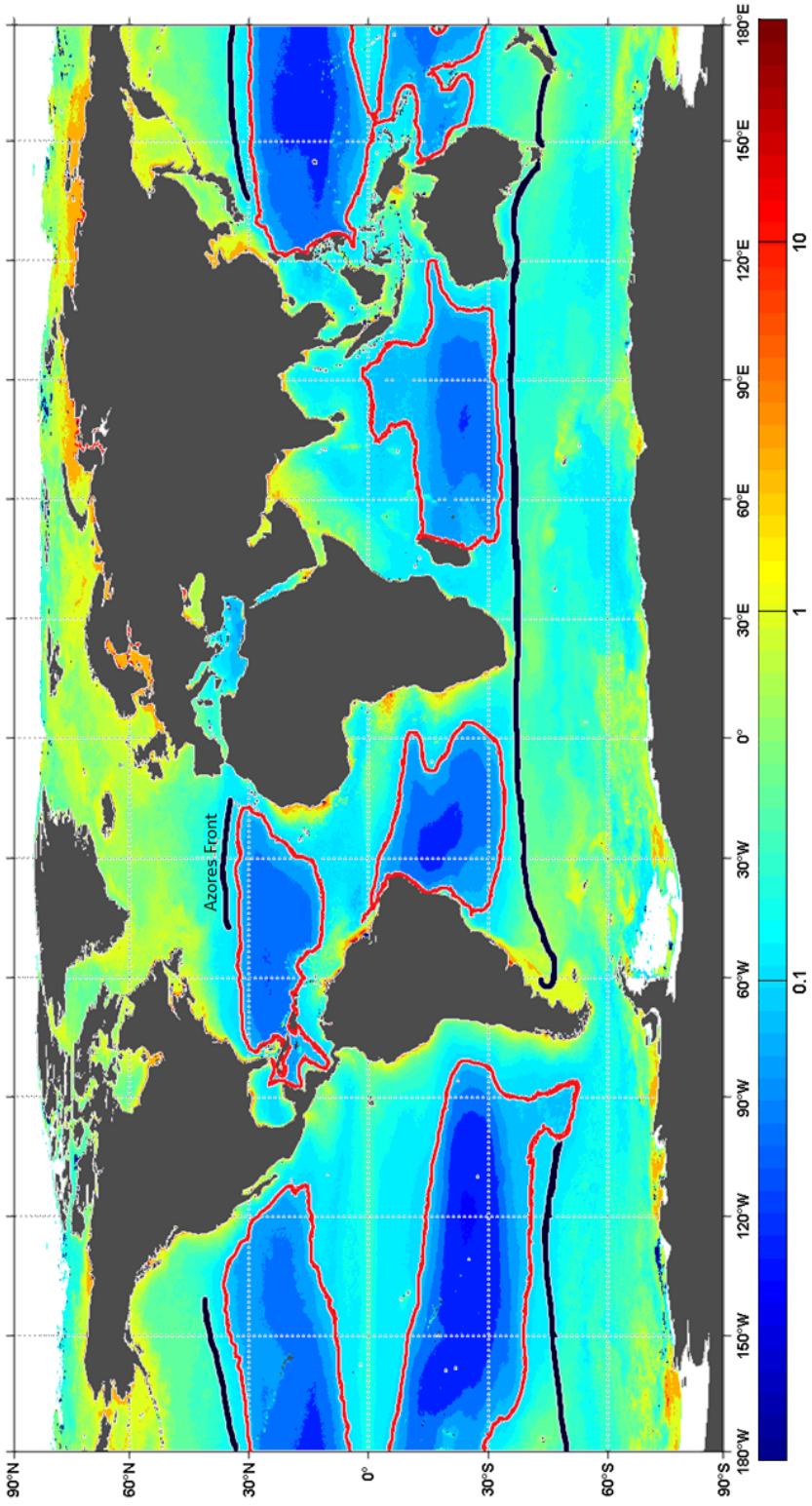

Figure 1.1: Global mean surface chlorophyll *a* concentrations in mg m^{-3} (indicated by the colorbar) from MODIS (average 2003 – 2011, 9 km resolution). The oligotrophic regions (chlorophyll *a* concentration < 0.9 mg m^{-3} after *Morel et al.* [2007]) are marked by red borders. Furthermore, the positions of the global subtropical fronts are given by dark blue lines.

In the northeastern part of the North Atlantic Subtropical Gyre, the Azores Front (Fig. 1.1) forms the boundary between the colder and nutrient enriched subpolar North Atlantic and the oligotrophic 18 °C Mode Water in the south [*Käse and Siedler*, 1982; *Klein and Siedler*, 1989; *Schiebel et al.*, 2002]. Measurements of export production were recorded by sediment traps in the frontal region in the Madeira Basin at the mooring site Kiel 276 (33°N, 22°W) since 1993 [*Waniek et al.*, 2005a,b]. High interannual variability of the particle flux was analysed, however, strong export events could not be linked to the primary production at surface derived from chlorophyll *a* measurements by satellites above the mooring site [*Waniek et al.*, 2005a; *Brust et al.*, 2011, see their fig. 2b]. The mooring site is located at the northeastern edge of the North Atlantic Subtropical Gyre with the Azores Front as the boundary to the subpolar gyre. The propagation of the Azores Front leads to different water masses in the catchment areas of the sediment trap of Kiel 276, deducing changes of growth conditions for phytoplankton. Detection of the position of the Azores Front by satellite measurements of the sea surface temperature is constrained because this front does not have any surface indication. Regarding this, the following questions arose which are discussed in the first part of the presented work (Chapter 3).

- How variable is the north- and southward propagation of the Azores Front?
- What are the forcing mechanisms of the propagation of the front?
- Which influence do the Azores Front and its propagation have on the primary and export production at Kiel 276?

To analyse the long-term variability of primary production, methods were developed to derive the primary production by chlorophyll *a* measurements by satellites [*Sathyendranath et al.*, 1991; *Antoine and Morel*, 1996; *Behrenfeld and Falkowski*, 1997; *Uitz et al.*, 2006]. The remote measurements of chlorophyll *a* were taken by the Coastal Zone Color Scanner from 1976 until 1986 and have permanently been accomplished by SeaWiFS since 1997 [*McClain*, 2009; *Boyce et al.*, 2010]. The resulting time series of primary production are still too short to detect long-term variability forced by low-frequency climatic pattern as the Atlantic Multidecadal Oscillation [*Enfield et al.*, 2001] or the North Atlantic Oscillation [*Hurrell*, 1995]. To distinguish between this natural variability and changes related to anthropogenic forced climate change in biological data

sets, time series of 40 years and more are necessary [*Henson et al.*, 2010]. *Boyce et al.* [2010] combined measurements of ocean transparency and *in-situ* chlorophyll *a* data to detect long-term changes of global primary production since 1899. However, deriving primary production from transparency measurements can be affected by large systematical errors and has therefore been intensively discussed [*Mackas*, 2011; *Rykaczewski and Dunne*, 2011; *McQuatters-Gollop et al.*, 2011; *Boyce et al.*, 2011].

One objective of the present thesis is hence to develop a new method to recalculate a chlorophyll *a* field over several past decades based on validated *in-situ* measurements (Chapter 4). One focal point of this method is to obtain a good resolution of the chlorophyll *a* distribution over the entire euphotic zone because remotely measured data just cover the upper 20 to 25 m [*Boyce et al.*, 2010; *Kemp and Villareal*, 2013] and do not deliver any information of the deep chlorophyll maximum in the subtropical oceans.

To analyse long-term changes of primary production in the Madeira Basin, the method introduced in chapter 4 is applied to this region. Besides identifying the long-term variability of primary production in the Madeira Basin, the following questions will be addressed in chapter 5.

- What are the natural forcing mechanisms of the long-term variability of primary production?
- Does the primary production show a long-term trend with impact on the oceanic carbon uptake in the last century?

Answering these questions will provide an insight especially on the variabilities of the deep chlorophyll maximum in the subtropical ocean for the first time.

2 Material and Methods

2.1 Study Area

The study area is situated in the Madeira Basin in the north-eastern part of the North Atlantic Subtropical Gyre (Fig. 2.1). As part of the global wind-driven upper layer circulation, the anticyclonic gyre is forced by the Westerlies in the mid-latitudes and the eastward blowing Trade Winds in low latitudes [*Siedler et al.*, 2001]. The gyre is delimited in the west by the Gulf Stream; its eastward flowing branch, the Azores Current, forms the boundary to the subpolar gyre in the north, and feeds the southward flowing Canary Current as the eastern boundary. To the south, the gyre is closed by the westward flowing North Atlantic Equatorial Current (Fig. 2.1). Related to the Sverdrup Balance, the recirculation is given by strong equatorward transports which are mainly located in the western boundary currents due to vorticity conservation [*Siedler et al.*, 2001], and only a small part of recirculation occurs in the eastern basin of the subtropical gyre [*Stramma*, 1984; *Stramma and Siedler*, 1988].

In the upper water column, the Azores Current and its associated Azores Front influence the hydrodynamics [*Fründt and Waniek*, 2012; *Fründt et al.*, 2013] and form the boundary between the 18 °C Mode Water in the south and the 15 °C regime in the north [*Gould*, 1985]. The salinity in the surface waters of this region ranges around 36 [*Lalli and Parsons*, 1993; *Stewart*, 2008]. The seasonal thermocline extends to about 100 m in winter and is shallower pronounced in summer. The main thermocline down to 600 m [*Waniek et al.*, 2005a; *Siedler et al.*, 2005] exhibits no seasonality. Beneath the permanent thermocline, in 600 m to 1300 m the outflow of the Mediterranean Water through the strait of Gibraltar prevails. This water mass is characterised by density compensated temperature and salinity anomalies of ΔT 2 – 3 °C and ΔS 1 – 2 compared to the overlying North Atlantic Central Water [*Siedler et al.*, 2005; *Fusco et al.*, 2008]. Associated with the Mediterranean Water tongue are high temperature (maximum near 13 °C) and

salt (maximum near 36.5) water lenses or eddies (Meddies) [*Siedler et al.*, 2005]. In the deeper levels below 1300 m, the North Atlantic Deep Water is found [*Tomczak and Stuart*, 1994]. This water mass was built by deep winter convection in the Greenland Sea [*Meincke et al.*, 1997] and in the Norwegian Sea [*Mauritzen*, 1996] and is identified by temperatures of 2 – 4 °C and salinities of 34.9 – 35 [*Brown*, 1995].

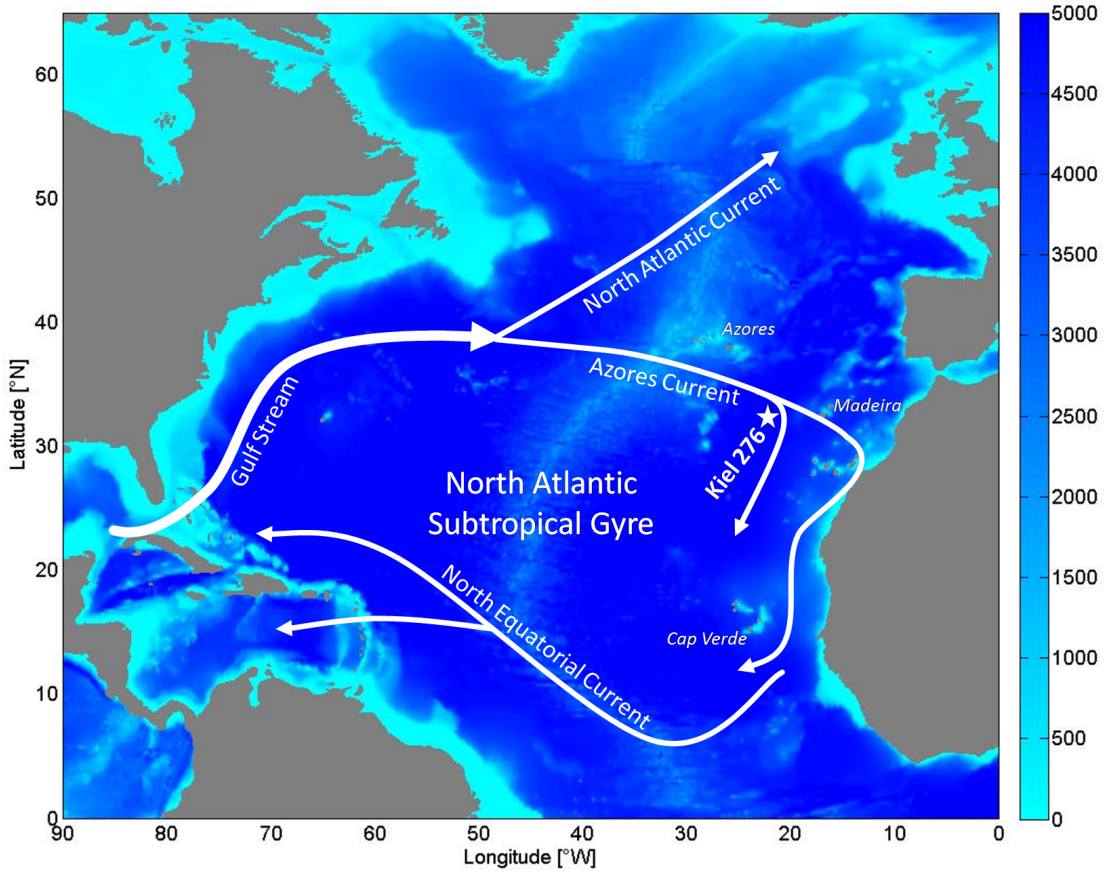

Figure 2.1: Main currents of the subtropical and tropical North Atlantic (after *Rogerson et al.* [2004]). The colour bar indicates water depth in metre. Additionally, the position of the mooring site Kiel 276 is given (white star).

Ecologically, the Madeira Basin belongs to the eastern North Atlantic Subtropical Gyral Province (NAST-E) which is delimited by the Azores Current at about 40° – 42°N and at about 25° – 30°N where the Westerlies and Trade Winds converge [*Longhurst*, 1998]. Typically in autumn, crossing of atmospheric cold fronts causes convective mix-

ing to about 125 – 150 m depth and leads to formation of the 18°C Mode Water [*Worthington*, 1976; *Longhurst*, 1998]. The increasing mixed layer imports new nutrients from beneath the nitracline in approximately 100 m depth and results in the phytoplankton bloom near the surface in late winter to early spring [*Cullen*, 1982]. In this oligotrophic region, the primary production is dominated by *Emiliana huxleyi* and other calcifying species whilst the opal forming diatoms play a minor role [*Waniek et al.*, 2005a]. After nutrient consumption near the surface, the phytoplankton forms the deep chlorophyll maximum in approximately 80 – 100 m depth and the primary production rate reaches its minimum in late summer [*Teira et al.*, 2005; *Waniek et al.*, 2005a].

2.2 Data

2.2.1 Measurements from the mooring site Kiel 276

Within the Madeira Basin basin, the mooring site Kiel 276 (33°N, 22°W) is deployed in approximately 5300 m water depth [Fig. 2.1, *Siedler et al.*, 2005; *Waniek et al.*, 2005a; *Fründt et al.*, 2013]. This mooring (33°N, 22°W) has been providing temperature and current measurements since April 4th, 1980, from the near-surface layer down to the bottom layer in 5300 m depth with an hourly and later (since 1989) two hourly resolution [*Müller and Siedler*, 1992; *Waniek et al.*, 2005a]. Mass flux has been measured by sediment traps in 2000 m and 3000 m since 1993.

The deployments (28 until 2013) were performed with different periods of 6 to 24 months and gaps in between of up to one week. Instrument failures can induce longer gaps of several months. The mooring positions were within $\pm$ 0.2° in latitude and $\pm$ 0.2° in longitude of the nominal mooring position of 33°N, 22°W. Current measurements were performed by Aanderaa current metres (Fig. 2.2, RCM 4/5 until 1993, RCM 7/8 replaced the RCM 4/5 from 1989 on, completing the process in 1993) additionally equipped with temperature and, mostly at near-surface, pressure sensors with sampling intervals of one hour and later two hours [*Müller and Siedler*, 1992; *Waniek et al.*, 2005a].

Figure 2.2: Aanderaa current meter of the mooring site Kiel 276.

The sensors have an accuracy of ± 0.2 bar in pressure, ± 0.05 °C in temperature, ± 0.1 cm s^{-1} in velocity, and ± 5° in direction (Aanderaa Instruments, 1978). Calibration and sensor stability were checked with CTD profiles performed prior to each recovery. For further analysis, the data were low-pass filtered over 40 hours removing inertial and higher frequencies and daily means were calculated resulting in a data set with a daily resolution. For further details of the mooring deployments see *Müller and Waniek* [2013]. The temperature and current measurements of the main thermocline were analysed by *Fründt et al.* [2013]. In the present thesis, daily current measurements from the near surface layer down to 1600 m depth were examined to calculate the catchment areas of the sediment traps. The used data are summarised in table 3.2. The method of calculation of the catchment areas is described in detail in *Waniek et al.* [2000].

Measurements of the mass flux were performed by 0.5 m^2 funnel type sediment traps at which an attached carousel with sampling bottles (400 cm^3 polypropylene cups) allows different sampling intervals between 5 and 62 days depending on the seasonality of primary production (Fig. 2.3). *Kremling et al.* [1996] provides detailed information about the instrument. Cleansing of the cone, rotator and the bottles followed the standard procedure for trace elements analysis *Kuss and Kremling* [1999]. A 4:1 mixture of *in-situ* seawater and sodium acid (NaN_3 5 % stock solution in high purity water) was used as solution in the sampling bottles. Finally, NaCl was added to reach a salt content of 38 g l^{-1} [*Lee et al.*, 1992; *Brügmann and Kremling*, 1999; *Waniek et al.*, 2005a]. A rinse-period of 1 – 2 weeks was scheduled before sampling started. A detailed description of the determination of particle flux is given in *Waniek et al.* [2005a,b].

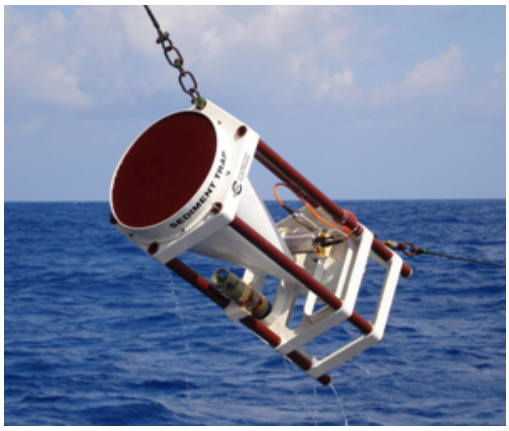

Figure 2.3: Recovering of a sediment trap at the mooring site Kiel 276 (Photo: A. Bauer).

In this thesis, the mass flux data from the 2000 m sediment trap were analysed from 1993 to 2007. Data gaps occurred between June 1997 and February 1999 as well as

2000 and 2001 due to mooring failure [*Waniek et al.*, 2005a]. Prior to the analysis, the different sampling intervals were standardised to monthly mean values.

2.2.2 *In-situ* measurements

In-situ data of temperature, nitrate and chlorophyll *a* were taken from several cruises by the research vessel Poseidon in the Madeira Basin and from data sets provided by the Pangaea database (http.//www.pangaea.de/). The data are summarised in table 3.1 and 4.1. Data of the Poseidon cruises are, on the one hand, calibrated temperature measurements by CTD casts, and on the other hand, nitrate and chlorophyll *a* data which were sampled in different depths using the Niskin-bottles of the CTD rosette. The nitrate concentrations were determined using an autoanalyzer (EVOLUTION III, Alliance Instruments) according to standard methods [*Grasshoff et al.*, 1999], and chlorophyll *a* concentration by a calibrated fluorometer (TURNER 10-AU, Gamma Analysen Technik GmbH) after the *JGOFS* [1994] protocol. For the nitrate measurements, the detection limit is 0.05 mmol l^{-1} and for the chlorophyll *a* concentrations 0.03 mg m^{-3}.

2.2.3 Modeled Data

Different data sets used in this thesis are delivered from global models providing atmospheric and hydrographic parameters.

As temperature data set for the Madeira basin, the output of the Simple Ocean Data Assimilation Parallel Ocean Program (SODA POP) was used [*Carton et al.*, 2005; *Carton and Giese*, 2008]. To detect the position of the Azores Front (chapter 3), the versions 1.4.2 and 2.0.4 were combined to one data set. The first version delivers temperature data from January 1958 until December 2001 and is forced by wind data from the European Centre for Medium - Range Weather Forecasts (ECMWF). The second version seamlessly attaches the first, beginning in January 2002 until December 2007, and uses wind measurements provided by the satellite QuikSCAT (Quick Scatterometer). In chapter 4 and 5, the temperature field from the version 2.1.6 was applied which provides data from January 1871 until December 2008. As forcing, the wind data from the European Reanalysis ERA 40 are used. All versions have a spatial resolution of $0.5^\circ \times 0.5^\circ \times 40$ depth levels and a temporal resolution of one month. The data are freely available at http://apdrc.soest.hawaii.edu/data/data.php.

Zonal and meridional wind components at 10 m depth level were provided by NCEP (National Centers for Environmental Prediction) since January 1948 [*Kalnay*, 1996]. The spatial resolution of this data set is 2.5° × 2.5°, and in this thesis the temporal resolution was chosen as one month. The data set is freely available at http://www.esrl.noaa.gov.

Furthermore, the downward solar radiation flux at surface was provided by NOAA-CIRES (National Oceanic and Atmospheric Administration – Cooperative Institute for Research in Environmental Sciences) 20th Century Reanalysis Version II from January 1871 until December 2008 [*Compo et al.*, 2004]. The data set has a spatial resolution of 2° × 2° and is monthly resolved. Download of the data set is freely available on http://www.esrl.noaa.gov.

2.2.4 Satellite Data

Satellites provide remotely measured near surface chlorophyll *a* data in high temporal and spatial resolution to a maximum depth of 25 % of the euphotic depth [*Gordon and McCluney*, 1975]. Data by SeaWiFS (SEA-viewing Wide Field of-view Sensor) in 8-day resolution from August 29th, 1997 until December 18th, 2010 are used in chapter 4. These data were provided by the online portal Giovanni (Goddard Earth Sciences Data and Information Services Center Interactive Online Visualization ANd aNalysis Infrastructure, *Acker and Leptoukh* [2007]) and can be downloaded at http://gdata1.sci.gsfc.nasa.gov/daac-bin/G3/gui.cgi?instance_id=ocean_month. To reduce the lack of data due to cloudiness and the effect of patchiness, data in an area around the mooring site Kiel 276, 30° – 35°N, 20° – 25°W, were chosen. For the analysis in chapter 4, spatial mean values over this area were calculated.

2.2.5 Climate and Oceanic Indices

To determine possible forcing mechanisms of the frontal dynamics and the long-term variability of primary production, different climate and oceanic indices were considered from the Atlantic, where the study area is located, as well as from the Pacific, whose climate pattern can be linked with the Atlantic via teleconnections.

The **North Atlantic Oscillation** (NAO) is known as the dominant mode of climate variability in the North Atlantic [*Eden and Jung*, 2001; *Marshall et al.*, 2001]. This

atmospheric oscillation influences precipitation, sea level pressure, and temperatures from North America to central Europe and the subtropical West Africa [*Hurrell and Deser*, 2009]. The NAO-index describes the normalised sea level pressure anomalies between Lisbon, Portugal, and Stykkisholmur, Iceland [*Hurrell*, 1995]. In this study, the monthly NAO-index is used as well as the winter NAO-index calculated as the mean from December to March because the NAO is most pronounced in these months. Both time series are available at https://climatedataguide.ucar.edu/climate-data/hurrell-north-atlantic-oscillation-nao-index-station-based. The NAO is discussed in chapters 3 – 5.

The shifts in the position of the Gulf Stream are described by the **Gulf Stream Northern Wall** (GSNW) index. This index is calculated as the first principal component of the position of the Northern Wall of the Gulf Stream [*Taylor and Stephens*, 1998]. The units of the GSNW index are equivalent to a meridional shifting of 0.03° at 79°W and 0.3° at 65°W [*Taylor et al.*, 1998]. The data are available at www.pml-gulfstream.org.uk. This index is used in chapter 3.

The following indices are used in the discussion of chapter 5.

The **Atlantic Multidecadal Oscillation** (AMO) is a natural mode of climate variability with a period of 60 – 80 years and is expressed in the sea surface temperature of the North Atlantic Ocean [*Schlesinger and Ramankutty*, 1994; *Kaplan et al.*, 1998; *Enfield et al.*, 2001]. The AMO effects air temperature as well as rainfall in wide areas of the Northern Hemisphere and is mostly stated in North America and northern Europe. The AMO index is calculated by averaging the detrended time series of sea surface temperature of the North Atlantic between 0° – 70°N and subtracting the climatological mean between 1901 and 1970. The AMO index is available from 1856 until present on http://www.esrl.noaa.gov/psd/data/timeseries/AMO/.

North of the trade wind zone, the dominant large scale mode of climate variability in the Northern Hemisphere is the **Arctic Oscillation** (AO, *Thompson and Wallace* [1998, 2000]; *Higgins et al.* [2000]) which is characterised by the wind field in the Arctic at around 55°N. Because the AO has a larger horizontal scale than the associated NAO, it influences the surface air temperature of the Northern Hemisphere to a larger amount. The index of the AO is calculated by projecting the so called "loading pattern" to the daily anomaly of the surface pressure field over 20° – 90°N. This loading pattern is the first mode of the EOF analysis of the monthly surface pressure anomaly from 1979 to 2000 over the same area. The data can be freely downloaded on http://www.cpc.ncep.

noaa.gov/products/precip/CWlink/daily_ao_index/ao.shtml.

The **Atlantic Meridional Mode** (AMM) is a climate mode centred in the tropical Atlantic which is characterised by the cross-equatorial meridional gradient of the sea surface temperature [*Chiang and Vimont*, 2004; *Doi et al.*, 2010; *Foltz et al.*, 2012]. The AMM is correlated with the meridional displacement of the Intertropical Convergence Zone and therefore impacts the weather conditions from South to North America as well as in Africa. This climate mode is known to be the dominant source of coupled ocean-atmosphere variability in the Atlantic [*Chiang and Vimont*, 2004]. The calculation of the AMM index bases on a Maximum Covariance Analysis of the sea surface temperature and the meridional wind component. The calculation method and the data are available on http://www.esrl.noaa.gov/psd/data/timeseries/monthly/AMM/.

The **East Atlantic Pattern** (EAP) is a North Atlantic climate mode of low frequency variability similar to the NAO [*Barnston and Livezey*, 1987]. However, its north-south dipole spanning the North Atlantic from east to west is displaced southeastward causing a strong subtropical link. Contrary to the NAO which is mostly apparent in winter, the EAP acts as a leading mode all year. The EAP influences temperatures and precipitation from North America to Europe. The EAP index used in this thesis is derived from a rotated principal component analysis of the normalised 500 hPa height anomalies of the Northern Hemisphere from 1950 until 2010 and standardised by the 1981 – 2010 climatology. The data are available on http://www.cpc.ncep.noaa.gov/data/teledoc/ea.shtml.

As global dominant mode of the natural climate variability, the **El Niño / Southern Oscillation** (ENSO) is centred in the tropical Pacific with a period between three and seven years [*Bradley et al.*, 1987; *Rahmstorf*, 2002]. The ENSO events persist for 6 to 18 months [*Mantua and Hare*, 2002]. The coupling from ocean and atmosphere of this mode effects fluctuations in precipitation, wind, ocean currents, and sea surface temperature from the pacific to the east of Africa [*Tomczak and Stuart*, 1994; *Bigg*, 2003]. The ENSO index describes the anomalies of the sea surface temperatures in the Niño 3.4 region (5°N – 5°S, 170° – 120°W). The time series is available on http://www.esrl.noaa.gov/psd/enso/enso.current.html\#indices.

The **Pacific Decadal Oscillation** (PDO) is a pattern of the climate variability of the Pacific with similarities to ENSO [*Trenberth and Hurrell*, 1994; *Mantua and Hare*, 2002]. However, the events of the PDO are more long-living, in the 20th century

they lasted for 20 to 30 years. Two dominant periods of the PDO were identified by *Minobe* [1999, 2000] with 15 to 20 years and from 50 to 70 years. Implications on climate as well as terrestrial and marine ecosystems are largest in the Pacific region, however, correlations were found all over the globe [*Mantua and Hare*, 2002]. The index of the PDO is defined as the leading principal component of the monthly sea surface temperature in the North Pacific poleward from 20°N. The data are available on http://www.esrl.noaa.gov/psd/data/climateindices/list/.

2.3 Methods

2.3.1 Reconstruction of past chlorophyll *a* fields

The chapter 4 in this thesis focusses on the development of a method to reconstruct a chlorophyll *a* field. This method bases on *in-situ* measurements of temperature, nitrate and chlorophyll *a*. After calculation of the correlation between these temperature and nitrate measurements, this correlation is applied to a modeled temperature field resulting in a nitrate field. The relationship between chlorophyll *a* and both temperature and nitrate are applied to their respecting fields to gather the chlorophyll *a* field. A detailed description of the used data (Tab. 4.1 and the method is given in chapter 4. In this thesis, a past chlorophyll *a* field in the Madeira Basin was calculated based on the modeled temperature field provided by SODA POP (see sec. 2.2.3).

2.3.2 Catchment areas of the sediment traps

The catchment areas of the sediment trap at the mooring Kiel 276 in 2000 m span up to a few hundred square kilometres with strong variations due to the high eddy activity in the region of the Azores Front [*Waniek et al.*, 2005a]. The calculation of the catchment areas is based on the backward trajectories of the sinking particles from the sediment trap to the surface. For this, the daily current measurements of the mooring Kiel 276 in different depths between surface and 1600 m are averaged between discrete depth levels to gain vertical velocity profiles for each day. Using the settling velocity of 100 m day^{-1}, the vertical displacement of a particle is calculated day to day rising from the sediment trap to the surface. The method is described in detail in *Waniek et al.* [2000]. The used

data and the discrete depth levels are given in table 3.2. The calculations were done with MATLAB by using the m-files written by J. J. Waniek within chapter 3.

2.3.3 Ekman transport

The Ekman transport describes the wind induced mass transport in the upper, wind effected layer of the ocean (Ekman layer) [*Ekman*, 1905].

The zonal (U_E) and meridional (V_E) components of the Ekman transport are calculated with

$$U_E = \frac{\rho_a \, C_d}{\rho_w \, f} \left(W_x^2 + W_y^2\right)^{1/2} W_y, \tag{2.1}$$

$$V_E = -\frac{\rho_a \, C_d}{\rho_w \, f} \left(W_x^2 + W_y^2\right)^{1/2} W_x, \tag{2.2}$$

where W is the wind speed at 10 m, ρ_a = 1.3 kg m^{-3} the air density, C_d the dimensionless drag coefficient, ρ_w = 1025 kg m^{-3} the mean sea water density, and f the Coriolis parameter [*Alvarez et al.*, 2008]. The drag coefficient C_d depends on the wind speed with [*Gill*, 1985]

$$C_d = 1.1 \cdot 10^{-3} \quad \text{for W} < 6 \text{ m s}^{-1}, \tag{2.3}$$

$$C_d = (0.61 + 0.063 \cdot W)10^{-3} \quad \text{for } 6 \leq \text{W} < 22 \text{ m s}^{-1}. \tag{2.4}$$

As wind data, the output provided by NCEP was used (see sec. 2.2.3). Calculations of the Ekman transport are analysed in chapter 3.

2.3.4 Wavelet Analysis

Contrary to Fourier analysis, Wavelet analysis allows to study dominant periods in non-stationary time series. A detailed description of the wavelet method is given in *Lau and Weng* [1995]; *Torrence and Compo* [1998]; *Grinsted et al.* [2004]. Using this method, the time series is decomposed into its time-frequency space allowing determination of the dominant modes and their variability in time.

The wavelet analysis bases on the convolution of a time series $x(t)$ with a set of

functions $\psi_{a,b}(t)$ which are derived from the so-called "mother wavelet" ψ:

$$\psi_{a,b}(t) = \frac{1}{a^{1/2}}\psi\left(\frac{t-b}{a}\right), \quad a > 0, b \in \Re, \tag{2.5}$$

with a corresponding to the scale (dilation) and b denoting the position (translation) of the wavelet in space or time according to the spatial or temporal resolution of the time series. The functions $\psi_{a,b}(t)$ are called "daughter wavelets". The normalization factor $a^{-1/2}$ ensures energy conversation between the mother and daughter wavelets [*Lau and Weng*, 1995].

In this thesis, the Morlet-wavelet was used as mother wavelet

$$\psi_0(\eta) = \pi^{-1/4} e^{i\omega_0\eta} e^{-\eta^2/2}, \tag{2.6}$$

with η representing the dimensionless time and ω_0 = 6 the wave number which gives the number of oscillations within the wavelet. Wavelet transformation of a time series $x(t)$ is then calculated by the convolution of $x(t)$:

$$W^x_\psi(b,a) = \frac{1}{a^{1/2}} \int \psi^* \left(\frac{t-b}{a}\right) x(t)dt \tag{2.7}$$

with ψ^* as the complex conjugate of ψ.

To identify on which periods two time series x and y behave concurrent by considering the phase differences, the wavelet coherence is defined as

$$R^2(a) = \frac{\left|\langle(a^{-1}W^{xy}(a)\rangle\right|^2}{\left\langle a^{-1}\left|W^x(a)\right|^2\right\rangle \cdot \left\langle\left|a^{-1}W^y(a)\right|^2\right\rangle} \tag{2.8}$$

with $W^{xy} = W^x\ W^{y*}$ [*Torrence*, 1999], and $\langle\ \rangle$ indicating smoothing in time and space ensuring that $0 \leq \mathrm{R}^2(a) \leq 1$. This coherence can be treated as a localised correlation in the time-period-space [*Grinsted et al.*, 2004]. Calculation was done using the wavelet coherence package by A. Grinsted (http://noc.ac.uk/using-science/crosswavelet-wavelet-coherence). The wavelet coherence is applied in chapter 4 and 5.

2.3.5 Empirical Orthogonal Function Analysis

The Empirical Orthogonal Function (EOF) analysis or Principal Component Analysis is a method to deduce the dominant patterns of variability from a statistical field [*Storch and Zwiers*, 2003]. The method's advantage is the reduction of dimensionality of the data field to gain the patterns which describe the variability at best. In doing so, the first EOF explains most of the variability, the second EOF second most, and so on. Thus, the variability of the data field can be described by using only few EOFs.

Let $\vec{F}(x,t)$ be a data field with $x = 1 \ldots X$ data points in time and $t = 1 \ldots T$ data points in space. To describe the variability, the anomalies $\vec{F}'(x,t)$ are formed and then expanded into a series of k EOFs

$$\vec{F}'(x,t) = \sum_{i=1}^{k} \alpha_i(t)\vec{e}_i(r) + \sum_{i=k+1}^{X} \alpha_i(t)\vec{e}_i(r) \tag{2.9}$$

with time coefficients $\alpha_i(t)$ and the EOF patterns $\vec{e}_i(x)$. Because the first k EOFs describe most of the variability, the second part of equation 2.3.5 represents the noise and is usually neglected. For calculation of the EOFs, first the eigenvectors of the covariance matrix $\mathbf{B} = \mathbf{F}\mathbf{F}^{\mathbf{T}}$ with $\mathbf{F}^{\mathbf{T}}$ as the transposed matrix are determined by composing $\mathbf{B}$ in an eigenanalysis

$$\mathbf{B}\mathbf{E} = \mathbf{\Lambda}\mathbf{E} \tag{2.10}$$

with $\mathbf{E}$ the matrix containing the orthonormal eigenvectors $\vec{e_i}$, which are EOF patterns, and $\mathbf{\Lambda}$ the eigenvalues λ_i which describe the amount of explained variability. To determine the development of the data field in time, the time coefficients of the EOF were calculated by using $\mathbf{F}$ that can be rewritten as

$$\mathbf{F} = \mathbf{E}\mathbf{A} \tag{2.11}$$

with the matrix $\mathbf{A}$ containing the time coefficients α_i. Because the EOFs are orthonormal, the time coefficients are

$$\mathbf{A} = \mathbf{E}^{\dagger}\mathbf{F} \tag{2.12}$$

with $\mathbf{E}^{\dagger}$ the conjugate transpose of $\mathbf{E}$. More details of the EOF analysis is given in *Storch and Zwiers* [2003]. The EOF analysis is used in chapter 4 and 5.

3 Impact of the Azores Front Propagation on Deep Ocean Particle Flux

Fründt, B. and Waniek, J. J. published 2013 in Central European Journal of Geosciences 4(4), 531–544.

3.1 Abstract

The Azores Current originating as a branch of the Gulf Stream is a highly dynamic system in the subtropical North Atlantic. The associated front forms the northeastern boundary of the North Atlantic Subtropical Gyre. In this study, we analysed 42 years of assimilated modeled temperature fields to localize the position of the Azores Front at 22°W and observed a fast north- and southward propagation between 30° and 37.5°N on monthly to decadal time scales. The North Atlantic Oscillation with correlated changes of the wind direction was identified as one driving mechanism. As the front is acting as a guide for Rossby waves, the signal of the front's propagation is transferred to the western Atlantic and, among other atmospheric forcing mechanisms, induces a shifting of the Northern Wall of the Gulf Stream with one year delay. Shallower mixed layer depths in the northern frontal region of the Azores Current caused by the rise of the isotherms lead to nutrient supply and primary production different from those found in the southern frontal region of the current system. A high interannual variability is manifested in deep ocean particle flux, derived from a sediment trap in 2000 m water depth at the mooring site Kiel 276 (33°N, 22°W) from 1993 to 2008, which is directly related to the phytoplankton bloom in the euphotic zone. This variability is explained by the propagation of the front and strong variations in the catchment areas of the sediment trap due to the associated eddy activity in the frontal region.

3.2 Introduction

South of Newfoundland, near 39°N, the Gulf Stream branches into the North Atlantic Current and the Azores Current [*Gould*, 1985; *Krauß*, 1994]. The Azores Current itself transports 10 Sv in the upper 800 m of the water column across the Atlantic Ridge south of the Azores between 32°N and 36°N [*Klein and Siedler*, 1989] and then feeds the southwestward flowing North Equatorial Current [*Krauß*, 1994]. Accompanied to the eastward flow of the meandering Azores Current is a high mesoscale eddy activity causing recirculation and advection [*Schiebel et al.*, 2002]. The northern boundary of the Azores Current is formed by the Azores Front (Fig. 3.1) characterised by strong temperature and salinity gradients [*Pérez et al.*, 2003], located between 30° and 38°N [*Käse and Siedler*, 1982], whereby the front simultaneously represents the northeastern border of the North Atlantic Subtropical Gyre. The Azores Front separates the warmer and saltier 18 °C Western North Atlantic Water (WNAW) originating from the Sargasso Sea to the south from the colder Eastern North Atlantic Water (ENAW) to the north [*Schiebel et al.*, 2002; *Teira et al.*, 2005] and in this study is defined by rising of the 15 °C - isotherm from depths below 300 m to above 200 m [*Gould*, 1985].

The northwestern boundary of the North Atlantic Subtropical Gyre is formed by the Gulf Stream. North- and southward drifting of the Gulf Stream has been observed and studied before [e.g. *Taylor et al.*, 1998; *Taylor and Stephens*, 1998; *Joyce et al.*, 2000; *Frankignoul et al.*, 2001]. Combined surface, aircraft and satellite observations have been used to observe the north wall of the Gulf Stream since 1966 [*Taylor and Stephens*, 1998]. A major factor in establishing the position of the Gulf Stream was found in changes of the atmospheric forcing related to the North Atlantic Oscillation (NAO) being the dominant mode in the climatic variability of the North Atlantic [*Eden and Jung*, 2001; *Marshall et al.*, 2001]. Correlated to the NAO, changes in wind forcing and the sea surface temperature (SST) pattern influence the north- and southward shift of the Gulf Stream [*Joyce et al.*, 2000; *Frankignoul et al.*, 2001]. The origin of the Azores Current as a branch of the Gulf Stream suggests a correlation of their propagation.

In contrast to the large scale physical forcing mechanisms from the atmosphere and in the ocean, subtropical fronts generate highly dynamic systems that can maintain a strong biological response caused both by their large spatial extent and temporal persistence as well as their jet-like flows [*Fernández and Pingree*, 1996]. Closely located to the

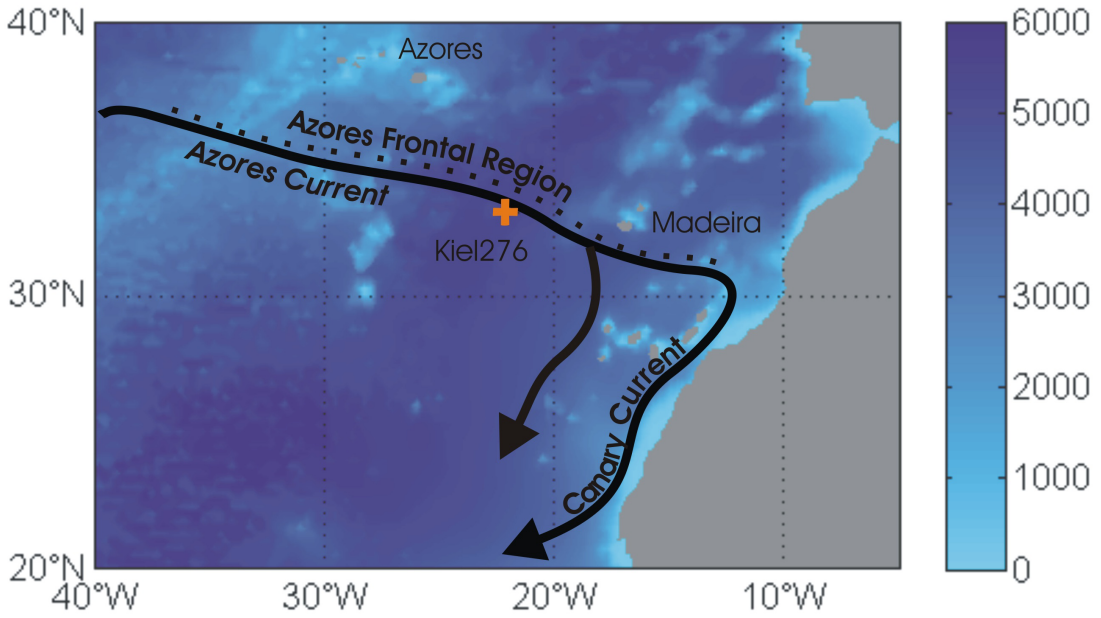

Figure 3.1: The Azores Frontal Region in the subtropical Northeast Atlantic. Indicated are the Azores Current with its accompanied Azores Frontal Region building the transition area between the surface waters of the cold waters of the temperate Atlantic and the warm waters of the subtropical and tropical Atlantic, and the Canary Current. The time series station Kiel 276 is located on 33°N, 22°W.

Azores Front is the mooring station Kiel 276 (33°N, 22°W, Fig. 3.1) where particle flux was sampled in 2000 m from 1993 onwards. This particle flux time series will be used to study the influence of the propagation and the water mass separation of the front on the biological environment in the upper water column and associated export production. Many studies of the biological production in the region of the Azores Front have been carried out, e.g. by *Fasham et al.* [1985]; *Fernández and Pingree* [1996]; *Pérez et al.* [2003]; *Teira et al.* [2005] with analyses of biological and chemical data sampled on different cruises. However, no long time series of *in-situ* chlorophyll *a* or primary production which are relevant for studies of the biogenic particle flux are available. *Fasham et al.* [1985] found in the colder water north to the front higher concentrations than in the warmer water in the south caused by either more nutrient supply or generally higher nutrient concentrations. However, there was no evidence of higher chlorophyll *a* values in the frontal zone, and also no indication for differences in the integrated production rates down to 80 m water depth north and south of the Azores Front [*Fernández and*

Pingree, 1996]. Contrary to *Fasham et al.* [1985], *Fernández and Pingree* [1996] measured 2 to 3 times higher chlorophyll *a* values at the frontal boundary. *Teira et al.* [2005] summarised the results of 13 cruises in the frontal region and found no significant differences in primary production rates related to the position of the front. Interannual variability in the biogenic particle flux [*Waniek et al.*, 2005a] could not be explained before since related dynamics on the upper water column caused by propagation of the Azores Front were not well understood. *Waniek et al.* [2005a] showed high variability in surface production based on model results and remotely measured chlorophyll a, but did not provide any explanation for processes responsible for that. In this study, we analyse the north- and southward propagation of the Azores Front using assimilated model data from 1966 to 2007. At first, we identify driving mechanisms as well as consider the interaction with the Gulf Stream. Secondly, the influence of the front on the deep ocean particle flux is analysed regarding the special growth conditions in the frontal zone as a narrow transition area between the oligotrophic subtropics and the more productive temperate North Atlantic.

3.3 Material and Methods

The Azores Front does not have any surface indication throughout the year, especially in summer, as it is masked by the seasonal thermocline ruling out detection via satellite observations of the sea surface temperature. Also the use of the remotely measured sea surface height is hindered because these signals are dominated by mainly atmospherically forced temperature changes of the uppermost water column above the front in 200 to 300 m water depth. However, these temperature changes do not influence the position of the Azores Front.

For studying the propagation of the Azores Front on monthly to decadal time scales, modeled temperature fields in the Northeast Atlantic have been used, as *in-situ* measurements of the front are rare (Tab. 3.1). Temperature data from the Simple Ocean Data Assimilation Parallel Ocean Program (SODA POP) were used. The model provides oceanographic fields with a mean spatial resolution of $0.5^\circ \times 0.5^\circ \times 40$ depth levels and monthly resolution between 1958 and 2007. This ocean model assimilates hydrographic data, temperature and salinity data from moorings, CTD measurements and ARGO floats, surface temperature and salinity observations of different kinds and

Table 3.1: Cruises in the Northeast Atlantic from which temperature measurements were used to reconstruct the position of the Azores Front (Fig. 3.2).

Site no.	Cruise	Cruise period	Research Vessel	Reference
1	P86	15/03/82 – 27/04/82	Poseidon	*Käse and Siedler* [1982]
2	P104	17/10/83 – 22/10/83	Poseidon	
3	M2T069-5-6	21/10/84 – 21/11/84	Meteor II	
4	MET006	01/11/87 – 09/11/87	Meteor III	
5	M10/1	19/03/89 – 27/04/89	Meteor III	*Zeitzschel et al.* [1990]
6	M36/2	21/06/96 –18/07/96	Meteor III	*Mienert et al.* [1998]
7	AZORES I	August 1998	BIO Hesperides	*Pérez et al.* [2003]
8	P247/2	January 1999	Poseidon	*Schiebel et al.* [2002]
9	P259	10/04/00 – 21/04/00	Poseidon	
10	P267	13/01/01 – 29/01/01	Poseidon	
11	P297	17/04/03 – 28/04/03	Poseidon	
12	P321	02/05/05 – 11/05/05	Poseidon	
13	P334	15/03/06 – 03/04/06	Poseidon	
14	P349	05/04/07 – 24/04/07	Poseidon	

nightly infrared satellite SST data. For more details see *Carton et al.* [2005] and *Carton and Giese* [2008].

To obtain the frontal position, the temperature distribution at 22°W between 20° to 40°N from surface to 400 m water depth was determined by linearly interpolating 18 depth levels of the model to a vertical resolution of one metre. According to the definition of the Azores Front [*Gould*, 1985], the position of the front in north-south direction was set where the 15 °C - isotherm crosses 250 m water depth.

The 22°W longitude was chosen to compare the position of the Azores Front determined from the SODA POP model data with *in-situ* measurements of the front made along 22°W transects between 1982 and 2007 (Tab. 3.1) which are independent from the model assimilation.

All the analyses carried out in this study are confined to a region which ranges from the southernmost position of the Azores Front in the time series to the northernmost position. Furthermore, one degree in latitude is added, respectively, regarding the slope of the 15 °C - isotherm at the front's position. Thus, in this study the so called frontal region extends from 29°N to 38.5°N.

The influence of the atmospheric forcing on the position of the Azores Front is analysed by considering the NAO. The NAO-index describes the difference of the normalised sea level pressure anomaly between the Azores High and the Iceland Low [*Hurrell*, 1995]. Here, both the monthly NAO-index and the winter NAO-index covering December to March, were used. The data are available at http://www.cgd.ucar.edu.

Additionally, the wind direction over the North Atlantic was taken into account. Wind directions on 22°W were calculated from monthly means of NCEP (National Centers for Environmental Prediction) zonal and meridional wind components (available at http://www.esrl.noaa.gov) [*Kalnay*, 1996]. Anomalies of the wind direction were calculated by subtracting the long-term mean from the actual wind direction. The wind components were also used to calculate the Ekman transport on 22°W [*Gill*, 1985; *Alvarez et al.*, 2008].

In this study, the Gulf Stream Northern Wall (GSNW) index calculated as the first principal component of the position of the North Wall Gulf Stream by *Taylor and Stephens* [1998] was applied from 1966 to 2007, and obtained from www.pml-gulfstream.org.uk. The units of the GSNW-index are equivalent to a meridional shifting of 0.03° at 79°W and 0.3° at 65°W [*Taylor et al.*, 1998].

To distinguish the conditions for the biological production north and south of the Azores Front, the mixed layer depth (MLD) was derived from the temperature profiles of SODA-POP as the depth where the difference between the SST and the temperature in depth exceeds 0.5 °C [*Ward and Waniek*, 2007]. The winter mixing is one of the crucial parameters that influence the strength of the phytoplankton bloom [*Neuer et al.*, 2007]. According to the depth of the mixed layer different amounts of nutrients are delivered to the euphotic zone. For the determination of the MLD north and south of the Azores Front, the temperature profiles 1° north and south of the calculated position of the Azores Front were used.

Variability of the biological export production in the upper water column was analysed by using particle flux data from a sediment trap in 2000 m from the mooring station Kiel 276 (Tab. 3.2, *Waniek et al.* [2005a]) located at 33°N, 22°W, which is frequently passed by the Azores Front. From satellite derived chlorophyll *a* data an estimate of the biological production in the whole euphotic zone cannot be made due to the deep chlorophyll maximum (DCM) at approximately 100 m water depth. This DCM is a consistent oceanographic feature of the subtropical ocean [*Pérez et al.*, 2006]. The

Table 3.2: Sample series of the deep ocean particle flux from the mooring station Kiel 276 (33°N, 22°W). Additionally the current meter data are given from which the catchment areas were calculated [*Waniek et al.*, 2000, 2005a].

Sample Series	Start of deployment	End of deployment	Current meter depth [m]
14	20/09/1993	05/08/1994	SODA-POP
15	27/09/1994	29/08/1995	240, 500, 970, 1120
16	01/11/1995	12/06/1996	378, 1008, 1600
17	14/07/1996	15/06/1997	270, 500, 1000, 1600
19	01/02/1999	01/11/1999	SODA-POP
21	03/02/2001	31/07/2001	SODA-POP
22	24/02/2002	01/04/2003	240, 500, 1000, 1600
23	24/04/2003	16/03/2004	240, 500, 1000, 1600
24	20/03/2004	01/04/2005	240, 500, 1038, 1594
25	10/05/2005	01/04/2007	240, 500, 1015, 1570
26	01/05/2007	01/11/2008	240, 500, 1015, 1572

particle flux used in this study is directly coupled to the phytoplankton development and decay in the euphotic zone [*Waniek et al.*, 2005a] with a delay of one and a half to two months [*Brust et al.*, 2011]. The particle flux data were sampled with 0.5 m^2 sediment traps in 2000 m depth. These instruments, consisting of fibre glass reinforced cone with a funnel slope [*Waniek et al.*, 2005a], are described in detail by *Kremling et al.* [1996]. The sampling bottles (400 cm^3 polypropylene cups) were attached to a carousel which allows temporally separated sampling intervals of 5 to 62 days. Choice of sampling interval length depends on the seasonality of biological production [*Waniek et al.*, 2005a; *Brust et al.*, 2011]. The data gaps both between June 1997 and February 1999 and between 2000 and 2001 are caused by mooring failure [*Waniek et al.*, 2005a]. For a detailed description of the sample treatment and the determination of the particle flux see *Waniek et al.* [2005a,b]. For a better comparison with the monthly resolved SODA-POP data and derived quantities such as MLD, monthly mean values of the particle flux were calculated with the assumption that the means of the different sampling intervals are valid for each day of the associated interval.

As the mooring station Kiel 276 is located close to the Azores Front, changes in the

catchment areas of the sediment trap due to variances in the current directions can determine whether the particle flux originates from north or south of the front. The catchment areas were calculated by using the method introduced in *Waniek et al.* [2000]. Daily current measurements of Aanderaa current meters (RCM 7 and 8) from the mooring in different depths between surface and 1600 m water depth were used (see tab. 3.2). The currents are shown in e.g. *Siedler et al.* [2005] (1980-2000) and *Waniek et al.* [2005a] (1995-2002). The catchment areas of winter and spring 1994 as well as from February 1999 to July 2001 were calculated using monthly current data of SODA-POP in their highest depth-resolution because, due to instrument failures, no *in-situ* measurements from the mooring are available. For all calculations a settling velocity of 100 m day^{-1} of the sinking particles in the water column down to 2000 m is used [*Waniek et al.*, 2000]. Catchment areas from 1994 to 2001 are described in detail by *Waniek et al.* [2005a].

Nitrate samples of the Poseidon cruise P349 in April 2007 (Tab. 3.1) determined by an autoanalyzer (EVOLUTION III, Alliance Instruments) according to standard methods [*Grasshoff et al.*, 1999] were used to calculate exemplary the supply of dissolved nitrate to the upper water column after the deepening of the mixed layer in winter both north and south of the Azores Front. The cruise took place after the spring bloom, which occurs between January and March in the subtropical Northeast Atlantic [*Waniek et al.*, 2005a], therefore nitrate was depleted in the upper water column. Discrete measurements were carried out for samples from 10, 30, 70 (90), 130, 200, 400 or 500 m water depth (brackets indicate depths of water sample taken south of the front according to different depths of the nitracline).

3.4 Results and Discussion

3.4.1 Driving Mechanisms

The position of the Azores Front shows a large month to month variability (Fig. 3.2a) caused by eddies moving across 22°W influencing the depth of the 15 °C - isotherm and therefore the frontal position according to our definition.

In 42 years, from 1966 to 2007, the northernmost position of the front was found in 1975 and 2004 at 37.5°N while the southernmost position was seen at 30°N in 2004

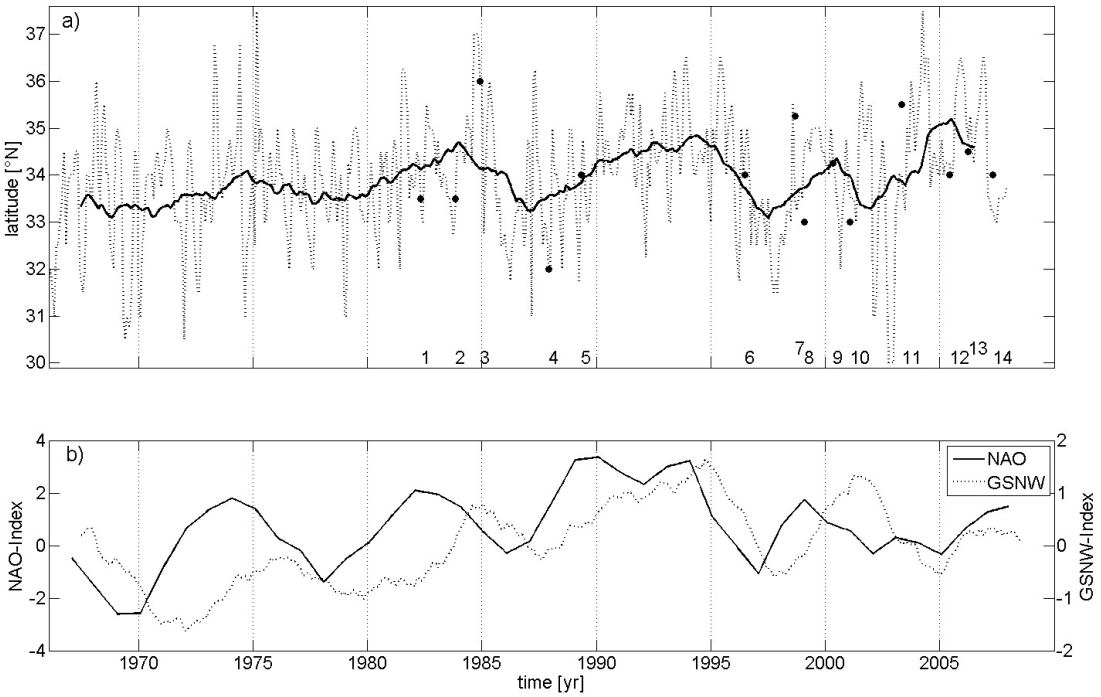

Figure 3.2: a) Position of the Azores Front at 22°W from 1966 to 2007 derived from the SODA POP temperature distribution in monthly resolution (dashed line) and a running mean over 36 months (solid line). The circles and numbers indicate *in-situ* measurements of the Azores Front at 22°W (see tab. 3.2). b) Running mean over 3 years of the winter-NAO-index (solid line) and running mean over 36 months of the GSNW-index (dashed line) from 1966 to 2009.

(Fig. 3.2a). The mean position between 1966 and 2007 was estimated at 33.9° $\pm$ 1.3°N.

The long-term changes of the front's propagation are becoming clearer after applying a running mean over 36 months. At the beginning of the time series until 1970, the Azores Front on average remains approximately at 33.2°N, from 1970 to 1974 a northward movement is seen reaching 34.1°N in 1974. In the following three years, the Azores Front shifted southward to reach 33.4°N in 1977. For the next seven years, the Azores Front propagates northward to approach 34.7°N in 1984, followed by three years southward propagation and the Azores Front is detected at 33.2°N in 1987. After seven years northward moving, the Azores Front can be detected at 34.8°N in 1994. The Azores Front repeatedly drifted southward over three years to 33.1°N in 1997, followed by a three years northward propagation to 34.4°N (Fig. 3.2a).

A shorter period of southward propagation follows from 2000 to 2002. From 2002 on, the Azores Front tends northward to the northernmost position determined in the running-mean time series at 35.2°N in 2005, and to the end of the time series a southward drift proceeds (Fig. 3.2a). From 1977 to 1997, the propagation of the Azores Front shows a repeated pattern of three years southward followed by seven years northward movement with the southward movement being faster (150 ± 40 m day^{-1}) than the northward movement (93 ± 16 m day^{-1}). From 1997 onwards, an obvious period of northward or southward propagation of the front is no longer clearly detectable (Fig. 3.2a). Over the entire time series, a linear northward propagation of the Azores Front of 6 m day^{-1} was calculated.

Measurements from 14 expeditions (Tab. 3.1), which are to our knowledge not assimilated into the SODA-POP model, are also included in figure 3.2 to estimate the quality of the SODA POP model data. The measured data compared to the model output show an agreement in the position of the Azores Front within 0.5°; this is the same as the spatial resolution in latitude of the model data, the distances between the stations of the cruises are similar with approximately 30 nautical miles.

The influence of the NAO on the ocean dynamics in the permanent thermocline in the subtropical Northeast Atlantic was shown in previous studies [e.g. *Siedler et al.*, 2005]. The time series of the running mean over three years of the winter NAO-Index (Fig. 3.2b) shows a similar pattern as the latitudinal movement of the position of the Azores Front. From 1970 to 1990, the NAO-index ascends and descends with a period of eight years. After 1990, this period decreases, and at the end of the time series no period can be recognised.

The position of the Azores Front seems to respond to the NAO with a delay of approximately one year. Significant correlations (significance level > 95 %) were found with a lag of 9 – 12 months with the largest coefficient of $\rho = 0.15$ (Tab. 3.3). Correlation coefficients between the winter NAO-index and an annual mean of the position of the Azores Front were calculated, because the NAO is most pronounced in winter [*Marshall et al.*, 2001]. Significant correlations ($\rho = 0.57$) can be seen where the Azores Front lags the NAO by 1 year (Fig. 3.3, Tab. 3.3).

As the dominant atmospheric feature over the North Atlantic, the NAO is associated with changes in wind direction, especially of the surface Westerlies between roughly 40°N and 60°N, but also in the horse latitudes between approximately 25°N and 35°N

[*Marshall et al.*, 2001]. In this region where the Azores Front is mostly located, fluctuations of the wind directions (0° pointing northwards, 90° pointing eastwards) directly associated with the NAO have been determined.

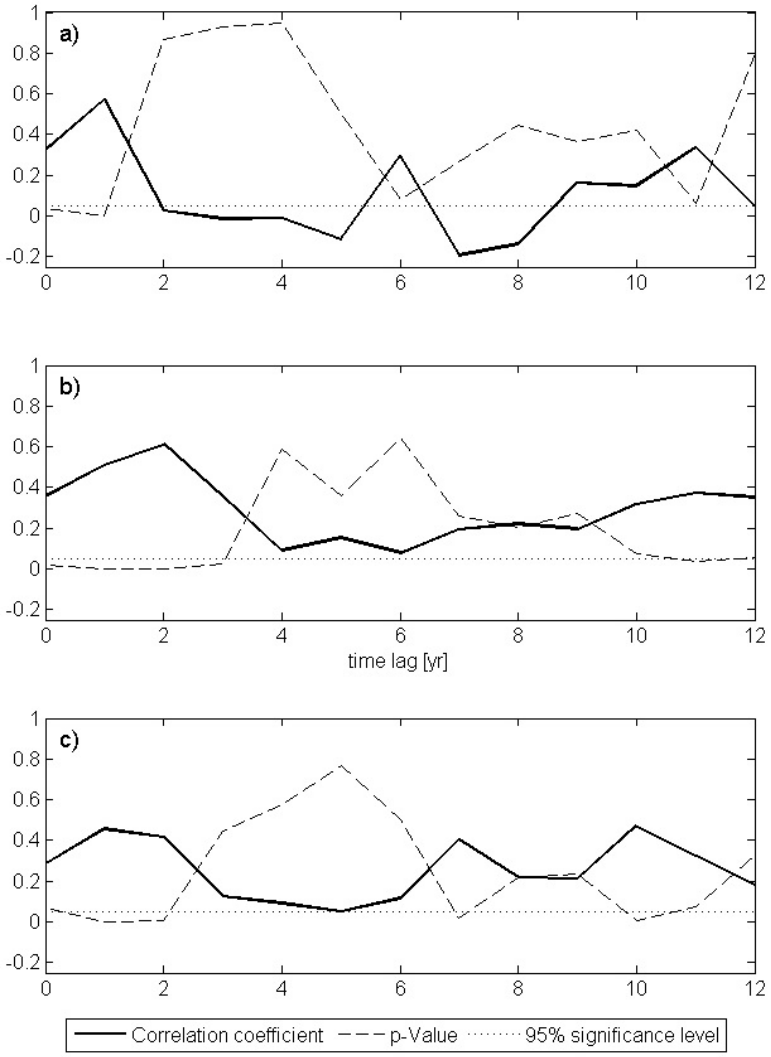

Figure 3.3: Lagged correlation coefficients between a) winter NAO and the annual mean position of the Azores Front, b) winter NAO and annual mean of GSNW, c) annual mean position of the Azores Front and annual mean of GSNW, the first parameter is leading respectively (solid lines). P-values (dashed lines) greater than 0.05 (i.e. 95 % significance level, dotted lines) indicate the level for no correlation and independent samples.

Table 3.3: Time lags of calculated correlation coefficients (in brackets) with their significance level (1: 95 %, 2: 99 %, 3: 99.9 % as superscript numbers) between NAO and GSNW, NAO and position of the Azores Front (AF), position of the Azores Front and GSNW, and GSNW and position of the Azores Front in monthly and annual resolution with the first variable leading the second, respectively. For time ranges over several months the highest coefficient is given.

NAO & GSNW		NAO & AF		AF & GSNW		GSNW & AF	
monthly	annual	monthly	annual	monthly	annual	monthly	annual
8–12 (0.13)^2	0 (0.36)^1	9–12 (0.15)^2	0 (0.32)^1	0–21 (0.23)^3	1 (0.45)^2	0 (0.15)^2	
21–23 (0.16)^3	1 (0.51)^3	14–15 (0.1)^1	1 (0.57)^3	24–28 (0.14)^2	2 (0.41)^2	45–47 (0.12)^2	
29–32 (0.16)^3	2 (0.61)^3	20–21 (0.12)^2		77–90 (0.19)^3	7 (0.4)^1	53-56 (0.15)^2	
	3 (0.35)^1			115–120 (0.23)^3	10 (0.47)^2		
	11 (0.37)^1						

Considering the wind direction anomaly at 22°W directly north (35°N) and south (32.5°N) of the mean position of the front (Fig. 3.4), deviations from the mean directions influence the position of the Azores Front. The mean direction at these latitudes are both southward (170° ± 80° at 35°N and 190° ± 70° at 32.5°N) connected to a strong variability indicated by high standard deviations. Changes in the wind direction which are directly associated with the NAO are one explanation for a propagation of the Azores Front (Fig. 3.4). This fact is supported by the study of *Volkov and Fu* [2011] who calculated the highest correlation between the wind stress curl and the Azores Front characterised by the eddy kinetic energy at a time lag of about seven months. Both results are in the same order of magnitude, however, the difference of two months in comparison to our calculation (Tab. 3.3) may be related to the different definitions of the position of the Azores Front; in this study the temperature distribution is used whereas the eddy kinetic energy was used by *Volkov and Fu* [2011]. The time lag between the NAO and the position of the Azores Front of several months is caused by the adjustment of the upper water column to the large scale atmospheric forcing [*Volkov and Fu*, 2011].

According to the southward mean wind direction in the frontal area, a positive anomaly corresponds to a westward and a negative anomaly to an eastward deviation of the mean wind direction. A westward directed wind leads to a northward displacement of the Azores Front relative to the mean position while an eastward directed wind effects a more southern position of the front, causing the front to move approximately 90° right

to the wind direction, pointing towards a wind induced Ekman transport affecting north- and southward shifting of the front (Fig. 3.4). To confirm this approach the meridional Ekman transport V_E in the frontal area was calculated (Fig. 3.5).

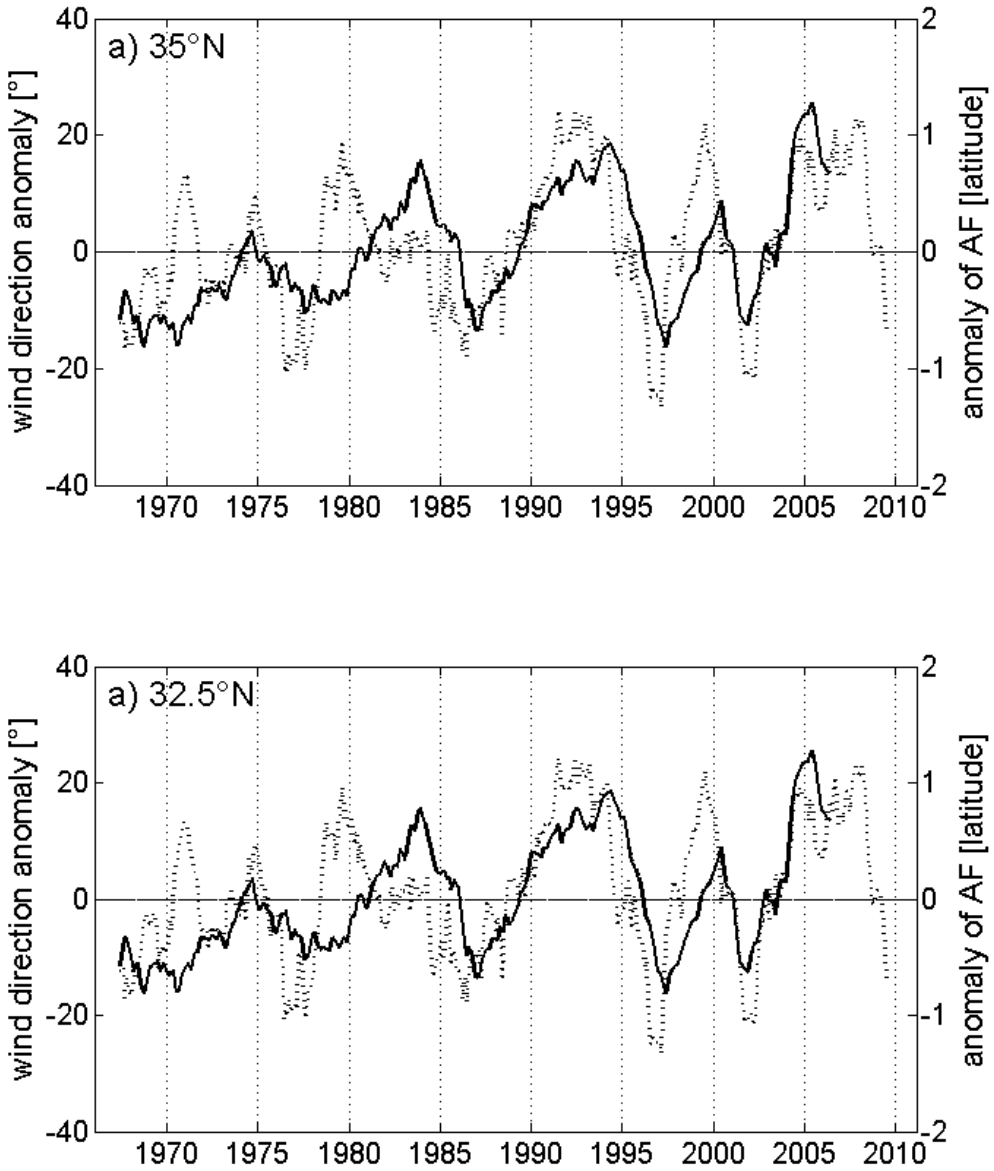

Figure 3.4: Anomaly of the 36 month running mean of the wind direction (dotted lines) at 22°W and running mean over 36 months of the anomaly of the position of the Azores Front (solid lines) at a) 35.0°N and b) 32.5°N. At both latitudes the mean wind direction is southward, so that a positive anomaly indicates a westward and a negative anomaly an eastward deviation.

Directly north of the front the transport points mainly towards the south with a mean transport of -0.03 $\pm$ 0.29 $m^2\ s^{-1}$. Contrary to that, directly south of the front a northward pointing Ekman transport (0.05 $\pm$ 0.26 $m^2\ s^{-1}$) is calculated. At the front, the transport is variable with a small northward tendency (0.01 $\pm$ 0.28 $m^2\ s^{-1}$). The meridional Ekman transports north and south of the front form a convergence area within which the Azores Front is located. The north- and southward moving of the front is partially caused by the variability of these transports. Especially changes in the mean direction of the Ekman transports from south- to northward (e.g. 1991 – 1993, 1998 – 1999, Fig. 3.5a) north of the Azores Front lead to pronounced positive anomalies of the position of the front (cf. Fig. 3.4, black line) while the zero crossings of the transport south of the front (1977 and 1996, Fig. 3.5c) lead to negative anomalies. From 2003 onwards, the meridional transport north of the Azores Front vanishes causing the northward persistent moving of the front leading to the northernmost position in 2005 (Fig. 3.2a). In the same time period (from 2003 to 2007), the correlation between the NAO and the associated wind direction with the propagation of the Azores Front seems to change because the leading effect of the NAO with a one year time lag is terminated (Fig. 3.2 and 3.4). To secure this trend with a statistically significant result, further studies with longer time periods, spanning the dominant period of the NAO (approx. 11 years) in minimum, are required.

These results of the influence of the NAO, the associated winds and Ekman transports in the frontal region on the propagation of the Azores Front represent just few of the possible driving mechanisms. Among this wind driven forcing of the front's propagation, the impact on the Azores Current of the Mediterranean Outflow was shown, by postulating that the Azores Current is possibly conceptionally generated by β - plumes [*Jia*, 2000; *Özgökmen et al.*, 2001; *Kida et al.*, 2008; *Lamas et al.*, 2010]. *Lamas et al.* [2010] confirm with observational evidence that both mechanisms are coupled leading to the assumption that variability of the Mediterranean Outflow would influence propagation of the Azores Front as well. However, this issue is subject to further investigations. The focus here lied on the atmospheric forcing because the variability of the atmospheric conditions mainly influences the uppermost water column where the biological production occurs. Changes of the amount of the production are then mirrored in the deep ocean particle flux [*Waniek et al.*, 2005a]. In this context of dominant climatic features over the North Atlantic, among the NAO the Atlantic Multidecadal Oscillation (AMO)

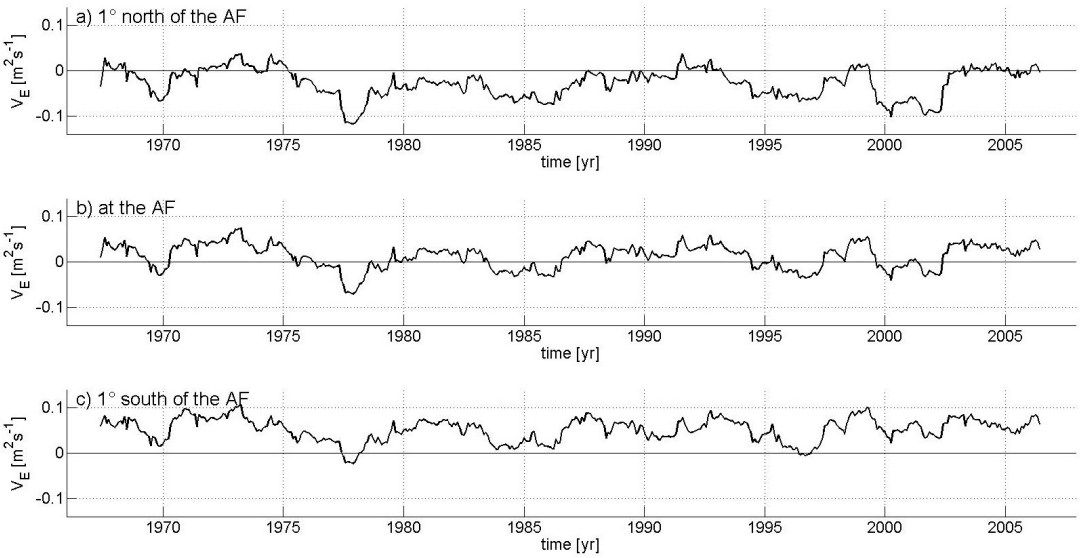

Figure 3.5: 36 month running mean of the meridional component of the Ekman transport at 22°W a) 1° north of the Azores Front, b) at the Azores Front, and c) 1° south of the Azores Front.

has to be regarded. In the observed period from 1966 to 2007 the AMO-index shifted from negative to positive in 1997. Nevertheless, a statistically significant influence of this shift from a colder to warmer period in 1997 of the position of the Azores Front cannot be seen, as the dominant period of the AMO of 60 to 80 years [*Kerr*, 2005] is nearly twice as long as the time series in which the position of the Azores Front is observed.

3.4.2 The Front's Impact on the Gulf Stream

Among the atmospheric forcing by the NAO on the Azores Front, the coherence of the meridional propagation of the Gulf Stream with the NAO on one side and with the Azores Front on the other side is considered by using the GSNW index which is derived from the position of the Northern Wall of the Gulf Stream.

The meandering of the Gulf Stream is characterised by a high month to month variability which can be removed by calculating a running mean over 36 months (Fig. 3.2b). The shifting of the northern wall of the Gulf Stream as the northwestern boundary of the

North Atlantic Subtropical Gyre shows a similar pattern as the position of the Azores Front with alternating north- and southward movements. A response to the NAO was also seen in the GSNW position in previous studies [e.g. *Taylor et al.*, 1998; *Taylor and Stephens*, 1998] caused by changes in the wind driven currents. *Taylor and Stephens* [1998] found that drift of the Gulf Stream was correlated with the NAO with a 2-year lag, whilst *Joyce et al.* [2000] found highest correlations with zero or one year lag. In this study, correlations show significant coefficients with lags of zero to three years and of eleven years (ρ = 0.37), with the highest coefficient (ρ = 0.61) at a two years lag (Fig. 3.3, Tab. 3.3). The adjustment of the Gulf Stream position to the changes in forcing is determined by westward propagation of baroclinic Rossby waves which may take several years to cross the North Atlantic [*Frankignoul et al.*, 2001]. Comparing the correlations between NAO and the position of the Azores Front on one side and the NAO and the GSNW on the other side, the GSNW seems to respond later to the NAO than the Azores Front (Fig. 3.3, Tab. 3.3).

Therefore, correlation coefficients between the position of the Azores Front and the GSNW were calculated for both the monthly and annually averaged time series (Tab. 3.3). First considering the correlation where the shift of the Azores Front is a response to changes of the GSNW, only low correlations ($\rho \leq 0.15$, Tab. 3.3) at different lags were found in monthly resolution, whereas in annual resolution no significant correlations were determined at all. Compared to the atmospheric forcing of the propagation of the Azores Front by the NAO, motions of the Gulf Stream seem to affect the Azores Front less.

Considering the results of the correlation between the NAO and both the GSNW and the position of the Azores Front, correlation coefficients for the GSNW lagging the Azores Front were calculated (Tab. 3.3). In monthly resolution significant correlations were found when the GSNW is responding to the shifting of the Azores Front, at a lag of 14 months with the highest coefficient of ρ = 0.23, and at a lag of 26 months (ρ = 0.14), then with a lag of 87 months (ρ = 0.19), and at last where the GSNW lags the position of the Azores Front by 117 months (ρ = 0.23). In contrast to the correlations where the Azores Front responds to the GSNW, here a response of the GSNW to the Azores Front is also reflected in the annual calculations (Fig. 3.3): significant correlations were calculated at lags of one (ρ = 0.45), two (ρ = 0.41), seven (ρ = 0.4) and ten years (ρ = 0.47). These results indicate that the NAO first affects the Azores Front with a

lag of one year, when the ocean has adjusted to the associated modification of the wind system. The changes of the position of the Azores Front then influence the drift of the North Wall of the Gulf Stream most rapidly with a lag of one year. This implies that the correlation between the GSNW and the NAO can be explained by a direct response of the GSNW to the position of the Azores Front whereby the influence of the NAO on the GSNW is most likely caused by an indirect signal transfer via the Azores Front.

The NAO has a high impact on the SST pattern of the North Atlantic with a largest correlation at a zero lag [*Visbeck et al.*, 2003]. Bearing in mind that in this study the position of the Azores Front was considered at 22°W, *Molinari* [2011] shows, in his figure 18 that a positive NAO-index leads to a positive temperature anomaly and vice versa. This temperature anomaly pattern is transferred across the Atlantic as Rossby Waves. *Cipollini et al.* [1997] have shown that the Azores Current can amplify the westward propagating Rossby Waves and has a similar waveguide effect as observed in the Antarctic Circumpolar Current [*Hughes*, 1996]. The correlation coefficients of the annual means have shown four different time lags in the range of one to ten years between the latitude of the Azores Front and the GSNW-index. This slow signal transfer across the North Atlantic is in the same order as the magnitude of Rossby Wave propagation. With a typical wave speed of 10 – 15 cm s^{-1} [*Chu et al.*, 2007], the NAO induced SST pattern in the region of the Azores Front needs one to two years to reach the west coast of the Atlantic where the drift of the Gulf Stream is observed. Much lower wave speeds have been quantified by *Cipollini et al.* [1997], with 0.9 cm s^{-1} and 1.9 cm s^{-1}. These speeds indicate that the signals are able to cross the Atlantic in seven and ten years; time lags for which high correlations between the Azores Front and the GSNW were found (Fig. 3.3).

3.4.3 Impact on Deep Ocean Particle Flux

The deep ocean particle flux from 1994 to 2008 is shown in figure 3.6. A detailed description of the particle fluxes from 1994 to 2002 is given in *Waniek et al.* [2005a]; the period from February 2002 to March 2005 was analysed by *Brust and Waniek* [2010] and *Brust et al.* [2011]. The particle flux time series show a high seasonal and interannual variability mirroring the variability in primary production [*Waniek et al.*, 2005a].

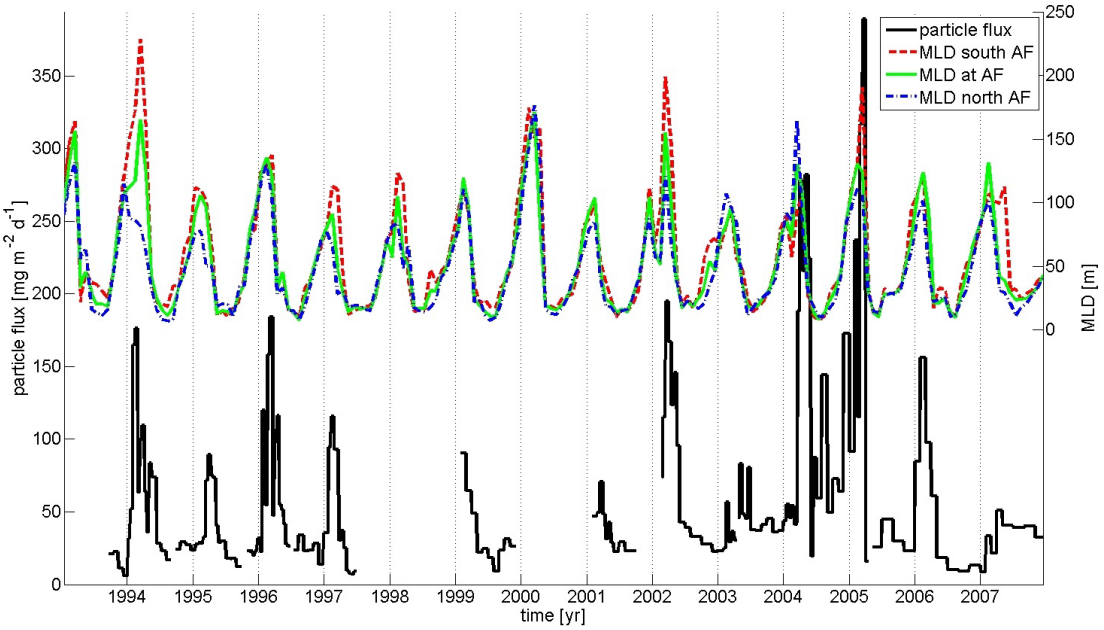

Figure 3.6: Particle flux at 2000 m depth at Kiel 276 (black line) and mixed layer depths at the position of the Azores Front (green line), 1° latitude north of the front (dot-dashed blue line) and 1° latitude south of the front (dashed red line). The gaps in particle flux between June 1997 and February 1999 and between April 2000 and 2001 are caused by mooring failure.

The annual maximum of particle flux varies in time from February to May. The highest values are found in 2004 with more than 250 mg m^{-2} day^{-1} and in 2005 with 350 mg m^{-2} day^{-1}. The seasonal variability follows directly the phytoplankton development and decay within the euphotic zone [*Waniek et al.*, 2005a]. The annual maximum is initiated by the decay of the bloom with a delay of approximately one month resulting from a mean sinking velocity of 100 m day^{-1} [*Waniek et al.*, 2000]. Comparison of independently predicted primary production with the particle flux in 2000 m depth shows a direct correlation between these two variables, but any influence of the variability in the catchment areas of the sediment trap was overlaid by the stronger signal of the seasonal cycle [*Waniek et al.*, 2005a]. *Waniek et al.* [2005a] suggested that the interannual variability is caused whether the winter mixed layer reaches the nitracline or not. The coupling of the seasonality of the winter mixed layer depth and the seasonality of phytoplankton biomass was postulated by *Neuer et al.* [2007] for the ESTOC station near the Canary Islands. In the region of the Madeira Basin, where the mooring station

Kiel 276 is located, the deepening of the winter mixed layer reaches its maximum in winter to early spring (Fig. 3.6).

The maximum varies from nearly 80 m north of the Azores Front in 1995 to 190 m in 2005 south of the Azores Front caused by a lifting of the isotherms by the front in the north (Fig. 3.7). *Fasham et al.* [1985] found values of 150 – 170 m in the region of the Azores Front in the winter 1980/81 derived from the deep stability maximum, a MLD depth range that is in good agreement with the magnitude of the mixed layer depth derived from assimilated modeled temperature fields. In spring and summer, the seasonal stratification begins and the mixed layer shallows to its minimum in autumn. If the mixed layer is deeper than the nutricline, new nutrients are supplied to the upper water column followed by phytoplankton growth. A comparison of the timing of the deepest mixed layer, which corresponds with the maximum of phytoplankton abundance in the euphotic zone, and the maximum in particle flux shows a delay of about 30 days due to the sinking velocity. Due to the coarse monthly resolution of the MLD in addition to the sampling intervals of the particle flux of two weeks to two months, *Brust et al.* [2011] estimated slightly longer time lags ranging from 30 to 60 days (Fig. 3.6).

To investigate the influence of the Azores Front on the interannual variability of the particle flux, the different biological environments north and south of the Azores Front are considered. Using remotely measured chlorophyll *a* values in this region allows only to account for particular issues, e.g. beginning of the spring bloom, but not for the existence of the deep chlorophyll maximum (DCM) in 50 – 120 m [*Teira et al.*, 2005] which is not detectable by satellite measurements. *Fasham et al.* [1985] found higher integrated chlorophyll *a* values as well as a higher maximum chlorophyll *a* concentration in the DCM in the Eastern North Atlantic Water (ENAW) that is colder and generally lies north to the Azores Front, in comparison to the warmer Western North Atlantic Water (WNAW) south to the Azores Front. Also the zooplankton biomass was significantly higher in ENAW than in WNAW. Due to the lower integrated chlorophyll *a* values the euphotic zone (1 % light level) in the WNAW was 14 m deeper causing a 20 m deeper DCM [*Fasham et al.*, 1985]. In contrast, *Teira et al.* [2005] analysed 13 cruises from 1992 to 2001 in the Azores Frontal Region and found no significant latitudinal trend in depth-integrated chlorophyll *a*. The integrated primary production showed high values both north and south of the Azores Front, as well as in the frontal boundary. In agreement with *Fasham et al.* [1985], a 20 m shallower DCM north of the Azores Front was

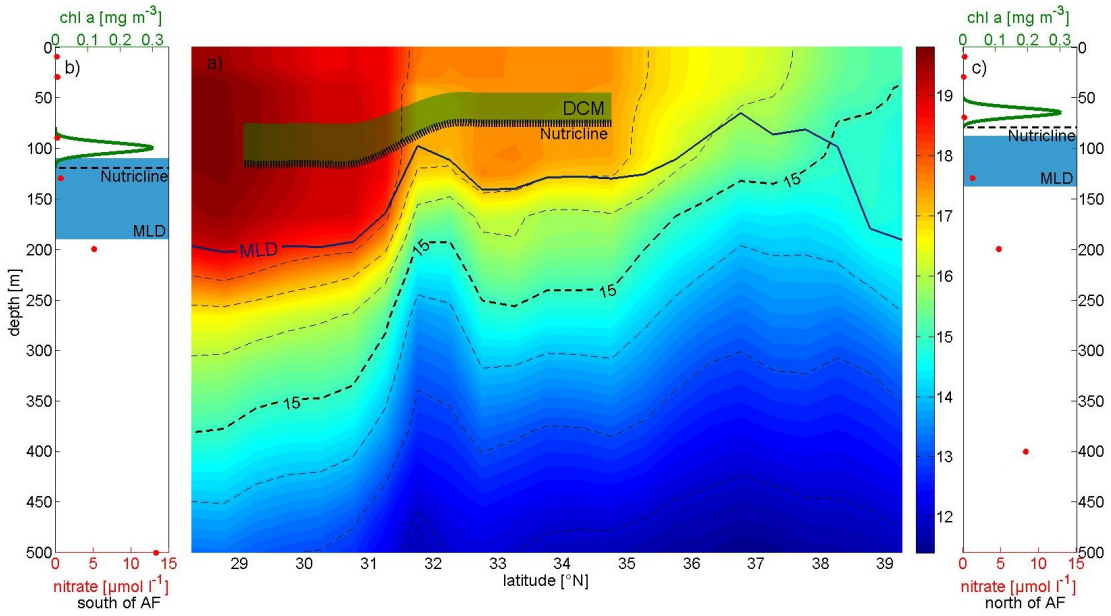

Figure 3.7: a) Temperature distribution from March 2002 derived from SODA POP and the mixed layer depth (MLD) is shown. In the region directly located at the Azores Front (31.5°N) the deep chlorophyll maximum (DCM) and the nutricline is schematically assigned. b) and c) Schema of the DCM in 80 – 120 m south to the Azores Front and in 50 – 80 m north to the front as well as the nitracline. Furthermore the depth range of the winter MLD derived from SODA POP is displayed. *In-situ* nitrate measurements of the cruise P349 (red circles) in April 2007 are also shown.

seen by *Teira et al.* [2005], but they explained the upward trend of the DCM towards northern latitudes with cooler surface waters and shallower mixed layers. It should be noted, that the sampling resolution cannot resolve the mesoscale activity [*Teira et al.*, 2005] which can induce high primary production [cf. *Fasham et al.*, 1985] caused by eddies affecting up- or downwelling relative to their direction of rotation [*Stewart*, 2008]. It is one of the most important requirements for the phytoplankton bloom that the MLD reaches the nutricline depth in winter to supply new nutrients by mixing. The depth of the nutricline is highly correlated with the depth of the DCM [*Teira et al.*, 2005], so that a mean difference of the nutricline depth of 20 m is expected between positions north of the Azores Front (shallower) and south of the Azores Front (deeper).

Assuming the same winter mixed layer depth north and south of the front, more nutrients would be supplied in the north due to mixing because the water column generally contains higher nutrient concentrations than south of the Azores Front, where the nu-

trients are depleted to a greater depth. In addition to the northward trend of the MLD shallowing within the frontal region because of lower surface temperatures, the Azores Front lifts the mixed layer by rising of the isotherms (Fig. 3.7). Generally, a deeper mixed layer can be seen south of the Azores Front (Fig. 3.6 and 3.7). Further north, in the North Atlantic Drift Province north of the frontal region the winter mixed layer starts to deepen to reach 350 m in March [*Longhurst*, 1998]. From 1966 to 2007, a mean difference in the MLD of 10 m was calculated with 50 $\pm$ 40 m north of the Azores Front and 60 $\pm$ 50 m south of the Azores Front. The high standard deviation is caused by the high seasonal variability with a shallow mixed layer of approximate 10 m in summer. Just considering the annual maximum MLD in winter, a difference of about 40 m between south (150 $\pm$ 40 m) and north (113 $\pm$ 25 m) of the Azores Front was determined. The lifting of the lower isotherms in the water column by the front is superimposed by mesoscale eddy activity acting on the MLD so that a high interannual variability both in the depth of the mixed layer and the difference relative to the front is seen (Fig. 3.6). Assuming that there are no or only small differences between the MLD north and south of the Azores Front (e.g. 1996), a higher primary production north of the Azores Front is expected due to a shallower nitracline (Fig. 3.7) providing more nutrients. In contrast, in March 1994, the MLD north and south of the Azores Front shows a difference of nearly 150 m which provides more nutrients to the south expecting an enhanced primary production at the southern frontal boundary (Fig. 3.7). *In-situ* nitrate measurements north and south of the Azores Front from April 2007 are used to estimate exemplary the amount of dissolved nitrate supplied to the euphotic zone by deepening of the mixed layer in winter by integrating the nitrate content over the MLD. Assuming the different mean maximum MLDs with their standard deviations derived from SODA POP, in this case south of the front twice as much nitrate (69^{+123}_{-36} mmol m^{-2}) is delivered as north of the frontal system (33^{+32}_{-18} mmol m^{-2}).

The mooring station Kiel 276, located on 33°N, is frequently passed by the Azores Front so that catchment areas of the sediment trap of up to a few hundred kilometres [*Waniek et al.*, 2005a] have to be considered for relating the MLD, depending on the Azores Front, with the particle flux. Even if the time series station is located south of the Azores Front, a catchment area of a few hundred kilometres can deliver particles originating north of the Azores Front and vice versa. Induced by the high eddy activity at the frontal boundary, the currents in the upper water column down to 1000 m show

high variability in velocity and direction values [e.g. *Siedler et al.*, 2005; *Waniek et al.*, 2005a] leading to high variations in extent and orientation of the catchment areas of the sediment trap.

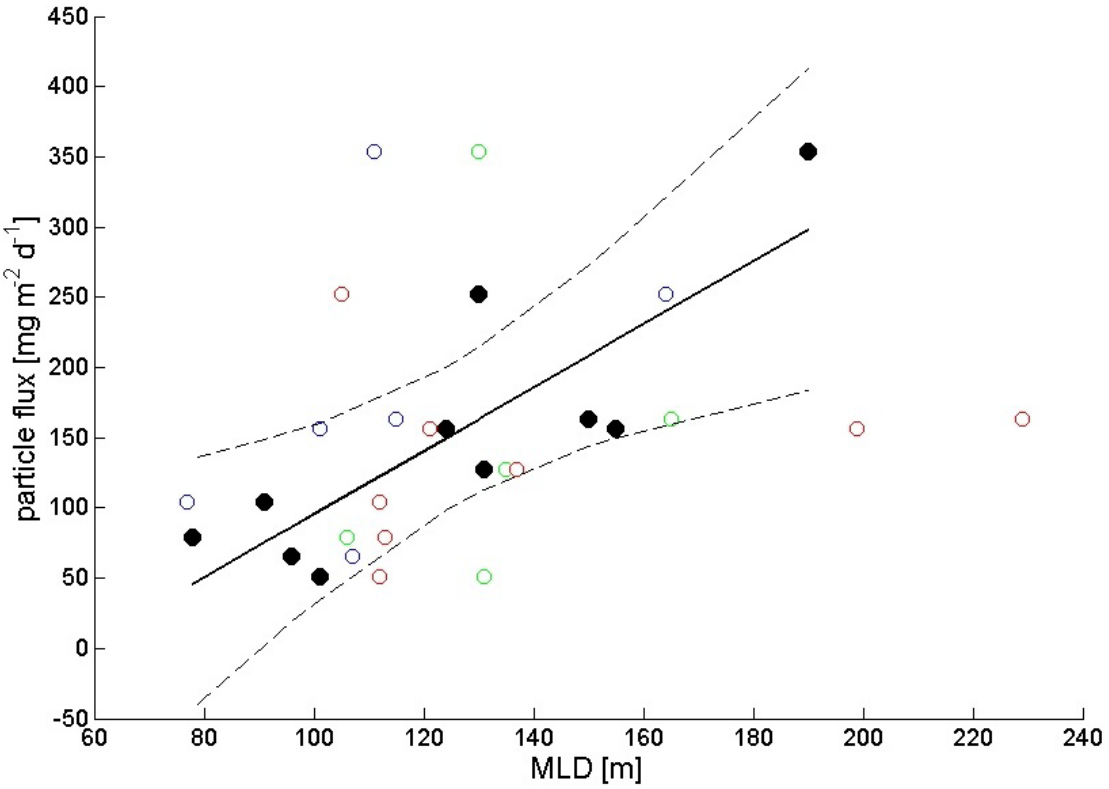

Figure 3.8: Annual maxima of the particle flux in 2000 m depth (1994 – 1997, 2002 – 2007) are assigned to the annual maxima of the MLD (black circles). The location of the catchment areas according to the position of the Azores Front either north, south or at the front was taken into account. A linear regression (solid line) with the 95 % significance levels (dashed lines) was calculated. Additionally the annual maxima of the particle flux north (blue circles) and south (red circles) of the Azores Front as well as at the front (green circles) in relation to the annual maxima of the MLD are shown.

The catchment areas as well as the position of the Azores Front at the time when the MLD reaches the maximum in winter were used to determine if the particle flux originated north, south or at the front. These considerations provide the information which maximum MLD, the generally deeper in the southern frontal region or the shallower in the northern part, has existed in the origin area of the annual maximum particle flux.

The relationship between this annual maximum MLD in winter and the particle flux are shown in figure 3.8 (black circles). A regression line of

$$\text{Particle flux}\left[\frac{mg}{m^2\ day}\right] = 2.25\left[\frac{mg}{m\ day}\right] \times \text{MLD}\,[m] - 130\left[\frac{mg}{m^2\ day}\right] \tag{3.1}$$

was calculated. With one exception, all values are within the 95 % significance level. The correlation coefficient of 0.84 (99 % significance level) between the particle flux and its corresponding MLD justifies the linear regression in this frontal region.

If the catchment areas as well as the position of the front are not taken into account, no relationship between the winter MLD north, south or at the front and the particle flux exists which is evident from the wide scattering (Fig. 3.8). Applying the regression line (3.1) (Fig. 3.8), the particle flux would be depleted when the MLD is shallower than 58 m. This result agrees well with the measured depths of the deep chlorophyll maximum between 50 and 80 m in the northern frontal region [*Teira et al.*, 2005], because a MLD of 58 m would not reach the nutricline located below the DCM and no nutrients would be delivered to the euphotic zone causing termination of the primary production and eventually of particle flux. Thus the winter MLD is the determinant for the interannual variability of the primary production leading to the observed variability in particle flux.

3.5 Conclusions

The analyses of the position of the Azores Front derived from assimilated modeled temperature fields between 1966 and 2007, show that this front is a highly dynamic system with a great variability of north- and southward propagation on monthly to decadal time scales. The southernmost position was found at 30°N (2004) and the northernmost at 37.5°N (1975 and 2004) with an overlying northward shifting trend of 6 m day^{-1}.

The propagation of the front is mainly forced by atmospheric conditions determined by the North Atlantic Oscillation. Wind direction changes over the North Atlantic correlated with the NAO cause advection and convergence/divergence which induces periodical movement of the front. The Ekman transports, due to the wind field in the frontal region, lead to a convergence zone with northward transport south to the front and southward transport north to the front. Variability of these transports additionally

causes meridional shifting of the front. Maybe a change in trend of the correlation between the NAO and the propagation of the Azores Front occurred in 2003, but further investigations are needed for a statistically significant result.

Due to the front's location further to the east in the North Atlantic than the Gulf Stream, fluctuations of the atmospheric patterns centred in the western North Atlantic impact the Azores Front and its associated currents faster than the western boundary currents. Rossby waves, modified by movement of the Azores Front, then transport the atmospherically initiated signals over the North Atlantic so that the front's shift is mirrored in the variance of the position of the Northern Wall of the Gulf Stream.

The deep ocean particle flux and the concurrent biological production in the upper water column are closely related to the migration of the Azores Front. Correlated variability in the winter mixed layer depth influences the amount of nutrient supply and leads to a high variability in primary production and consequently in particle flux. The front forms a transition zone with particular growth conditions between the cooler and generally more productive water to the north and the warmer less productive WNAW to the south where the general latitudinal trend of increasing primary production to the north is masked. To understand the interannual variability of the deep ocean particle flux, it is important to consider the propagation of the Azores Front as well as the associated mesoscale eddy activity at the frontal boundary, which influences the deepening of the mixed layer, and furthermore the variability of the catchment areas due to changes in the current velocities and directions. The resulting variances of the hydrographic conditions in the frontal area are directly mirrored in the strength of primary production in the upper water column and the associated particle flux.

3.6 Acknowledgments

The authors thank all colleagues involved in obtaining the time series data since 1980, and the crew and masters of the RV Poseidon and RV Meteor and two anonymous referees for their comments on earlier versions of the manuscript. This work is financially supported by DFG (Contract numbers WA2157/3-1 and WA2157/5-1).

4 Chlorophyll *a* reconstruction from *in-situ* measurements, Part I: Method description

Fründt, B., Dippner, J. W., and Waniek, J. J. published 2015 in Journal of Geophysical Research: Biogeosciences 120, 237-245.

4.1 Abstract

Understanding the development of primary production is essential for projections of the global carbon cycle in the context of climate change. A past chlorophyll *a* field, as an indicator of primary production, was calculated by fitting *in-situ* measurements of nitrate and chlorophyll *a* to those of temperature and by adapting the fitting functions to a modeled temperature field. The method was applied to observations from the Madeira Basin, in the northeastern part of the oligotrophic North Atlantic Subtropical Gyre, and yielded a chlorophyll *a* field from 1989 to 2008 with a monthly resolution that was validated with remotely measured surface chlorophyll *a* data. The chlorophyll *a* field determined with our method resolved the seasonal and inter-annual variability in the phytoplankton biomass of the euphotic zone as well as the deep chlorophyll maximum. Moreover, it will allow an estimation of carbon uptake over long time scales.

4.2 Introduction

Primary production in the oceans accounts for half of the global carbon fixation, and a large part of this carbon is exported into the intermediate and deep oceans [*Field et al.*, 1998; *Schwab et al.*, 2012]. Long-term changes in the growth conditions of phytoplankton in response to atmospheric forcing or an increase in temperature, as in recent decades [*Levitus et al.*, 2005, 2009; *Denman et al.*, 2007], can affect the Earth's climate and the global carbon cycle by changing the amount of carbon fixation. Understanding the changes in phytoplankton biomass occurring under past climate conditions will allow robust projections of the global carbon cycle. Studies analysing long-term variability of primary production have been pursued by *Boyce et al.* [2010] by combining *in-situ* measured chlorophyll *a* data, as primary production indicator, and early measurements of the ocean's transparency to analyse the trend in global primary production from 1899. The global drop in chlorophyll *a* since the late 1800s could be related to an increase of upper ocean stratification due to risen sea surface temperatures [*Behrenfeld et al.*, 2006; *Polovina et al.*, 2008]. Methods to measure chlorophyll *a* and primary production in the water column by satellite measurements have been developed [*Sathyendranath et al.*, 1991; *Antoine and Morel*, 1996; *Behrenfeld and Falkowski*, 1997; *Uitz et al.*, 2006] resulting in remotely measured chlorophyll *a* time series by the Coastal Zone Color Scanner from 1976 to 1986 and by SeaWiFS from 1997 until present [*McClain*, 2009; *Boyce et al.*, 2010].

In contrary to *Boyce et al.* [2010], *Dave and Lozier* [2013] found no significant trend in global chlorophyll *a* in measurements from 1997 until 2010. Furthermore, their previous studies [*Dave and Lozier*, 2010; *Lozier et al.*, 2011] confuted the hypothesis of the negative correlation of ocean stratification and chlorophyll *a* content on interannual time scales especially in the oligotrophic parts of the ocean. Nevertheless, the length of the remotely measured chlorophyll *a* time series is still insufficient to permit an analysis of long-term variability. Within the scope of the two contradictory studies by *Boyce et al.* [2010] and *Dave and Lozier* [2013], it is necessary to devise a new approach for deriving a chlorophyll *a* time series for a time period long enough detecting long-term trends and variability.

Here we present a method to reconstruct the chlorophyll *a* distribution of several past decades. The Madeira Basin, in the North Atlantic Subtropical Gyre (NAST),

was deemed appropriate as the study area because a continuous record of temperature measurements at the mooring site Kiel 276 (33°N, 22°W) has documented a clear temperature increase within the thermocline since 1980 [*Fründt et al.*, 2013]. Although chlorophyll *a* has been sparsely measured in this region (Fig. 4.1), the results of our method will provide an understanding of the consequences of altered environmental conditions for primary production.

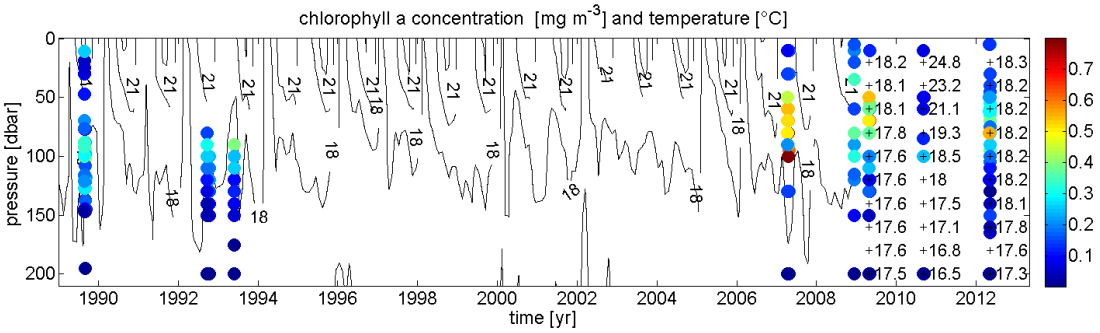

Figure 4.1: *In-situ* measurements of chlorophyll *a* (1989 - 2012, coloured circles and colour bar) in the Azores Frontal Region (29° – 38.5°N, 17° – 27°W). Isotherms [15, 18, 21, and 24 °C] from the SODA POP temperature field are shown from 1989 to 2008. Between 2009 and 2012, because no SODA POP data are available, temperature was obtained by CTDs (crosses).

4.3 Material and Methods

4.3.1 Data

To reconstruct the chlorophyll *a* field, a correlation of *in-situ* temperature and nitrate measurements was adapted to a modeled temperature field, yielding a nitrate field. Additional *in-situ* chlorophyll *a* data were related to both temperature and nitrate, and their respective fields were used to calculate the chlorophyll *a* field.

Given the relatively few measurements of chlorophyll *a* directly at the position of mooring site (33°N, 22°W), the data set was enlarged with measurements from the Azores Frontal Region (29° – 38.5°N, and 17° – 27°W, *Fründt and Waniek* [2012]) (Fig. 4.1). This also served to reduce the effects of patchiness. *In-situ* measurements were taken from different cruises within the Madeira Basin, and from data sets of the Pangaea database (http://www.pangaea.de/, tab. 4.1).

Table 4.1: Cruises in the Azores Frontal Region (AFR) and number of *in-situ* measurements of nitrate, when temperature data were available, and of chlorophyll *a* (CHL), when temperature and nitrate data were available. Both were used to calculate chlorophyll *a* on 33°N, 22°W, [1)] provided at http://www.geomar.de/en/centre/central-facilities/wasser/f-s-poseidon/.

cruise / station number	ship	time of sampling in AFR	data points of nitrate(T)	data points of CHL (T,N)	reference
NAPP89-1	RV Tyro	28.08. – 07.09.1989	111	47	*Rommets et al.* [1991a]
NAPP90-1	RV Tyro	28.04 – 10.05.1990	111	47	*Rommets et al.* [1991b]
HUD92/37	Hudson	24.09 – 12.10.1992	96	25	*Irwin* [2000]
HUD93/2	Hudson	29.05 – 30.05.1993	60	19	*Irwin* [2000]
M36/2	Meteor (1986)	23.06. – 01.07.1996	165	156	*Mienert et al.* [1998]
P349	Poseidon	09.04 – 22.04.2007	214	83	*Fründt and Waniek* [2012]
P377	Poseidon	08.12. – 13.12.2008	58	38	Waniek et al., cruise report, unpubl.
P383	Poseidon	22.04. – 02.05.2009	94	41	Waniek et al., cruise report, unpubl.
P404	Poseidon	03.09 – 08.09.2010	74	40	Waniek et al., cruise report [1)]
P432	Poseidon	03.05. – 10.05.2012	210	73	Krüger et al., cruise report [1)]

In-situ measurements taken near islands were removed from the application because these regions are affected by upwelling at the subsurface island slopes.

Temperature *in-situ* measurements of the Poseidon cruises were taken from calibrated CTD (Seabird 911) casts. Nitrate concentrations were measured using an autoanalyzer (EVOLUTION III, Alliance Instruments) according to standard methods [*Grasshoff et al.*, 1999]. The chlorophyll *a* concentration was determined with a fluorometer (TURNER 10-AU, Gamma Analysen Technik GmbH) calibrated after the *JGOFS* [1994] protocol.

The modeled temperature field was the output of the simple ocean data assimilation parallel ocean program (SODA POP) [*Carton et al.*, 2005; *Carton and Giese*, 2008] version 2.1.6 for 33.2°N, 22.2°W (available at http://apdrc.soest.hawaii.edu/datadoc/soda_2.1.6.php).

For validation, satellite chlorophyll *a* measurements in the Madeira Basin, made by SeaWiFS with an 8-day resolution between August 29, 1997 and December 18, 2010, were used. The data set is freely available at http://gdata1.sci.gsfc.nasa.gov/daac-bin/G3/gui.cgi?instance_id=ocean_8day.

The impact of atmospheric long-term changes is discussed using the winter North Atlantic Oscillation (NAO) index from December to March (freely available on https://climatedataguide.ucar.edu/, *Hurrell* [1995]).

Figure 4.2 (following page): Schema of the method to calculate the past chlorophyll *a* distribution. In the first step, assumptions are established and the data sets are prepared. In the second step, the nitrate field $g_1(t,z)$ is calculated using the fitting function $f_1(T)$. a) *In-situ* nitrate measurements with respect to temperature (blue stars) and the fitting function f_1 (red line). For error estimation, the lower and upper envelopes (red dashed lines) are given. b) The calculated nitrate field g_1 = Nitrate(t,z) in the upper 400 m from 1989 to 2008. In the third step, the chlorophyll *a* field $g_2(t,z)$ is calculated using the fitting function $f_2(T,N)$ and the euphotic depth $Z_{eu}(t)$. c) *In-situ* measurements of chlorophyll *a* with respect to temperature and nitrate (blue circles) and the linear surface fit f_2. d) The resulting vertically resolved past chlorophyll *a* field $g_2(t,z)$ in the upper 200 m from 1989 to 2008.

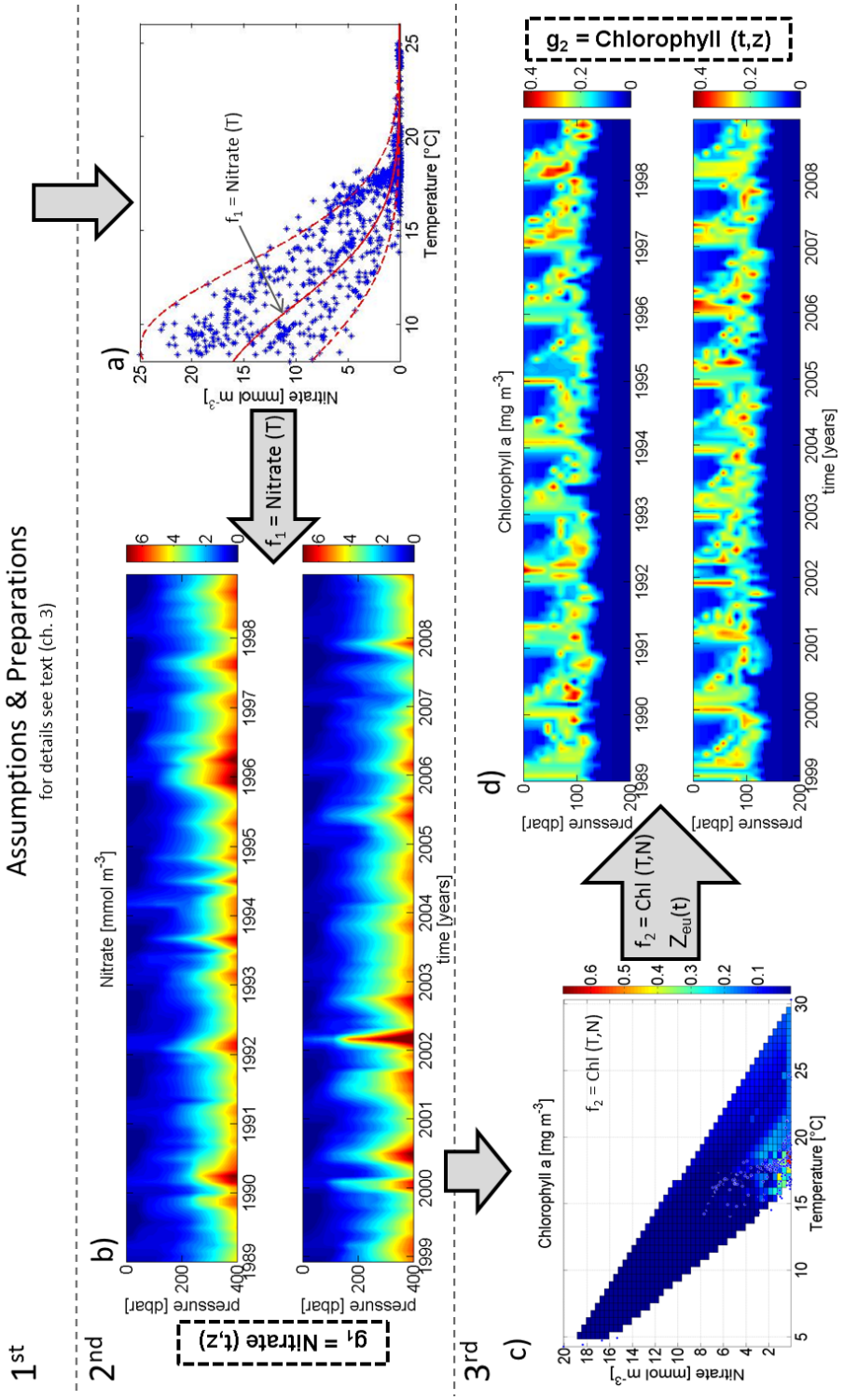

4.3.2 Methods

The euphotic depth was either derived from the Secchi depth or calculated using the exponential law of light attenuation [*Kirk*, 2011]. In our case, the depth of the euphotic layer varied between 93 m (Secchi depth) and 153 m (calculated after *Kirk* [2011]), depending on the integrated chlorophyll *a* content in the overlying water column:

$$Z_{eu}(CHL_{int})[m] = -1.7\ m^3\ mg^{-1} \cdot CHL_{int}\ [mg\ m^{-2}] + 160\ m \tag{4.1}$$

with CHL_{int} the vertical integrated chlorophyll *a* concentration.

Three steps were required to determine the past chlorophyll *a* field (Fig. 4.2): In the first, it was assumed that primary production in the Madeira Basin is nitrate-limited [*Mills et al.*, 2004], and no distinction between different phytoplankton species was made. The correlation between temperature, nitrate, and chlorophyll *a* was considered as conservative, i.e., at a given temperature and nitrate concentration, the chlorophyll *a* concentration was the same over time. For the temperature field, data from SODA POP at the position of Kiel 276 were extracted and the minimum and maximum euphotic depths were determined by Secchi depths or by calculation after the method of *Kirk* [2011]. In the second step, *in-situ* nitrate measurements were fitted to the temperature values after the removal of outliers (Fig. 4.2a), yielding the Gaussian first-order equation:

$$f_1 = Nitrate(T) = 17.01 \cdot exp(-((T - 6.45)/6.36)^2) \tag{4.2}$$

with $R^2 = 0.72$. For error estimation, two additional fits were calculated with the enveloping data points (Fig. 4.2a). Equation 4.2 was applied to each point of the temperature field resulting in a nitrate field (Fig. 4.2b).

In the third step, the chlorophyll *a* concentrations measured *in-situ* were surface-fitted to both temperature and nitrate (Fig. 4.2c). A piecewise linear surface interpolation (MATLAB, fittype *linearinterp*) was used, yielding the interpolant f_2 = CHL(T,N). Next, the temperature and nitrate fields were applied to f_2, resulting in a first chlorophyll *a* field. The euphotic depth $Z_{eu}(t)$ was calculated for each time step and used to remove the overshooting of chlorophyll *a* at higher depths because of the increase in nitrate. By applying $Z_{eu}(t)$ to the first chlorophyll *a* field, we obtained the final chlorophyll *a* field

(Fig. 4.2d).

To determine the skill factor of the method, the Nash-Sutcliffe coefficient of efficiency (E) [*Nash and Sutcliffe*, 1970; *Legates and Mc Cabe Jr.*, 1999] was calculated. Because the time series of the calculated chlorophyll *a* was not normally distributed, the data were first log-transformed and standardised. E was then calculated as:

$$E = 1 - \frac{\sum_i (S_i - M_i)^2}{\sum_i (S_i - \bar{S})^2} \tag{4.3}$$

where S is the satellite-measured data, $\bar{S}$ the mean of S, and M the chlorophyll *a* data calculated with our method. An efficiency of 1 (E = 1) corresponds to a perfect match between the calculated and the remotely measured data. An efficiency of 0 (E = 0) indicates that the variance of the calculated chlorophyll *a* is of the same size as the variance of the remotely measured data. Equation 4.3 is identical with the Brier-based skill score [*Livezey*, 1995].

For discussion, the chlorophyll *a* field is standardised, resulting in a zero mean value and unit variance for each depth. To examine the dominant patterns of the resulting chlorophyll *a* field, empirical orthogonal function (EOF) analysis is calculated with annual mean profiles [*Storch and Zwiers*, 2003]. Identifying the periods on which the time coefficients behave concurrent to the NAO, wavelet coherences and phase differences were calculated by applying a complex Morlet wavelet ($\omega_0 = 6$) as mother-wavelet [*Torrence and Compo*, 1998; *Grinsted et al.*, 2004].

4.4 Results

The method was applied to calculate a chlorophyll *a* field from 1980 to 2008, the same time period, in which *in-situ* measurements from the mooring site Kiel 276 demonstrate a marked temperature increase especially in the last decade [*Fründt et al.*, 2013].

The signal was dominated by the phytoplankton bloom from approximately December to March and was confined to the bottom of the euphotic layer until the new bloom developed (Fig. 4.3a), reproducing the deep chlorophyll maximum (DCM), with a mean depth of 70 ± 40 m.

For validation, the calculated surface chlorophyll *a* was compared to satellite-based chlorophyll *a* measurements (Fig. 4.4). The mean surface chlorophyll *a* concentra-

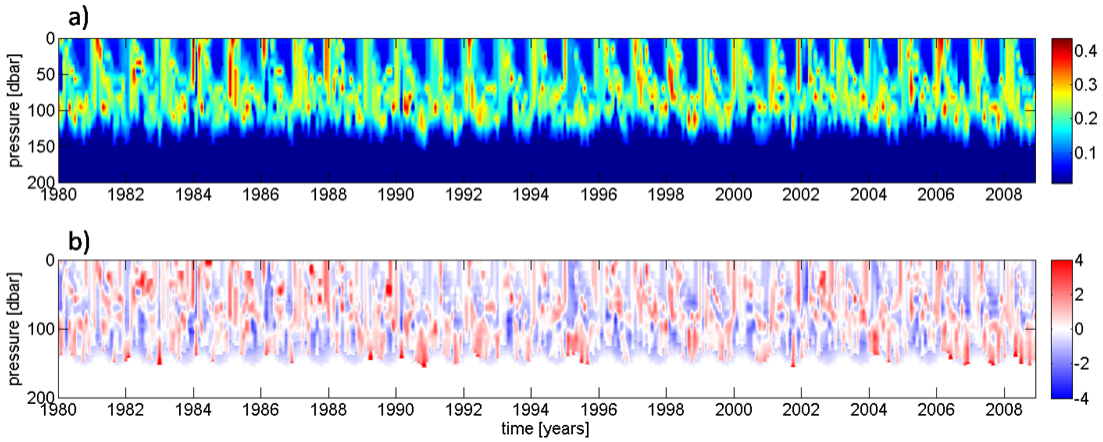

Figure 4.3: a) The calculated chlorophyll *a* field [mg m^{-3}] and b) the standardised chlorophyll *a* field from 1980 to 2008. Note that the standardised chlorophyll *a* field has no units.

tion (0.14 ± 0.09 mg m^{-3}) was similar to that determined by satellite measurements (0.12 ± 0.06 mg m^{-3}). The calculated chlorophyll *a* reproduced the beginning and the end of the phytoplankton bloom but did not exactly match the inter-annual variability.

The Nash-Sutcliffe coefficient of efficiency [*Nash and Sutcliffe*, 1970; *Legates and Mc Cabe Jr.*, 1999] resulted in a value of E = 0.3 indicating the method's relatively high capacity to reconstruct the seasonal to long-term variability of the chlorophyll *a* field, since 30 % of the natural variability was explained by the calculated chlorophyll *a* data.

The distinct DCM was found nearly all year and extended within the water column over a depth of roughly 50 m around a mean depth of approximately 100 m. The chlorophyll *a* concentration is typically low in the oligotrophic regions, with values of 0.2 – 0.3 mg m^{-3}. Single events, lasting one to two months, showed enhanced values of up to 0.45 mg m^{-3}. This intensification mostly occurred within the DCM spanning only few metres. In some years like 1984, 1985, and 1988, strong phytoplankton growth events spanned nearly the entire euphotic zone (Fig. 4.3a).

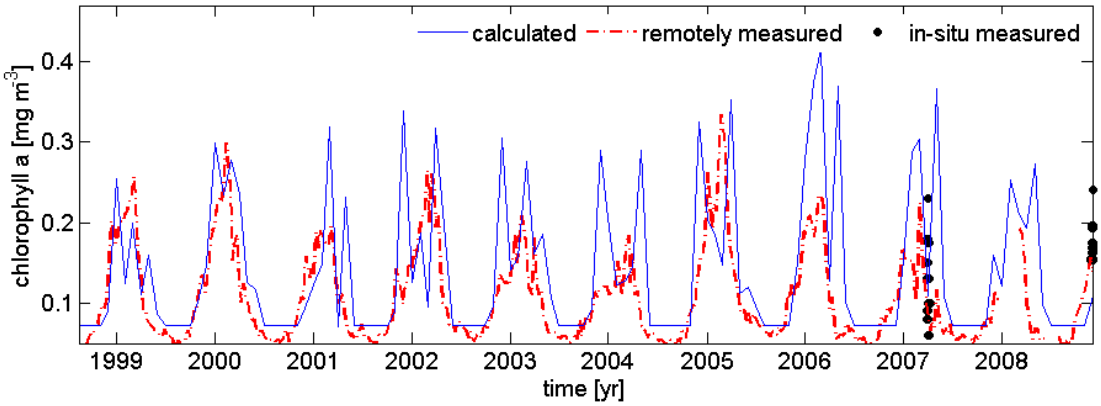

Figure 4.4: Validation of the calculated chlorophyll *a* concentration (solid blue line) using the surface chlorophyll *a* concentration measured remotely (dash-dot red line). *In-situ* (black circles) measured surface chlorophyll *a* is also given.

Because the chlorophyll *a* field holds a high seasonal variability, it was standardised with a mean annual field (Fig. 4.3b). This approach arose the opportunity for detecting variability of chlorophyll *a* concentrations differing from the mean annual cycle. The standardised chlorophyll *a* field was then used to calculate the EOFs and their time coefficients (Fig. 4.5). The first EOF explains 55.5 % and the second EOF 14.2 % of the variability. The time coefficients of both EOFs show a high interannual variability (Fig. 4.5b).

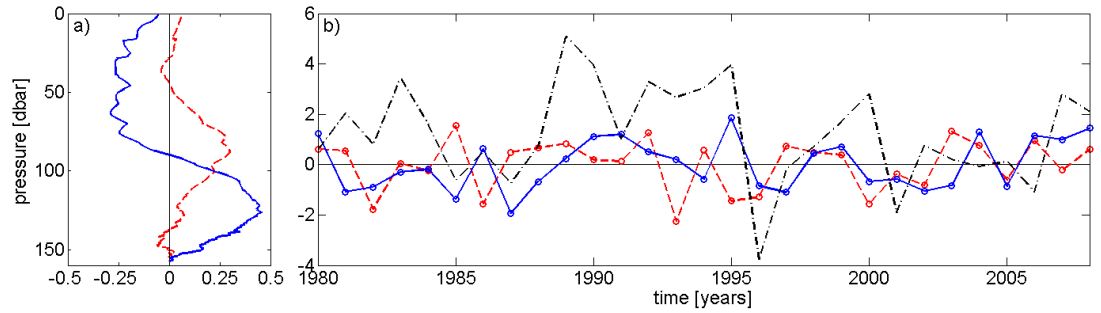

Figure 4.5: a) The first (blue line) and second EOF (red dotted line) and b) the time coefficients of the first EOF (blue line and circles) and second EOF (red dotted line and circles). Note that due to calculation with the standardised chlorophyll *a* field, they have no units. Additionally, the winter NAO-index is given (black dash-dotted line).

4.5 Discussion

The first and second EOF, together explaining nearly 70 % of the variability of the chlorophyll *a* field, emphasise the DCM as dominant pattern of the chlorophyll *a* field (Fig. 4.5a). Therefore, understanding the interannual variability of the DCM is highly important for an understanding of the chlorophyll *a* evolution in the entire euphotic zone. Pronounced DCMs were found at the begin of the time series 1982/83, from 1989 to 1991, 1995, and at the end of the time series from 2006 to 2008 (Fig. 4.3b). The same periods are characterised by positive NAO indices (Fig. 4.5b). Less distinct DCMs can be recognised in 1985, 1997/98, and 2003/04 where the NAO index is negative or around zero (Fig. 4.5b). This relationship between the DCM and the NAO is manifested in a significant correlation coefficient of the time coefficient of the first EOF and the winter NAO-index with 0.37 ($p < 0.05$). The wavelet coherences between the time coefficient of the first EOF and the NAO show the high correlation between these two time series at periods between 4 – 6 years with a curling phase difference of 270° in the 1980s to no phase difference in the 2000s (Fig. 4.6). This range of periods was previously reported by *Higuchi et al.* [1999] to be one of the dominant of the NAO. A correlation of the NAO on the same periods with no time lag was previously found with the currents directions in the permanent thermocline in the Madeira Basin [*Fründt et al.*, 2013]. The initial phase difference of 270° would correspond to a leading of the chlorophyll *a* concentration to the NAO by about one year. The coherences were calculated by using annual mean values of the time coefficient of the first EOF as well as the annual winter NAO-index (Fig. 4.6). The time lag in the 1980s seems to be biased by averaging, supposing a direct response with zero time lag for the 1980s, too.

The NAO as dominant atmospheric pattern over the North Atlantic has high influence on the lateral wind field even in the horse latitudes where the study area is located [*Marshall et al.*, 2001; *Fründt and Waniek*, 2012]. Changes in the wind speed intensities cause different depths of the upper mixed layer which is correlated with the amount of nutrient supply into the euphotic zone and new production. The approximate zero time lag between the NAO and chlorophyll *a* concentration indicates that the primary production is sensitive to wind induced changes of nutrient supply in the subsequent bloom.

An overlying long-term trend of the chlorophyll *a* concentration could not be de-

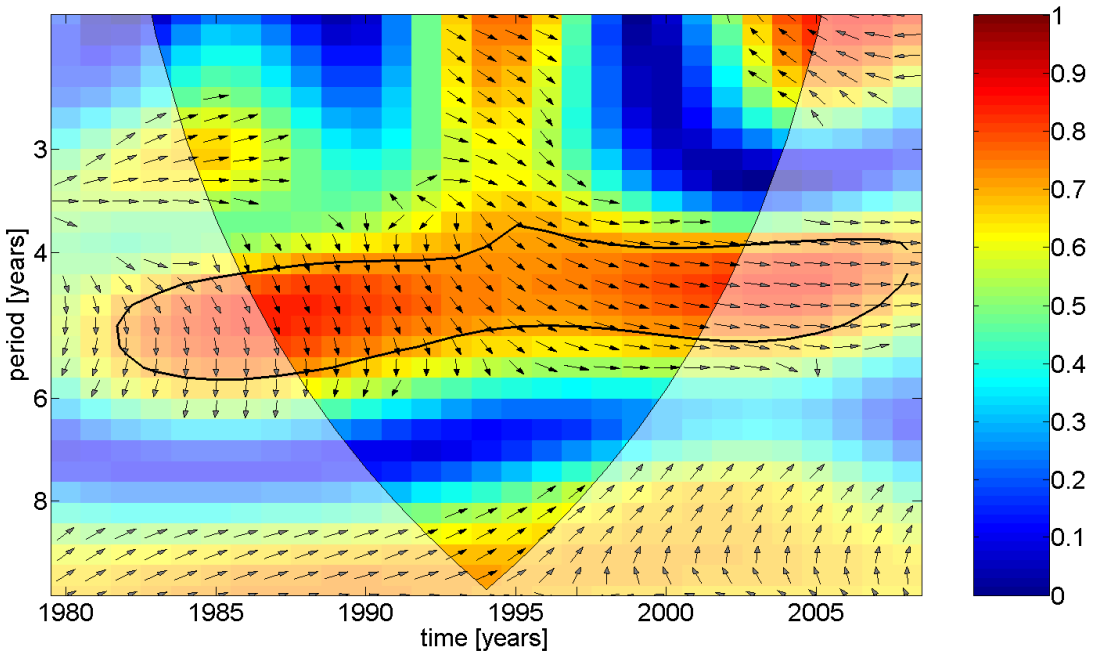

Figure 4.6: Wavelet coherence and phase between the winter NAO index and the time coefficient of the first EOF. Areas bordered by the black solid lines are within the 95 % confidence level using the red noise model. The arrows indicate the phase difference (0° is given by a horizontal arrow pointing to the right and a arrow pointing vertically upwards means the time coefficient lags the NAO by 90°). The U-shaped curve shows limits of the cone of influence (COI). All signals outside COI are statistically not certain.

tected within the studied time period. In the Madeira Basin, a temperature increase of 1.4 K was measured in 240 m between 1980 and 2008 [*Fründt et al.*, 2013]. Increasing ocean temperatures are predicted to cause a higher stratification which prevents nutrient input from below the euphotic zone leading to a decrease in phytoplankton growth [e.g. *Bopp et al.*, 2001; *Sarmiento et al.*, 2004; *Polovina et al.*, 2008; *Irwin and Oliver*, 2009]. However, the warming trend in 240 m is higher than reported trends in sea surface temperature [*Denman et al.*, 2007] which would rather lead to destratification than enhanced stratification. *Dave and Lozier* [2013] found the same trend of faster warming of the deeper levels than the surface. Therefore, our study can neither verify the hypothesis of decreasing phytoplankton productivity with increasing stratification nor the results by *Lozier et al.* [2011] and *Dave and Lozier* [2013] who reported no correlation of stratification and primary production on interannual time scales, because the

in-situ measured time series of temperature in 240 m does not allow to make estimations of the stratification variability on interannual time scales. In our study, no correlation between long-term temperature trends and chlorophyll *a* concentration was found. A change in species composition due to rising temperatures was found in the Northeast Atlantic as well as the North and Baltic Sea [*Beaugrand et al.*, 2002; *Daufresne et al.*, 2009]. However, the introduced method cannot distinguish between different phytoplankton species and therefore the influence of rising temperatures on species size and composition cannot be determined.

The observed period is characterised by a predominantly positive NAO as well as Atlantic Multidecadal Oscillation (AMO) gradient after the regime shift 1976–81 [*Graham*, 1994; *Trenberth and Hurrell*, 1994]. Further studies are necessary to determine if the correlation between NAO and chlorophyll *a* concentration resists even in a state of decreasing AMO.

Regarding the standardised chlorophyll *a* field (Fig. 4.3b), the phytoplankton concentration seems to be higher in the 1980s and the 2000s than in the 1990s. This probable variability with a period of approximately twenty years is too long to make any statistic significant statements especially in relation to low frequency climate indices yet. Further studies will focus on the multidecadal variability of primary production and probable forcing mechanisms by the atmosphere and the ocean in the subtropical Northeast Atlantic over the entire last century, especially emphasising the impact of the beginning of global warming in the last decades.

4.6 Conclusion

We introduced a method to reconstruct the chlorophyll *a* distribution of past decades based on occasional *in-situ* measurements of temperature, nitrate, and chlorophyll *a*. It is applicable as a simple technique with low computational cost. Although in this work the chosen study area was the Madeira Basin, the method can be adapted to other regions of the global ocean as long as *in-situ* data enabling the analysis of short- and long-term variability of primary production are available.

By utilizing full-length modeled data sets (e.g., SODA POP 1871 – 2008), our method allows primary production to be studied in the context of low-frequency climate indices or 20th-century temperature changes, particularly as a comparison between the era be-

fore and during the warming currently taking place in wide areas of the global ocean. This will extend the results of the interannual influence of the NAO found in this study by a focus on the multidecadal variability.

Moreover, an estimation of carbon uptake related to primary production can be extended to large oceanic regions. Application of the method described herein will provide essential information on the long-term variability of carbon uptake as response to changing climate conditions.

4.7 Acknowledgments

The authors thank all colleagues involved in obtaining the *in-situ* measurements since 1989, the crews and masters of the research vessels. The *in-situ* measurements of temperature and nitrate are available at the Pangaea database (http://www.pangaea.de/). The SODA-POP temperature data are available on http://apdrc.soest.hawaii.edu/datadoc/soda_2.1.6.php. This work is financially supported by DFG (Contract number WA2157/5-1).

5 Chlorophyll *a* reconstruction from *in-situ* measurements, Part II: Marked carbon uptake decrease in the last century

Fründt, B., Dippner, J. W., Schulz-Bull, D. E., and Waniek, J. J. published 2015 in Journal of Geophysical Research: Biogeosciences 120, 246-253.

5.1 Abstract

A calculated chlorophyll *a* field in the Madeira Basin from 1871 to 2008 was used to analyse the long-term variability in the oligotrophic, subtropical gyres in relation to the climate change of the last century. The deep chlorophyll maximum (DCM), as dominant pattern of the chlorophyll *a* field, showed a fast decrease in its strength in the 1940s. An absolute minimum was reached between 1967 and 1973 when no DCM established with a recovering to the end of the time series. Long-term variability of the DCM was related to the North Atlantic Oscillation with a time delay of 9 years. The marked decrease in the 1940s was correlated to the decrease in the solar radiation in transition from early brightening to global dimming. Caused by the influence of the solar radiation and maybe related to increasing global temperatures in the last century, the integrated chlorophyll *a* concentration decreased by about 0.7 mg m^{-2} in 2008 compared to 1871. The high resolved chlorophyll *a* field allows an estimation of the carbon uptake by the ocean due to primary production in the euphotic zone. A rough calculation over the area of the global subtropical oceans shows 700 Mt less carbon uptake in 2008.

5.2 Introduction

Marine primary production by phytoplankton plays a key role in the global carbon uptake and is therefore an important factor influencing the global climate [*Charlson et al.*, 1987; *Murtugudde et al.*, 2002; *Boyce et al.*, 2012]. Nearly half of the planetary primary production takes place in the euphotic zone, the uppermost water column of the global oceans [*Behrenfeld et al.*, 2006; *Boyce et al.*, 2010]. A large amount of carbon is subsequently transferred into the deep oceans, stored in sediments and removed from the atmosphere [*Field et al.*, 1998; *Denman et al.*, 2007; *Schwab et al.*, 2012].

The subtropical oceans spread up to 40 % of the planetary surface and their ecosystems contribute to 25 % of the global primary production [*Longhurst et al.*, 1995; *Polovina et al.*, 2008; *Schwab et al.*, 2012]. To estimate the primary production of the water column, measurements of chlorophyll *a* concentrations are commonly used as a proxy for the phytoplankton biomass [*Cullen*, 1982; *Uitz et al.*, 2006]. In the subtropical oceans, most of the primary production takes place near the surface during the bloom in late winter and early spring as an answer to enhanced wind mixing causing new nutrient import from beneath the nitracline which is deeper than 100 m in this regions [*Cullen*, 1982]. After depletion of nutrients at the surface, the phytoplankton descends to the edge of the euphotic zone in approximately 80 – 100 m water depth and forms the deep chlorophyll maximum (DCM) [*Teira et al.*, 2005]. The formation of the DCM depends on two main factors: the transport of nutrients upwards through the nutricline by turbulent diffusion as well as the amount of light from above [*Hodges and Rudnick*, 2004]. Therefore, the upper and lower boundary of the DCM are found between the lowest required concentration of nutrients and the deeper edge of the euphotic zone. Due to formation of the DCM, considerable carbon uptake takes place in the subtropical gyres even in summer and autumn whilst the surface chlorophyll *a* is depleted. This important contribution to the global carbon pump results in 50 % of the global ocean carbon export to the deep oceans and sediments within the subtropical gyres [*Schwab et al.*, 2012].

The sensitivity of phytoplankton growth to long-term changes in nutrient and light supply is still not understood and needs to be investigated for robust projections of the carbon export by the oceans in changing environments in the 21st century due to global temperature increase. To approach this task, we present an analysis of the long-term variability of the DCM using a chlorophyll *a* field in the Madeira Basin for more than

100 hundred years to identify the forcing mechanisms of primary production in low-light conditions like found in the DCM.

Besides the recorded variability of sea surface temperature in the last century [*Levitus et al.*, 2005; *Denman et al.*, 2007; *Levitus et al.*, 2009], the strength of solar radiation is also subject to high multidecadal variability [*Ohmura*, 2006; *Wild*, 2009] and may influence the strength of the DCM. In context of evaluated decrease of primary production in the last century due to global warming [*Behrenfeld et al.*, 2006; *Martinez et al.*, 2009; *Boyce et al.*, 2010], an estimation of the carbon export in the subtropical gyres over more than one century aims to determine the possible effects of global climate change.

5.3 Material and Methods

Due to a lack of continuous *in-situ* measurements of the DCM in the subtropical regions, we applied a method to reconstruct a chlorophyll *a* field in the Madeira Basin in the north eastern part of the oligotrophic North Atlantic Subtropical Gyre from 1871 – 2008 (Fig. 5.1). This method uses *in-situ* measurements of temperature and nitrate and their correlation is adapted to a modeled temperature field resulting in a nitrate field. In a next step, *in-situ* chlorophyll *a* measurements were fitted to both, *in-situ* temperature and nitrate measurements and this relation is finally used to calculate the chlorophyll *a* field. The *in-situ* measurements were taken from the Azores Frontal Region (29° – 38.5°N, and 17° – 27°W, *Fründt and Waniek* [2012]), a part of the Madeira Basin. The method and the *in-situ* measurements are described in detail in chapter 4 [*Fründt et al.*, 2015b]. As required modeled temperature field, we used the output of the simple ocean data assimilation parallel ocean program (SODA POP) [*Carton et al.*, 2005; *Carton and Giese*, 2008], version 2.1.6 in its entire length from 1871 to 2008, resulting in a chlorophyll *a* field of the same length (Fig. 5.1).

Empirical orthogonal function (EOF) analysis [*Storch and Zwiers*, 2003] was performed using annual mean profiles of the standardised chlorophyll *a* concentration. Furthermore, wavelet coherences and phase differences were computed by applying the complex Morlet wavelet ($\omega_0 = 6$) as mother wavelet to determine the periods on which two time series behave synchronously [*Torrence and Compo*, 1998; *Grinsted et al.*, 2004].

The impact of the dominant large-scale atmospheric patterns was determined by using

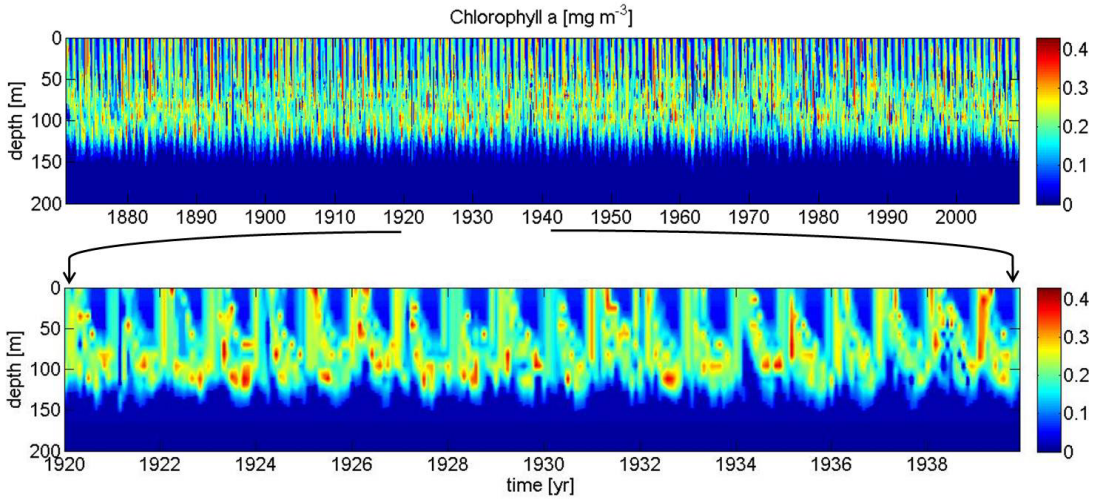

Figure 5.1: a) The calculated chlorophyll *a* field from 1871 to 2008 in the Madeira Basin. b) The calculated chlorophyll *a* field is shown from 1920 to 1939 indicating the transition from the strong DCM in the 1920s to the weaker DCM in the late 1930s.

the winter North Atlantic Oscillation (NAO) index from December to March [*Hurrell*, 1995]. Analogous analyses were done with further modes in the Atlantic: the Atlantic Multidecadal Oscillation (AMO, *Enfield et al.* [2001]), the Arctic Oscillation (AO, *Higgins et al.* [2000]), the Atlantic Meridional Mode (AMM, *Chiang and Vimont* [2004]), and the East Atlantic Pattern (EAP, *Wallace and Gutzler* [1981]). To determine the impact of global teleconnections, additionally the Pacific Decadal Oscillation (PDO, *Trenberth and Hurrell* [1994]), and the El Niño Southern Oscillation (ENSO, *Bradley et al.* [1987]) indices were used.

As solar radiation flux at surface, the data provided by NOAA-CIRES 20th Century Reanalysis Version II were used in the Azores Frontal Region from 1871 to 2008 [*Compo et al.*, 2004]. A mean value from August to November for each year and, enhancing the multidecadal variability of the time series [*Gulev et al.*, 2013], a running mean over ten years is calculated (Fig. 5.5). The same filtering method is applied to the chlorophyll *a* field.

The time series of chlorophyll *a* content over more than the 20th century allows estimation of the change in carbon uptake by the oceans due to changes in the amount of primary production. The difference in carbon uptake (ΔCU) in the subtropical gyres between 2008 and 1871 is calculated using

$$\Delta CU = \Delta_{CHL} \cdot R \cdot A \cdot \mu \tag{5.1}$$

with Δ_{CHL} the difference in integrated chlorophyll *a* content of the water column from surface to 465 m depth between 2008 and 1871, R = $carbon/chl\ a$ = 50 as a weighted mean between the ratio of 25 in DCMs [*Eppley*, 1968; *Cullen*, 1982] lasting all year and of 150 – 250 near the surface [*Beers et al.*, 1975; *Cullen*, 1982] contributing only during the bloom, the area of the subtropical gyres A = $2.04 \cdot 10^8$ km^2 [*Polovina et al.*, 2008] and the growth rate of phytoplankton μ = 0.26 day^{-1} in the North Atlantic Subtropical Gyre [*Maranón*, 2005]. This growth rate based on measurements of the photosynthesis rate per unit chlorophyll *a* all year and represents therefore an annual mean value over all phytoplankton species.

5.4 Results

In the second half of the year, between August and November, the DCM in a depth of about 90 to 130 m is most distinct with values typical for the oligotrophic waters in the North Atlantic Subtropical Gyre of 0.25 – 0.3 mg m^{-3} (Fig. 5.2a). Contrary to the surface, where chlorophyll *a* is completely depleted after the bloom due to exhausted nutrients, low chlorophyll *a* concentrations in the DCM are still found between December and July in most of the years.

Table 5.1: Mean chlorophyll *a* concentrations in the DCM (90 – 130 m) (CHL$_{DCM}$) from August to November for selected time periods.

time period	CHL$_{DCM}$ [mg m^{-3}]
1920 – 1939	0.20 ± 0.04
1940 – 1966	0.183 ± 0.025
1967 – 1973	0.15 ± 0.05
1974 – 2008	0.18 ± 0.04

Besides the interannual variability, the time series of 138 years of chlorophyll *a* concentration reveals a variability of the strength of the DCM on time scales of several decades (Fig. 5.2b). Beginning in the 19th century, the chlorophyll *a* concentration

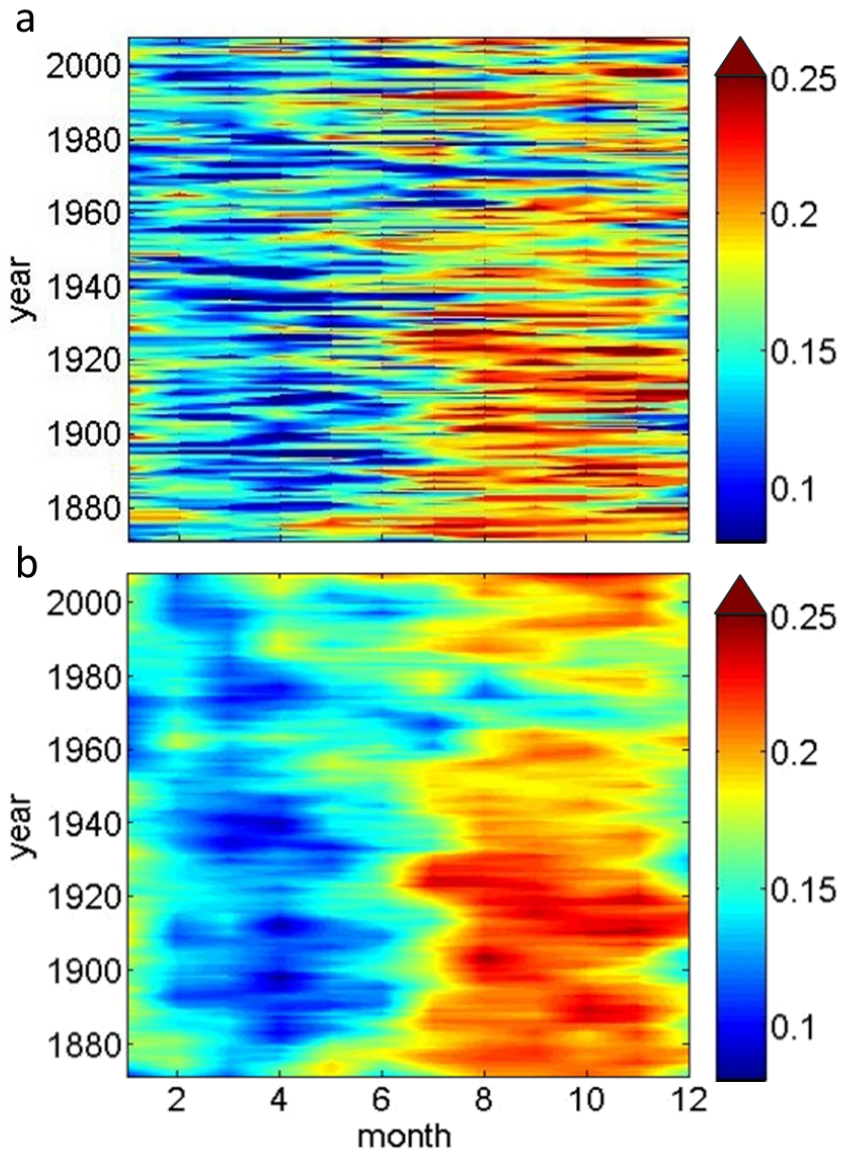

Figure 5.2: Hovmöller diagram of the mean chlorophyll *a* concentration [mg m^{-3}] between 90 and 130 m from 1871 to 2008 at depths of the DCM: a) shows the unfiltered annual values and b) a running mean over ten years.

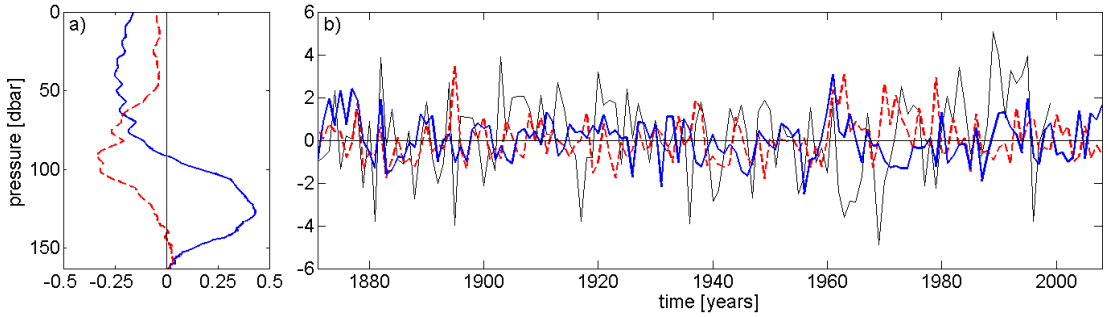

Figure 5.3: a) The first (blue line) and second EOF (red dashed line) and b) the time coefficients of the first EOF (blue line) and second EOF (red dashed line). Note that due to calculation with the standardised chlorophyll *a* field, they have no units. Additionally, the winter NAO-index (black line) with a time lag of 9 years is given.

continuously increases until the 1930s where a marked DCM lasts over 4 months. Afterwards, the chlorophyll *a* concentration rapidly decreases from the 1940s until the 1960s. In these more than 20 years, the chlorophyll *a* values remain nearly constant on the lowest level since 1871. A further decrease of the chlorophyll *a* concentration leads to the absolute minimum between 1967 and 1973 when no DCM is established, which holds for the entire upper 100 m. This exceptional situation is followed by a steady intensification until the last years of our time series. However, the chlorophyll *a* concentration does not reach the high values from the 1920s to 1930s.

The DCM as dominant pattern of the chlorophyll *a* field over the entire time period is manifested in the first, explaining 45.4 %, and second EOF, explaining 19.3 % (Fig. 5.3a,b). The integrated chlorophyll *a* content of our time series (mean value 24 $\pm$ 5 mg m^{-2}) shows a decrease (Δ_{CHL} = -0.72 mg m^{-2}) from 1871 to 2008.

5.5 Discussion

5.5.1 Long-term variability of the DCM

A correlation between the DCM and the NAO on a period of roughly 5 years was shown in chapter 4 with a shorter time series from 1980 to 2008, by applying EOF analysis. Application of the wavelet coherence between the time coefficient of the first EOF (Fig. 5.3b) and the NAO shows that the relationship between NAO and the DCM found

between 1980 and 2008 is less contributed to the long-term variability of the DCM since this relationship has not been established before the 1980s (Fig. 5.4). This is maybe linked to the regime shift 1976 – 1981 when the Atlantic Multidecadal Oscillation (AMO) as well as the NAO changed from a negative to a more positive trend related with a change from a colder to warmer period associated with variations in the wind field over the North Atlantic [*Kerr*, 2000; *Dima and Lohmann*, 2007; *Dippner et al.*, 2012] influencing mixed layer depths and nutrient supply into the euphotic zone from below. On periods in range of several years, no continuous relationship over the entire time series can be identified. On decadal scale, the DCM is significantly correlated with the NAO since 1910 on periods of 30 – 40 years with a consistent phase difference of 90°, i.e., a time lag of approximately 7 to 10 years (Fig. 5.4). The calculation of the correlation coefficients ρ between the NAO and the time coefficient of the first EOF shows significant results at a time lag of 0 years ($\rho = 0.17$, p = 0.041) and of 9 years ($\rho = 0.21$, p = 0.016, Fig. 5.3b) which corresponds to the phase difference as seen in the wavelet coherence. The direct correlation with NAO, i.e. no time lag, is diminished compared to the value found in chapter 4 when only the last 28 years were regarded, because a continuous correlation over the entire length was not found. The time lag of 9 years may be related to the transmission of NAO induced oceanic signals by slow Rossby waves with speeds of around 1 cm s^{-1} as reported by *Cipollini et al.* [1997].

Regarding the rapid decrease of the chlorophyll *a* concentration in the 1940s (Fig. 5.2), the NAO seems not to be the dominant forcing mechanism. Even though the NAO is in a predominantly negative phase from the 1940s to the 1960s (Fig. 5.3b), the negative trend of the NAO is not strong enough to explain the sudden decline in chlorophyll *a* concentration in the DCM. The analogous correlation analyses of the DCM with the further climate indices (AMO, AO, AMM, EAP, EAP, PDO, and ENSO) gave no significant results considering phase differences. Potentially, the regime shift in the North Atlantic 1957/58 with impact on the sea surface temperatures in the mid latitudes [*Yasunaka and Hanawa*, 2002] supports the decline in the strength of the DCM. However, the influence of this regime shift on the phytoplankton community in the subtropical regions is not studied yet.

Besides the hydrographic and atmospheric influences effecting the amount of nutrient supply into the DCM, its formation depends highly on the incoming solar radiation (Fig. 5.5). The planetary increase of the solar radiation in the first half of the 20th century,

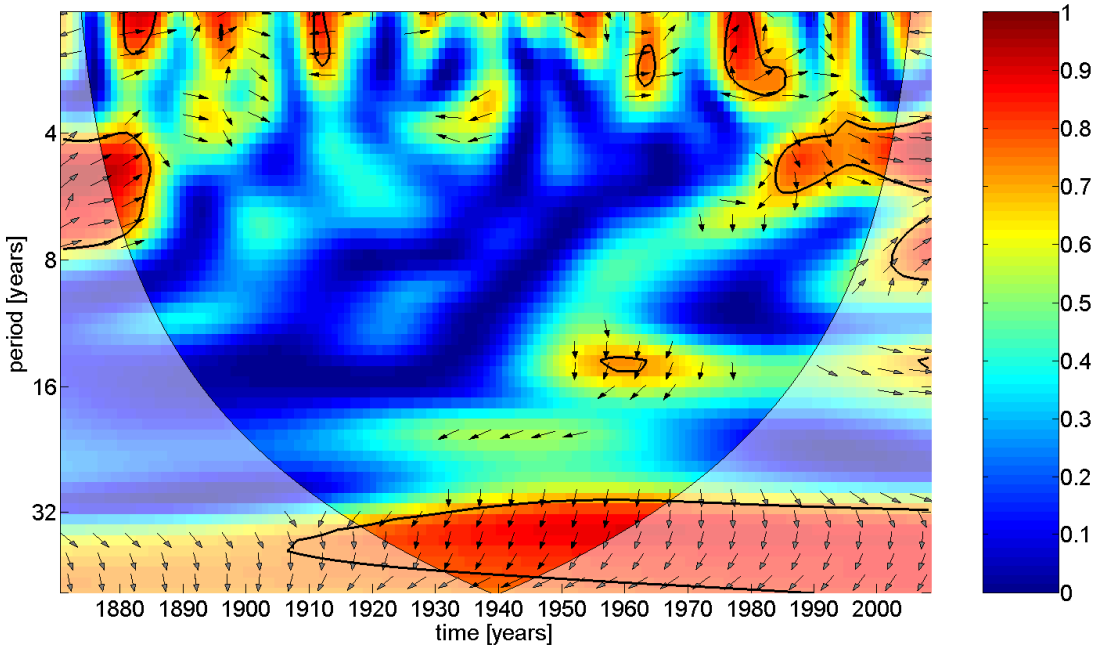

Figure 5.4: Wavelet coherence and phase between the winter NAO index and the time coefficient of the first EOF. Areas bordered by the black solid lines are within the 95 % confidence level using the red noise model. The arrows indicate the phase difference (0° is given by a horizontal arrow pointing to the right and a arrow pointing vertically upwards means the time coefficient lags the NAO by 90°). The U-shaped curve shows limits of the cone of influence (COI). All signals outside COI are statistically not certain.

especially in the 1930s and 1940s is known as the "early brightening" [*Ohmura*, 2006; *Wild*, 2009]. Afterwards, mostly caused by an increase of aerosols, clouds and their interaction, the "global dimming" reduces the solar radiation flux at the sea surface. On a planetary scale, changes in cloudiness and atmospheric transmission terminate the dimming in the 1980s followed by a "brightening" until nowadays [*Wild et al.*, 2005; *Wild*, 2009]. Most pronounced in the Madeira Basin is the moment from early brightening to global dimming in the 1940s (Fig. 5.5). The transition from brightening to dimming caused a reduction of the DCM strength until the 1970s (Fig 5.2b). With the start of the second brightening, the DCM intensifies again. The direct connection of the strength of the DCM and the solar radiation flux is manifested in a significant correlation coefficient of 0.25 (p-value 0.004) calculated with the annual mean chlorophyll *a* in 90 – 130 m.

Hence, the intensity of the solar radiation is a dominant factor explaining the long-

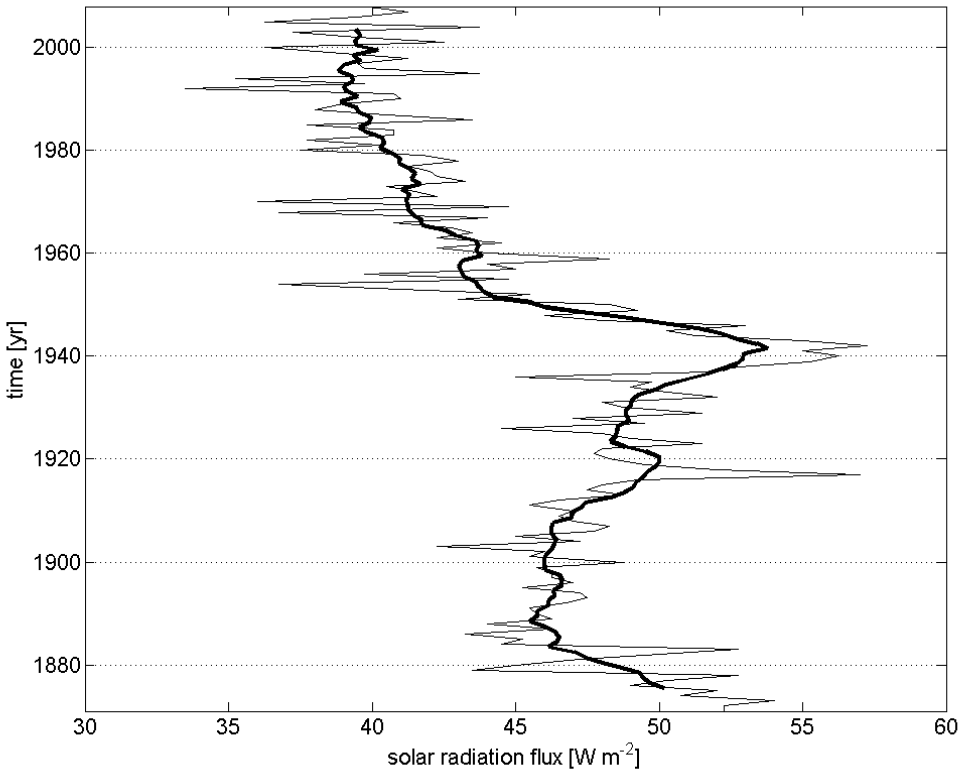

Figure 5.5: The solar radiation flux at surface from 1871 to 2008. Shown is the mean value between Augusts to November (thin line) during which months the DCM is mostly established, and a running mean over ten years (bold line).

term variability of the chlorophyll *a* concentration in the deeper levels of the euphotic zone where the phytoplankton is adapted to low-light conditions. Whereas the light saturated upper levels of the euphotic zone are not affected, smallest changes in the light intensity has high impact on the primary production in the DCM.

5.5.2 Effect of long-term trends of primary production on the global carbon cycle

It is worth considering which impact did the decrease of the DCM have for the carbon uptake by the oceans in the last century. In this region, the surface chlorophyll *a* is depleted after the bloom for almost half a year, making the DCM an important fraction

of the integrated chlorophyll *a* content.

Our method allows a calculation of the carbon uptake for the entire year with lower errorbars due to a more precise estimation of the integrated chlorophyll *a* over time and depth. The decrease of the integrated chlorophyll *a* is on the one hand caused by the long-term variability of the solar radiation flux and its impact on the DCM. On the other hand, changes in the growth conditions like varying sea surface temperature and associated stratification of the water column as well as mixing processes interfere or promote nutrient supply. The long lasting global warming of the upper water column has recently been reported by *Levitus et al.* [2009]. An increase of temperature led to a decrease of the globally integrated primary production [*Boyce et al.*, 2010]. Assuming both the solar radiation flux and the warming of the world's ocean are similarly manifested in the subtropical oceans, it concedes an estimation of the global change of carbon uptake by the decrease of primary production in the last 138 years. Comparison of the first (1871) with the last year (2008) of our time series shows a reduction in carbon uptake by the oceans of ΔCU = -700 Mt yr^{-1} in 2008.

The global carbon uptake by the oceans amount for 92.2 Gt yr^{-1} in the last years [*Denman et al.*, 2007]. The subtropical gyres contribute to 50 % of this global carbon export [*Emerson et al.*, 1997]. Therefore, the 700 Mt less carbon uptake in 2008 amounted to 1.5 % in the subtropical gyres nowadays compared to the 19th century. Integrating over the entire time period from 1871 to 2008 and assuming a linear decrease of the carbon uptake in these 138 years, the oceans stored 48 Gt less carbon, i. e. half of the annual carbon uptake nowadays.

The oceans' capability to take up and store carbon in intermediate and deep waters as well as in the sediment is considered as an important factor to reduce the CO_2 concentration in the atmosphere and hence the temperature increase until the end of the 21st century [*Denman et al.*, 2007]. Our back-of-the-envelope calculation above shows this capability decreased in the last century. Large parts of the subtropical gyres are oligotrophic. Especially these areas of the world's ocean for which we determined a reduced capacity of carbon uptake are extending [*Polovina et al.*, 2008]. This may result in even less global carbon uptake in the 21st century, further backed up by the accelerated warming of the oceans in the last decades of the 20th century [*Levitus et al.*, 2009].

5.6 Conclusion

The analysis of more than 100 years of chlorophyll *a* in the Madeira Basin shows the DCM as very sensitive to long-term changes in Northern hemisphere atmospheric pattern and in the solar radiation flux. This chlorophyll *a* field, spanning more than one century, offered the opportunity to highlight the direct influence of global dimming and brightening on the DCM for the first time. Identifying the influence of the NAO on periods of 30 – 40 years with a time delay of nine years required such a long time series, but needs further studies to understand the underlying mechanisms. In the subtropical gyres, the DCM greatly contributes to the integrated primary production and is an important factor in the global carbon cycle. Assuming a linear trend of carbon uptake between 1871 and 2008, this led to a reduction in carbon uptake in the order of magnitude of half an annual carbon uptake today. Similar studies in another regions of the world's ocean are needed to allow a global estimation of the variability in carbon uptake over the last one hundred years, especially before and during the period of increasing global temperatures. These results will help to comprehend the sensitivity of the primary production to changes in atmospheric and oceanic conditions and contribute to more solid projections of subsequent global climate conditions.

5.7 Acknowledgments

The authors thank all colleagues involved in obtaining the *in-situ* measurements since 1989, the crews and masters of the research vessels. The SODA-POP temperature data are available on http://apdrc.soest.hawaii.edu/datadoc/soda_2.1.6.php. The solar radiation flux is available on http://www.esrl.noaa.gov/psd/data/gridded/data.20thC_ReanV2.html. This work is financially supported by DFG (Contract number WA2157/5-1).

6 Summary and future perspectives

The present work analysed the interannual to interdecadal variability of primary production and export production in the northeastern part of the oligotrophic North Atlantic Subtropical Gyre in the context of natural variability as well as globally increasing temperatures in the 20th century. A time series of thirteen years of particle flux sampled in the deep ocean by sediment traps of the mooring Kiel 276 (33°N, 22°W) was related to the propagation of the Azores Front and its impact on the growth conditions for phytoplankton. To detect interdecadal variability and long-term trends of primary production, a new method was developed to derive a chlorophyll *a* field for several decades. Using this method, the calculated chlorophyll *a* field was correlated to the natural atmospheric variability in the North Atlantic as well as long-term trends due to global warming of the upper layers of the ocean.

The Azores Front, building the transition zone between the colder and nutrient enriched North Atlantic and the warmer and oligotrophic North Atlantic Subtropical Gyre, plays an important role in the ocean dynamics of the Madeira Basin and forms a narrow zone of enhanced primary productivity. The influence of the dominant North Atlantic atmospheric pattern on the meridional propagation of the front was determined. With reference to the scientific questions raised in chapter 1.2, following conclusions are drawn (see chapter 3, *Fründt and Waniek* [2012]):

- The latitudinal position of the Azores Front, derived from a high resolved modeled temperature field by SODA POP, shows a variability on monthly to decadal time scales. In the time period analysed from 1966 to 2007, the position ranged between 30°N and 37.5°N with a mean position of 33.9 $\pm$ 1.3°N. Additionally, an overlying northward trend was detected.

- The Azores Front's propagation is forced by the North Atlantic Oscillation (NAO). Significant correlation coefficients between the position and the NAO were cal-

culated with a time delay of approximately one year. The NAO induces changes in the wind field causing a convergence zone of the Ekman transport at the front. Variability in the strength of these transports north and south of the front, respectively, leads to the observed north- and southward propagation.

- Enhanced primary production was determined at the southern edge of the front, compared to the northern edge, because deeper mixed layers in winter stimulated increased nutrient supply into the euphotic zone. The interannual variability of the export production at the mooring Kiel 276 was caused by the north- and southward propagation of the Azores Front which changed the growth conditions for phytoplankton due to different mixed layer depths with associated nutrient supply in the catchment areas of the sediment traps at Kiel 276.

The time series of export production measured with the sediment traps of the mooring is still too short to detect long-term variability of primary production in the Madeira Basin. The use of *in-situ* measurements of chlorophyll *a*, as an indicator for primary production, was hindered by a lack of data in the last decades. Therefore, a new method was developed to calculate the past chlorophyll *a* distribution based on *in-situ* measurements of temperature, nitrate and chlorophyll *a* (see chapter 4, *Fründt et al.* [2015b]). The application requires as basis a modeled temperature field for which in this thesis the output of the assimilation model SODA POP was used. The relationship between temperature and nitrate measurements is applied to the modeled temperature field and results in a nitrate field. Subsequently, a fit of chlorophyll *a* to both temperature and nitrate measurements delivers the chlorophyll *a* field with a high depth resolution reproducing the chlorophyll *a* distribution in the entire euphotic zone, especially in the depth of the deep chlorophyll maximum. This method was validated with surface chlorophyll *a* measurements by satellites, and a coefficient of efficiency of 0.3 confirms the method's capability for reconstruction of seasonal to long-term variability of primary production. First results of reconstructed chlorophyll *a* concentrations in the Madeira Basin, monthly resolved from 1980 to 2008, show the NAO as a dominant forcing mechanism for the interannual variability in this region, especially in the depth and strength of the deep chlorophyll maximum (see chapter 4, *Fründt et al.* [2015b]).

To detect the long-term variability of primary production and its natural forcing mech-

anisms, the method developed in chapter 4 was applied to a modeled temperature field in the Madeira Basin from 1871 to 2008 (see chapter 5, *Fründt et al.* [2015a]). This results in a unique chlorophyll *a* field spanning a period of more than one hundred years in which most of the recent global temperature increase occurred.

As dominant pattern of the primary production in the Madeira Basin, the deep chlorophyll maximum in 90 to 130 m depth is identified with a pronounced multidecadal variability. The chlorophyll *a* concentrations in the deep chlorophyll maximum increased until the 1930s followed by a strong decrease until the 1970s when no deep chlorophyll maximum was established. Until the end of the time series, the chlorophyll *a* concentrations recovered to values found at the beginning of the 20th century. According to the scientific questions, the results of chapter 5 [*Fründt et al.*, 2015a] are summarised hereinafter.

- Two dominant forcing mechanisms of the long-term variability of the deep chlorophyll maximum were determined. At first, the NAO is highly correlated with the deep chlorophyll maximum on periods of roughly 30 years with a time lag of 9 years. This time lag is caused by the slow signal transfer via Rossby waves. After the regime shift in 1976 – 1981 until today, a correlation with the NAO established on shorter periods of 5 years with no time lag, which can be related to the shift of the Atlantic Multidecadal Oscillation and the NAO from a negative to a positive phase.

  Secondly, the sharp decrease of the strength of the deep chlorophyll maximum after the 1930s is caused by a decrease of solar radiation in transition from early brightening to global dimming inducing insufficient light irradiation to maintain photosynthesis in the depth of the deep chlorophyll maximum.

- A decrease of 3 % of the depth integrated chlorophyll *a* content was determined between 1871 and 2008. Applying this result to the global subtropical gyres, an estimation of the oceans' carbon uptake amounts to 700 Mt C, i.e. 1.5 % less global carbon uptake in 2008 compared to 1871. By combining both this decrease of carbon uptake and an expansion of the subtropical gyres, the capability of the oceans for carbon uptake will decrease with possibly high impact on future atmospheric CO_2 concentrations and hence global climate variability.

The present thesis does in no sense form a complete figure of the variability of primary and export production in the Madeira Basin, but provides an incentive for further studies in the context of global climate variability. A prolongation of the time series of particle flux at the mooring site Kiel 276 may offer the opportunity to detect the analysed correlation of the Azores Front propagation with the NAO directly in the sediment trap measurements. Until now, the mass flux time series is still too short to provide statistically significant results in correlation with dominant periods of the NAO.

Comparisons with the sediment trap flux data set of the Bermuda Atlantic Time Series (BATS) study in the northwestern part of the North Atlantic Subtropical Gyre, can give indication about differences and similarities in the atmosphere-ocean interaction over the entire subtropical North Atlantic. This study can continue the analysis made by *Brust* [2011] who concentrated on the source areas of lithogenic particle flux at both mooring sites, Kiel 276 and BATS.

The area of the Azores Front was identified as a region of increased primary production at the boundary to the oligotrophic subtropical gyre. Future measurements of the velocity field at the front, especially the vertical velocity inducing upwelling at the front, are necessary to gain a deeper understanding of the interaction of the hydrographic dynamics at the front and primary productivity.

The analyses of the position of the Azores Front show a northern displacement enlarging the oligotrophic area of the North Atlantic. This result is consistent with the study by *Polovina et al.* [2008] who examined the increasing global oligotrophic areas with chlorophyll *a* satellite measurements. Thus, a study about the propagation and possible displacements of the further global subtropical fronts in the Pacific and Southern Ocean (Fig. 1.1) could provide information about the velocity with which the oligotrophic areas are expanding and promotes the projection of global primary production.

The propagation of the Azores Front, as a boundary between two water masses, causes fast changes of the hydrographic conditions to which the phytoplankton and higher trophic levels have to adapt. The differences in the species composition of phytoplankton and mesozooplankton north and south of the front have been studied by *Fer-*

nández and Pingree [1996]; *Schiebel et al.* [2002]; *Head et al.* [2002], however, besides this spatial resolution, it is still insufficiently studied how the biocoenosis is influenced by a crossing of the front. For this investigation, the measurements of the sediment traps could be used due to their appropriate temporal resolution of several days to weeks. The results of this study could be used for projections of adaptions or migrations of phytoplankton in case of relatively slow hydrographical and biogeochemical changes induced by recent increasing global temperatures.

The global subtropical frontal zones span a large area of the world's ocean and new knowledge about these areas can be used to contribute to a more precise estimation and projection of global primary production which is highly important in the context of carbon uptake and prospective climate variability.

With the newly developed method, a chlorophyll *a* field was recalculated from 1871 to 2008 in the Madeira Basin, i.e. in the same area from which the samples of the sediment traps originate. A coupling of these two time series could be used, at first, to extend the mass flux data back into the past. Since the calculated chlorophyll *a* field provides no information about the dominant species, the samples of the sediment traps give indication of the phytoplankton population. Hence, secondly, the analysis of the long-term variability of the chlorophyll *a* field could be extended to the phytoplankton community especially in the context of the changes in hydrographical and atmospherical conditions in the last century. For this study, additional *in-situ* measurements of phytoplankton are necessary for the validation.

Related to the global carbon uptake by the oceans, the method could be applied to other regions of the world's ocean. At first, the focus should lie on the more productive regions of the subpolar gyres. Additionally, due to a higher amount of *in-situ* measurements in the high productive shelf seas and global upwelling areas, retrieving the chlorophyll *a* fields in those regions will easily be possible. Combined with the calculation in the subtropical oceans, all these regions cover most of the world's ocean areas. Hence, it would be possible to determine the impact, especially of the temperature increase in the last century, on global primary production as well as on global carbon uptake.

Besides this global point of view, the recalculation of the chlorophyll *a* fields could be expanded to single ocean basins to analyse the differences of forcing mechanisms causing long-term variability of primary production, especially between the Atlantic and Pacific Oceans. It can be studied if El Niño events or the phase of the Atlantic Multidecadal Oscillation influence primary productivity by teleconnections on a global scale, for example. These results will help to increase the knowledge of the interaction of global ecosystems with the current climate state and, hence, to give solid projections in case of changing climate.

References

Acker, J. G., and G. Leptoukh, Online Analysis Enhances Use of NASA Earth Science Data, *EOS*, *88*, 14–17, 2007.

Alvarez, I., M. Gomez-Gesteira, M. deCastro, and E. M. Novoa, Ekman transport along the Galician Coast (NW, Spain) calculated from QuikSCAT winds, *Journal of Marine Systems*, *72*, 101–115, 2008.

Antoine, D., and A. Morel, Oceanic primary production 1. Adaption of a spectral light-photosynthesis model in view of application to satellite chlorophyll observations, *Global Biogeochemical Cycles*, *10*, 43–55, 1996.

Antoine, D., A. Morel, H. R. Gordon, V. F. Banzon, and R. H. Evans, Bridging ocean color observations of the 1980s and 2000s in search of long-term trends, *Journal of Geophysical Research*, *110*, 1–22, 2005.

Barker, S., and H. Elderfield, Foraminiferal calcification response to glacial–interglacial changes in atmospheric CO_2., *Science*, *297*, 833–836, 2002.

Barnston, A. G., and R. E. Livezey, Classification, Seasonality and Persistence of Low-Frequency Atmospheric Circulation Patterns, *Monthly Weather Review*, *115*, 1083–1126, 1987.

Beaufort, L., I. Probert, T. de Garidel-Thoron, E. M. Bendif, D. Ruiz-Pino, N. Metzl, C. Goyet, N. Buchet, P. Coupel, M. Grelaud, B. Rost, R. E. M. Rickaby, and C. de Vargas, Sensitivity of coccolithophores to carbonate chemistry and ocean acidification, *Nature*, *426*, 80–83, 2011.

Beaugrand, G., P. C. Reid, F. Ibañez, J. A. Lindley, and M. Edwards, Reorganization of North Atlantic Marine Copepod Biodiversity and Climate, *Science*, *296*, 1692–1694, 2002.

Beers, J. R., F. M. H. Reid, and G. K. Stewart, Microplankton of the North Pacific central gyre. Population structure and abundance, *Internationale Revue der gesamten Hydrobiologie*, *60*, 607–638, 1975.

Behrenfeld, M. J., and P. G. Falkowski, Photosynthetic rates derived from satellite-based chlorophyll concentration, *Limnology and Oceanography*, *42*, 1–20, 1997.

Behrenfeld, M. J., R. T. O'Malley, D. A. Siegel, C. R. McClain, J. L. Sarmiento, G. C. Feldman, A. J. Milligan, P. G. Falkowski, R. M. Letelier, and E. S. Boss, Climate-driven trends in contemporary ocean productivity, *Nature*, *444*, 752–755, 2006.

Belkin, I. M., P. C. Cornillon, and K. Sherman, Fronts in Large Marine Ecosystems, *Progress in Oceanography*, *81*, 223–236, 2009.

Bigg, G. R., *The Oceans and Climate*, Cambridge University Press, Cambridge, 2003.

Bopp, L., P. Monfray, O. Aumont, J.-L. Dufresne, H. Le Treut, G. Madec, L. Terray, and J. C. Orr, Potential impact of climate change on marine export production, *Global Biogeochemical Cycles*, *15*, 81–99, 2001.

Boyce, D. G., M. R. Lewis, and B. Worm, Global phytoplankton decline over the past century, *Nature*, *466*, 591–596, 2010.

Boyce, D. G., M. R. Lewis, and B. Worm, Boyce et al. reply, *Nature*, 2011.

Boyce, D. G., M. Lewis, and B. Worm, Integrating global chlorophyll data from 1890 to 2010, *Limnology and Oceanography: Methods*, *10*, 840–852, 2012.

Boyd, P. W., and S. C. Doney, Modeling regional responses by marine pelagic ecosystems to global climate change, *Geophysical Research Letters*, *29*, 1–4, 2002.

Boyd, S. H., P. H. Wiebe, and J. L. Cox, Limits of *Nematoscelis megalops* in the Northeastern Atlantic in relation to Gulf Stream cold core rings. II. Physiological and biochemical effects of expatriation, *Journal of Marine Science*, *36*, 143–159, 1978.

Bradley, R. S., and P. D. Jonest, 'Little Ice Age' summer temperature variations: their nature and relevance to recent global warming trends, *The Holocene*, *3*, 367–376, 1993.

Bradley, R. S., H. F. Diaz, G. N. Kiladis, and J. K. Eischeid, ENSO signals in continental temperature and precipitation records, *Nature*, *327*, 497–501, 1987.

Brown, J., *Seawater : its composition, properties and behaviour*, Oceanography series, Butterworth-Heinemann, Oxford, 1995.

Brügmann, L., and K. Kremling, Sampling, in *Methods of Seawater Analysis*, edited by K. Grasshoff, Wiley-VCH, New York, 1999.

Brust, J., *Interannual variability of lithogenic particle fluxes in the subtropical North Atlantic*, Dissertation, Universität Rostock, Rostock, 2011.

Brust, J., and J. J. Waniek, Atmospheric dust contribution to deep-sea particle fluxes in the subtropical Northeast Atlantic, *Deep Sea Research Part I: Oceanographic Research Papers*, *57*, 988–998, 2010.

Brust, J., D. E. Schulz-Bull, T. Leipe, V. Chavagnac, and J. J. Waniek, Descending particles: From the Atmosphere to the deep ocean - A time series study in the subtropical NE Atlantic , *Geophysical Research Letters*, *38*, 1–5, 2011.

Bryden, H. L., C. Robinson, and G. Griffiths, Changing currents: a strategy for understanding and predicting the changing ocean circulation, *Philosophical Transactions of the Royal Society A: Mathematical, Physical and Engineering Sciences*, *370*, 5461–5479, 2012.

Brzezinski, M. A., T. A. Villareal, and F. Lipschultz, Silica production and the contribution of diatoms to new and primary production in the central North Pacific, *Marine Ecology Progress Series*, *167*, 89–104, 1998.

Carton, J. A., and B. S. Giese, A Reanalysis of Ocean Climate Using Simple Ocean Data Assimilation (SODA), *Monthly Weather Review*, *136*, 2008.

Carton, J. A., B. S. Giese, and S. A. Grodsky, Sea level rise and the warming of the oceans in the Simple Data Assimilation (SODA) ocean reanalysis, *Journal of Geophysical Research*, *110*, 1–8, 2005.

Cazenave, A., and R. S. Nerem, Present-day sea level change: observations and causes, *Reviews of Geophysics*, *42*, 2004.

Charlson, R. J., J. E. Lowelock, M. O. Andreae, and S. G. Warren, Oceanic phytoplankton, atmospheric sulphur, cloud albedo and climate, *Nature*, *326*, 655–661, 1987.

Chavez, F. P., M. Messié, and J. T. Pennington, Marine Primary Production in Relation to Climate Variability and Change, *Annual Review of Marine Science*, *3*, 227–260, 2011.

Chiang, J. C. H., and D. J. Vimont, Analogous Pacific and Atlantic Meridional Modes of Tropical Atmosphere–Ocean Variability, *Journal of Climate*, *326*, 4143–4158, 2004.

Chu, P. C., L. M. Ivanov, O. V. Melnichenko, and N. C. Wells, On long baroclinic Rossby waves in the tropical North Atlantic observed from profiling floats, *Journal of Geophysical Research*, *112*, 1–24, 2007.

Church, J. A., and N. J. White, A 20th century acceleration in global sea-level rise, *Geophysical Research Letters*, *33*, 2006.

Church, J. A., N. J. White, R. Coleman, K. Lambeck, and J. X. Mitrovica, Estimates of the Regional Distribution of Sea Level Rise over the 1950-2000 Period, *Journal of Climate*, *17*, 2004.

Church, J. A., N. J. White, L. F. Konikow, C. M. Domingues, J. G. Cogley, E. Rignot, J. M. Gregory, M. R. van den Broeke, A. J. Monaghan, and I. Velicogna, Revisiting the Earth's sea-level and energy budgets from 1961 to 2008, *Geophysical Research Letters*, *38*, L18,601, 2011.

Ciais, P., C. Sabine, G. Bala, L. Bopp, V. Brovkin, J. Canadell, A. Chhabra, R. DeFries, J. Galloway, M. Heimann, C. Jones, C. Le Quéré, R. B. Myneni, S. Piao, and P. Thornton, Carbon and Other Biogeochemical Cycles, in *Climate Change 2013: The Physical Science Basis. Contribution of Working Group I to the Fifth Assessment Report of the Intergovernmental Panel on Climate Change*, edited by T. F. Stocker, D. Qin, G.-K. Plattner, M. Tignor, S. K. Allen, J. Boschung, A. Nauels, Y. Xia, V. Bex, and P. M. Midgley, Cambridge University Press, Cambridge, United Kingdom and New York, NY, USA, 2013.

Cipollini, P., D. Cromwell, M. S. Jones, G. D. Quartly, and P. G. Challenor, Concurrent altimeter and infrared observations of Rossby wave propagation near 34°N in the Northeast Atlantic, *Geophysical Research Letters*, *24*, 889–892, 1997.

Compo, G. P., J. S. Whitaker, and P. D. Sardeshmukh, Feasibility of a 100 year reanalysis using only surface pressure data, *Bulletin of the American Meteorological Society*, *87*, 175–190, 2004.

Cullen, J. J., The Deep Chlorophyll Maximum: Comparing Vertical Profiles of Chlorophyll *a*, *Canadian Journal of Fisheries and Aquatic Sciences*, *39*, 791–803, 1982.

Daufresne, M., K. Lengfellner, and U. Sommer, Global warming benefits the small in aquatic ecosystems, *Proceedings of the National Academy of Sciences*, 2009.

Dave, A. C., and M. S. Lozier, Local stratification control of marine productivity in the subtropical North Pacific, *Journal of Geophysical Research*, *115*, 2–16, 2010.

Dave, A. C., and M. S. Lozier, Examining the global record of interannual variability in stratification and marine productivity in the low-latitude and mid-latitude ocean, *Journal of Geophysical Research: Oceans*, *118*, 3114–3127, 2013.

Denman, K. L., G. Brasseur, A. Chidthaisong, P. Ciais, P. M. Cox, R. E. Dickinson, D. Hauglustaine, C. Heinze, E. Holland, D. Jacob, U. Lohmann, S. Ramachandran, P. L. da Silva Dias, S. C. Wofsy, and X. Zhang, Couplings Between Changes in the Climate System and Biogeochemistry, in *Climate Change 2007: The Physical Science Basis. Contribution of Working Group I to the Fourth Assessment Report of the Intergovernmental Panel on Climate Change*, edited by S. Solomon, D. Qin, M. Manning, Z. Chen, M. Marquis, K. Averyt, M. Tignor, and H. Miller, Cambridge University Press, Cambridge, United Kingdom and New York, NY, USA, 2007.

Dima, M., and G. Lohmann, A hemisphere mechanism for the Atlantic multidecadal oscillation, *Journal of Climate*, *20*, 2706–2719, 2007.

Dippner, J. W., C. Möller, and J. Hänninen, Regime Shifts in North Sea and Baltic Sea: A comparison, *Journal of Marine Systems*, *105-108*, 115–122, 2012.

Dlugokencky, E., and P. P. Tans, Recent CO_2, NOAA, ESRL. Retrieved from http://www.esrl.noaa.gov/gmd/ccgg/trends/global.html, accessed 20.03.2014, 2014.

Doi, T., T. Tozuka, and T. Yamagata, The Atlantic Meridional Mode and Its Coupled Variability with the Guinea Dome, *Journal of Climate*, *23*, 455–475, 2010.

Doney, S. C., M. Ruckelshaus, J. E. Duffy, J. P. Barry, F. Chan, C. A. English, H. M. Galindo, J. M. Grebmeier, A. B. Hollowed, N. Knowlton, J. Polovina, N. N. Rabalais, W. J. Sydeman, and L. D. Talley, Climate Change Impacts on Marine Ecosystems, *Annual Review of Marine Science*, *4*, 11–37, 2012.

Eden, C., and T. Jung, North Atlantic Interdecadal Variability: Oceanic Response to the North Atlantic Oscillation (1865-1997), *Journal of Climate*, *14*, 676–691, 2001.

Ekman, W. K., On the influence of earth's rotation on ocean currents, *Arkiv för Matematik, Astonomi och Fysik*, *2*, 1905.

Emerson, S., P. Quay, D. Karl, C. Winn, L. Tupas, and M. Landry, Experimental determination of the organic carbon flux from open-ocean surfacewaters, *Nature*, *389*, 951–954, 1997.

Enfield, D. B., A. M. Mestas-Nuñez, and P. J. Trimble, The Atlantic multidecadal oscillation and its relation to rainfall and river flows in the continental U.S., *Geophysical Research Letters*, *28*, 2077–2080, 2001.

Eppley, R. W., An incubation method for estimating the carbon content of phytoplankton in natural samples, *Limnology and Oceanography*, *13*, 574–582, 1968.

Eppley, R. W., and B. J. Peterson, Dissolved organic matter in the ocean: A controversy stimulates new insights, *Nature*, *282*, 677–680, 1979.

Falkowski, P. G., The global carbon cycle: A test of our knowledge of Earth as a system, *Science*, *290*, 291–296, 2000.

Falkowski, P. G., and M. J. Oliver, Mix and Match: how climate selects phytoplankton, *Nature Reviews Microbiology*, *5*, 813–819, 2007.

Fasham, M. J. R., T. Platt, B. Irwin, and K. Jones, Factors affecting the spatial pattern of the deep chlorophyll maximum in the region of the Azores front, *Progress in Oceanography*, *14*, 129–165, 1985.

Feely, R. A., S. C. Doney, and S. R. Cooley, Ocean acidification: Present conditions and future changes in a high-CO_2 world, *Oceanography*, *22*, 36–47, 2009.

Fernández, E., and R. D. Pingree, Coupling between physical and biological fields in the North Atlantic subtropical front southeast of the Azores, *Deep Sea Research Part I: Oceanographic Research Papers*, *43*, 1369–1393, 1996.

Field, C. B., M. Behrenfeld, J. T. Randerson, and P. Falkowski, Primary production of the biosphere: Integrating terrestrial and oceanic components, *Science*, *281*, 237–240, 1998.

Foltz, G. R., M. J. McPhaden, and R. Lumpkin, A Strong Atlantic Meridional Mode Event in 2009: The Role of Mixed Layer Dynamics, *Journal of Climate*, *25*, 363–380, 2012.

Francois, R., S. Honjo, R. Krishfield, and S. Manganini, Factors controlling the flux of organic carbon to the bathypelagic zone of the ocean, *Global Biogeochemical Cycles*, *16*, 1–20, 2002.

Frankignoul, C., G. d. Coëtlogon, T. M. Joyce, and S. Dong, Gulf Stream Variability and Ocean-Atmosphere Interactions, *Journal of Physical Oceanography*, *31*, 3516–3529, 2001.

Fründt, B., and J. J. Waniek, Impact of the Azores Front Propagation on Deep Ocean Particle Flux, *Central European Journal of Geosciences*, *4*, 531–544, 2012.

Fründt, B., T. J. Müller, D. E. Schulz-Bull, and J. J. Waniek, Long-term changes in the thermocline of the subtropical Northeast Atlantic (33°N, 22°W), *Progress in Oceanography*, *116*, 246–260, 2013.

Fründt, B., J. W. Dippner, D. E. Schulz-Bull, and J. J. Waniek, Chlorophyll *a* reconstruction from in-situ measurements: 2. Marked carbon uptake decrease in the last century, *Journal of Geophysical Research: Biogeosciences*, *120*, 246–253, 2015a.

Fründt, B., J. W. Dippner, and J. J. Waniek, Chlorophyll *a* reconstruction from in-situ measurements: 1. Method description, *Journal of Geophysical Research: Biogeosciences*, *120*, 237–245, 2015b.

Fusco, G., V. Artale, Y. Cotroneo, and G. Sannino, Thermohaline variability of Mediterranean Water in the Gulf of Cadiz, 1948 – 1999, *Deep-Sea Research I*, *55*, 1624–1638, 2008.

Gattuso, J. P., M. Frankignoulle, I. Bourge, S. Romaine, and R. W. Buddemeier, Effect of calcium carbonate saturation of seawater on coral calcification, *Global and Planetary Change*, *18*, 37–46, 1998.

Gill, A. E., *Atmosphere-Ocean Dynamics*, Academic Press, New York, 1985.

Goes, J. I., T. Saino, H. Oaku, J. Ishizaka, C. S. Wong, and Y. Nojiri, Basin scale estimates of sea surface nitrate and new production from remotely sensed sea surface temperature and chlorophyll, *Geophysical Research Letters*, *27*, 1263–1266, 2000.

Goldman, J. C., Potential role of large oceanic diatoms in new primary production, *Deep Sea Research*, *40*, 159–186, 1993.

Gordon, H. R., and W. R. McCluney, Estimation of the Depth of Sunlight Penetration in the Sea for Remote Sensing, *Applied Optics*, *14*, 413–416, 1975.

Gould, W. J., Physical oceanography of the Azores front, *Progress in Oceanography*, *14*, 167–190, 1985.

Graham, N. E., Decadal scale climate variability in the tropical and North Pacific during the 1970s and 1980s: observations and model results, *Climate Dynamics*, *10*, 135–162, 1994.

Grasshoff, K., K. Kremling, and M. Ehrhardt, *Methods of Seawater Analysis*, Wiley-VCH, Weinheim, 1999.

Grinsted, A., J. C. Moore, and S. Jevrejeva, Application of the cross wavelet transform and wavelet coherence to geophysical time series, *Nonlinear Processes in Geophysics*, *11*, 561–566, 2004.

Gulev, S. K., M. Latif, N. Keenlyside, W. Park, and K. P. Koltermann, North Atlantic Ocean control on surface heat flux on multidecadal timescales, *Nature*, *499*, 464–467, 2013.

Hansell, D. A., C. A. Carlson, D. J. Repeta, and R. Schlitzer, Dissolved organic matter in the ocean: A controversy stimulates new insights, *Oceanography*, *22*, 202–211, 2009.

Head, R. N., G. Medina, I. Huskin, R. Anadon, and R. P. Harris, Phytoplankton and mesozooplankton distribution and composition during transects of the Azores Subtropical Front, *Deep Sea Research II*, *49*, 4023–4034, 2002.

Henson, S. A., J. L. Sarmiento, J. P. Dunne, L. Bopp, I. Lima, S. C. Doney, J. John, and C. Beaulieu, Detection of anthropogenic climate change in satellite records of ocean chlorophyll and productivity, *Biogeosciences*, *7*, 621–640, 2010.

Higgins, R. W., A. Leetmaa, Y. Xue, and A. Barnston, Dominant Factors Influencing the Seasonal Predictability of U.S. Precipitation and Surface Air Temperature, *Journal of Climate*, *13*, 3994–4017, 2000.

Higuchi, K., J. Huang, and A. Shabbar, Wavelet Characterization of the North Atlantic Oscillation Variation and its Relationship to the North Atlantic Sea Surface Temperature, *International Journal of Climatology*, *19*, 1119–1129, 1999.

Hodges, B. A., and D. L. Rudnick, Simple models of steady deep maxima in chlorophyll and biomass, *Deep Sea Research Part I: Oceanographic Research Papers*, *51*, 999–1015, 2004.

Hughes, C. W., The Antarctic Circumpolar Current as a Waveguide for Rossby Waves, *Journal of Physical Oceanography*, *26*, 1375–1387, 1996.

Hurrell, J. W., Decadal Trends in the North Atlantic Oscillation: Regional Temperatures and Precipitation, *Science*, *269*, 676–679, 1995.

Hurrell, J. W., and C. Deser, North Atlantic climate variability: The role of the North Atlantic Oscillation, *Journal of Marine Systems*, *78*, 28–41, 2009.

IPCC, in *Climate Change 2013: The Physical Science Basis, Contribution of Working Group I to the Fifth Assessment Report of the Intergovernmental Panel on Climate Change*, edited by T. F. Stocker, D. Qin, G.-K. Plattner, M. Tignor, S. K. Allen, J. Boschung, A. Nauels, Y. Xia, V. Bex, and P. M. Midgley, p. 1535, Cambridge University Press, Cambridge, United Kingdom and New York, NY, USA, 2013.

Irwin, A. J., and M. J. Oliver, Are ocean deserts getting larger?, *Geophysical Research Letters*, *36*, 1–5, 2009.

Irwin, B., Nutrient Data from the Atlantic. JGOFS Canada Data Sets 1989-1998, CD-ROM Version 1.0 Dec. 2000, *Tech. rep.*, Department of Fisheries and Oceans, 2000.

James, C., M. Tomczak, I. Helmond, and L. Pender, Summer and winter surveys of the Subtropical Front of the southeastern Indian Ocean 1997-1998, *Journal of Marine Systems*, *37*, 129–149, 2002.

James, R., *Marine biogeochemical cycles*, Oceanography series, Buuterworh-Heinemann, Oxford, 2005.

JGOFS, Protocols for the Joint Global Ocean Flux Study (JGOFS) Core Measurements, *Tech. rep.*, 1994.

Jia, Y., Formation of an Azores Current due to Mediterranean Overflow in a Modeling Study of the North Atlantic, *Journal of Physical Oceanography*, *30*, 2342–2358, 2000.

Jones, P. D., T. M. L. Wigley, and P. B. Wright, Global temperature variations between 1861 and 1984, *Nature*, *322*, 430–434, 1986.

Jones, P. D., M. New, D. E. Parker, S. Martin, and I. G. Rigor, Surface air temperature and its changes over the past 150 years, *Reviews of Geophysics*, *37*, 173–199, 1999.

Joyce, T. M., C. Deser, and M. A. Spall, The Relation between Decadal Variability of Subtropical Mode Water and the North Atlantic Oscillation, *Journal of Climate*, *13*, 2550–2569, 2000.

Kalnay, E., The NCEP/NCAR 40-Year Reanalysis Project, *Bulletin of the American Meteorological Society*, *77*, 437–471, 1996.

Kaplan, A., M. A. Cane, Y. Kushnir, A. C. Clement, M. B. Blumenthal, and B. Rajagopalan, Analyses of global sea surface temperature 1856–1991, *Journal of Geophysical Research*, *103*, 18,567–18,589, 1998.

Käse, R. H., and G. Siedler, Meandering of the subtropical front south-east of the Azores, *Nature*, *300*, 245–246, 1982.

Keeling, C. D., R. B. Bacastow, A. E. Bainbridge, C. A. Ekdahl, P. R. Guenther, L. S. Waterman, and J. F. S. Chin, Atmospheric carbon dioxide variations at Mauna Loa Observatory, Hawaii, *Tellus*, *28*, 538–551, 1976.

Kemp, A. E. S., and T. A. Villareal, High diatom production and export in stratifies waters – A potential negative feedback to global warming, *Progress in Oceanography*, *119*, 4–23, 2013.

Kerr, R. A., A North Atlantic pacemaker for the centuries, *Science*, *288*, 1984–1986, 2000.

Kerr, R. A., Atlantic climate pacemaker for millennia past, decades hence?, *Science*, *309*, 41–43, 2005.

Kida, S., J. F. Price, and J. Yang, The Upper-Oceanic Response to Overflows: A Mechanism for the Azores Current, *Journal of Physical Oceanography*, *38*, 880–895, 2008.

Kirk, J. T. O., *Light and Photosynthesis in Aquatic Ecosystems, Third Edition*, Cambridge University Press, New York, 2011.

Kirtman, B., S. B. Power, J. A. Adedoyin, G. J. Boer, R. Bojariu, I. Camilloni, F. J. Doblas-Reyes, A. M. Fiore, M. Kimoto, G. A. Meehl, M. Prather, A. Sarr, C. Schär, R. Sutton, G. J. van Oldenborgh, G. Vecchi, and H. J. Wang, Near-term Climate Change: Projections and Predictability, in *Climate Change 2013: The Physical Science Basis. Contribution of Working Group I to the Fifth Assessment Report of the Intergovernmental Panel on Climate Change*, edited by T. F. Stocker, D. Qin, G.-K. Plattner, M. Tignor, S. K. Allen, J. Boschung, A. Nauels, Y. Xia, V. Bex, and P. M. Midgley, Cambridge University Press, Cambridge, United Kingdom and New York, NY, USA, 2013.

Klaas, C., and D. E. Archer, Association of sinking organic matter with various types of mineral ballast in the deep sea: Implications for the rain ratio, *Global Biogeochemical Cycles*, *16*, 1–13, 2002.

Klein, B., and G. Siedler, On the Origin of the Azores Current, *Journal of Geophysical Research*, *94*, 6159–6168, 1989.

Kleypas, J. A., R. W. Buddemeier, D. Archer, J.-P. Gattuso, C. Langdon, and B. N. Opdyke, Geochemical Consequences of Increased Atmospheric Carbon Dioxide on Coral Reefs, *Science*, *284*, 118–120, 1999.

Krauß, W., *Nr. 258. Sonderforschungsbereich 133. Warmwassersphäre des Atlantiks - Eine Dokumentation*, Berichte aus dem Institut für Meereskunde., Kiel, 1994.

Kremling, K., U. Lentz, B. Zeitzschel, D. E. Schulz-Bull, and J. Duinker, New type of time-series sediment trap for the reliable collection of inorganic and organic trace chemical substances, *Review of Scientific Instruments*, *67*, 4360–4363, 1996.

Kuss, J., and K. Kremling, Particulate trace element fluxes in the deep northeast Atlantic Ocean, *Deep-Sea Research Part I: Oceanographic Research Papers*, *46(1)*, 149–169, 1999.

Lalli, C. M., and T. R. Parsons, *Biological Oceanography: An Introduction*, Pergamon, Tarrytown, N. Y., 1993.

Lamas, L., A. Peliz, I. Ambar, A. Barbosa-Aguiar, N. Maximenko, and A. Teles-Machado, Evidence of time-mean cyclonic cell southwest of Iberian Peninsula: The Mediterranean Outflow-driven β-plume?, *Geophysical Research Letters*, *37*, 1–5, 2010.

Lau, K.-M., and H. Weng, Climate Signal Detection Using Wavelet Transform: How to Make a Time Series Sing, *Bulletin of the American Meteorological Society*, *76*, 1995.

Lee, C., J. I. Hedges, S. G. Wakeham, and N. Zhu, Effectiveness of various treatment in retarding microbial activity in sediment trap material and their effects on the collection of swimmers, *Limnology and Oceanography*, *37*, 117–130, 1992.

Legates, S., and G. J. Mc Cabe Jr., Evaluating the use of "goodness-of-fit" measures in hydrologic and hydroclimatic model validation, *Water Resources Research*, *35*, 233–241, 1999.

Leuliette, E. W., R. S. Nerem, and G. T. Mitchum, Calibration of TOPEX/Poseidon and Jason Altimeter Data to Construct an Continuous Record of Mean Sea Level Change, *Marine Geodesy*, *27*, 79–94, 2004.

Levitus, S., J. I. Antonov, and T. P. Boyer, Warming of the world ocean, 1955-2003, *Geophysical Research Letters*, *32*, 1–4, 2005.

Levitus, S., J. I. Antonov, T. P. Boyer, R. A. Locarnini, and H. E. Garcia, Global ocean heat content 1955-2008 in light of recently revealed instrumentation problems, *Geophysical Research Letters*, *36*, 1–5, 2009.

Levitus, S., J. I. Antonov, T. P. Boyer, O. K. Baranova, H. E. Garcia, R. A. Locarnini, A. V. Mishonov, J. R. Reagan, D. Seidov, E. S. Yarosh, and M. M. Zweng, World ocean heat content and thermosteric sea level change (0-2000 m), 1955-2010, *Geophysical Research Letters*, *39*, 1–5, 2012.

Lewis, C. V. W., C. S. Davis, and Gawarkiewicz, Wind forced biological-physical interactions on an isolated offshore bank, *Deep-Sea Research II*, *41*, 51–73, 1994.

Livezey, R. E., The evaluation of forecast, in *Analysis of Climate Variability*, edited by H. von Storch and A. Navarra, pp. 177–196, Springer, Berlin, 1995.

Longhurst, A., *Ecological Geography of the Sea*, Academic Press, New York, 1998.

Longhurst, A., S. Sathyendranath, T. Platt, and C. Caverhill, An estimate of global primary production in the ocean from satellite radiometer data, *Journal of Plankton Research*, *17*, 1245–1271, 1995.

Lozier, M. S., A. C. Dave, J. B. Palter, L. M. Gerber, and R. T. Barber, On the relationship between stratification and primary productivity in the North Atlantic, *Geophysical Research Letters*, *38*, L18,609, 2011.

Mackas, D. L., Does blending of chlorophyll data bias temporal trend?, *Nature*, *472*, E4–E5, 2011.

Mahaffey, C., R. G. Williams, G. A. Wolff, N. Mahowald, W. Anderson, and M. Woodward, Biogeochemical signatures of nitrogen fixation in the eastern North Atlantic , *Geophysical Research Letters*, *30*, 1–4, 2003.

Mantua, N. J., and S. R. Hare, The Pacific Decadal Oscillations, *Journal of Oceanography*, *58*, 35–44, 2002.

Maranón, E., Phytoplankton growth rates in the Atlantic subtropical gyres, *Limnology and Oceanography*, *50*, 299–310, 2005.

Marshall, J., Y. Kushnir, D. Battisti, P. Chang, A. Czaja, R. R. Dickson, J. W. Hurrell, M. S. McCartney, R. Saravanan, and M. Visbeck, North Atlantic Climate Variability: Phenomena, Impacts and Mechanisms, *International Journal of Climatology*, *21*, 1863–1898, 2001.

Martinez, E., D. Antoine, F. D'Ortenzio, and B. Gentili, Climate-Driven Basin-Scale Decadal Oscillations of Oceanic Phytoplankton, *Science*, *326*, 1253–1256, 2009.

Mauritzen, C., Production of dense overflow waters feeding the North Atlantic across the Greenland–Scotland Ridge. Part 1: Evidence for a revised circulation scheme, *Deep-Sea Research I*, *43*, 769–806, 1996.

McClain, C. R. A., A decade of satellite ocean color observations, *Annual Review of Marine Science*, *1*, 19–42, 2009.

McGillicuddy, D. J., A. R. Robinson, D. A. Siegel, H. W. Jannasch, R. Johnson, T. D. Dickey, J. McNeil, A. F. Michaels, and A. H. Knap, Influence of mesoscale eddies on new production in the Sargasso Sea, *Nature*, *394*, 263–266, 1998.

McQuatters-Gollop, A., P. C. Reid, M. Edwards, P. H. Burkill, C. Castellani, S. Batten, W. Gieskes, D. Beare, R. R. Bidigare, E. Head, R. Johnson, M. Kahru, J. A. Koslow, and A. Pena, Is there a decline in marine phytoplankton?, *Nature*, *472*, E6–E7, 2011.

Meincke, J., B. Rudels, and H. J. Friedrich, The Arctic Ocean – Nordic Seas thermohaline system, *ICES Journal of Marine Science*, *54*, 283–299, 1997.

Michaels, A. F., and M. W. Silver, Primary production, sinking fluxes and the microbial food web, *Deep Sea Research Part A. Oceanographic Research Papers*, *35*, 473–490, 1988.

Mienert, J., G. Graf, C. Hemleben, K. Kremling, O. Pfannkuche, and D. E. Schulz-Bull, Nordatlantik 1996, Cruise No. 36, 6 June 1996 - 4 November 1996, *Tech. rep.*, Institut für Meereskunde der Universität Hamburg, 1998.

Miller, L., and B. C. Douglas, Mass and volume contributions to twentieth-century global sea level rise, *Nature*, *428*, 406–409, 2004.

Mills, M. M., C. Ridame, M. Davey, J. La Roche, and R. J. Geider, Iron and phosphorus co-limit nitrogen fixation in the eastern tropical North Atlantic, *Nature*, *429*, 292–294, 2004.

Minobe, S., Resonance in bidecadal and pentadecadal climate oscillations over the North Pacific: Role in climatic regime shifts, *Geophysical Research Letters*, *26*, 855–858, 1999.

Minobe, S., Spatio-temporal structure of the pentadecadal variability over the North Pacific, *Progress in Oceanography*, *47*, 381–408, 2000.

Molinari, R. L., Information from low-density expendable bathythermograph transects: North Atlantic mean temperature structure and quasi-decadal variability, *Progress in Oceanography*, *88*, 131–149, 2011.

Morán, X. A. G., A. López-Urrutia, A. Calvo-Díaz, and W. K. W. Li, Increasing importance of small phytoplankton in a warmer ocean, *Global Change Biology*, *16*, 1137–1144, 2010.

Morel, A., Y. Huot, B. Gentili, P. J. Werdell, S. B. Hooker, and B. A. Franz, Examining the consistency of products derived from various ocean color sensors in open ocean (Case 1) waters in the perspective of a multi-sensor approach, *Remote Sensing of Environment*, *111*, 69–88, 2007.

Moy, A. D., W. R. Howard, S. G. Bray, and T. W. Trull, Reduced calcification in modern Southern Ocean planktonic foraminifera, *Nature Geosciences*, *2*, 276–280, 2009.

Müller, T. J., and G. Siedler, Multi-year current time series in the eastern North Atlantic Ocean, *Journal of Marine Research*, *50*, 63–98, 1992.

Müller, T. J., and J. J. Waniek, KIEL276 Time Series Data from Moored Current Meters Madeira Abyssal Plain 33°N, 22°W, 5285 m water depth March 1980 - April 2011 Background Information and Data Compilation, *Tech. rep.*, GEOMAR Report, N. Ser. 013 . GEOMAR, Kiel, Germany, 2013.

Murtugudde, I., R. J. Beauchamp, C. R. McClain, M. R. Lewis, and A. Busalacchi, Effects of penetrative radiation on the upper tropical ocean circulation, *Journal of Climate*, *15*, 470–486, 2002.

Nakamura, H., *Tuna distributions and migrations*, Fishing News, London, 1969.

Nash, J. E., and J. V. Sutcliffe, River flow forecasting through conceptual models, I, A discussion of principles, *Journal of Hydrology*, *10*, 282–290, 1970.

Neftel, A., E. Moor, H. Oeschger, and B. Stauffer, Evidence from polar ice cores for the increase in atmospheric CO_2 in the past two centuries, *Nature*, *315*, 45–47, 1985.

Neuer, S., A. Cianca, P. Helmke, T. Freudenthal, R. Davenport, H. Meggers, M. Knoll, J. M. Santana-Casiano, M. González-Davila, M.-J. Rueda, and O. Llinás, Biogeochemistry and hydrography in the eastern subtropical North Atlantic gyre. Results from the European time-series station ESTOC, *Progress in Oceanography*, *72*, 1–29, 2007.

Ohmura, A., Observed long-term variations of solar irradiances at the Earth's surface, *Space Science Reviews*, *125*, 111–128, 2006.

Olson, D. B., G. L. Hitchcock, A. J. Mariano, C. J. Ashjian, G. Peng, R. W. Nero, and G. P. Podestá, Life on the edge: marine life and fronts, *Oceanography*, *7*, 52–60, 1994.

Orr, J. C., V. J. Fabry, O. Aumont, L. Bopp, S. C. Doney, R. A. Feely, A. Gnanadesikan, N. Gruber, A. Ishida, F. Joos, R. M. Key, K. Lindsay, E. Maier-Reimer, R. Matear, P. Monfray, A. Mouchet, R. G. Najjar, G.-K. Plattner, K. B. Rodgers, C. L. Sabine, J. L. Sarmiento, R. Schlitzer, R. D. Slater, I. Totterdell, M.-F. Weirig, Y. Yamanaka, and A. Yool, Anthropogenic ocean acidification over the twenty-first century and its impact on calcifying organisms, *Nature*, *437*, 681–686, 2005.

Oschlies, A., Nutrient supply to the surface water of the North Atlantic: A model study, *Journal of Geophysical Research*, *107*, 14, 2002.

Osterhammel, J., *Die Verwandlung der Welt: Eine Geschichte des 19. Jahrhunderts*, C. H. Beck, München, 2011.

Özgökmen, T. M., E. P. Chassignet, and C. G. H. Rooth, On the Connection between the Mediterranean Outflow and the Azores Current, *Journal of Physical Oceanography*, *31*, 461–480, 2001.

Pak, H., D. A. Kiefer, and J. C. Kitchen, Meridional variations in the concentration of chlorophyll and microparticles in the North Pacific Ocean, *Deep-Sea Research*, *35*, 1151–1171, 1988.

Palko, B. J., G. L. Bearsley, and W. J. Richards, Synopsis of the biology of the swordfish, *Xiphias gladius Linnaeus*, *Tech. rep.*, FAO Fisheries Synopsis No. 127, NOAA Technical Report NMFS Circular 441, 1981.

Pérez, F. F., M. Gilcoto, and A. F. Ríos, Large and mesoscale variability of the water masses and the deep chlorophyll maximum in the Azores Front, *Journal of Geophysical Research*, *108*, 3215, 2003.

Pérez, V., E. Fernández, E. Marañón, X. A. G. Morán, and M. V. Zubkov, Vertical distribution of phytoplankton biomass, production and growth in the Atlantic subtropical gyres, *Deep Sea Research Part I: Oceanographic Research Papers*, *53*, 1616–1634, 2006.

Pielke Sr, R. A., A broader view of the role of humans in the climate system, *Physics Today*, *61*, 54–55, 2008.

Polovina, J. J., E. A. Howell, and M. Abecassis, Ocean's least productive waters are expanding, *Geophysical Research Letters*, *35*, 1–5, 2008.

Ragueneau, R., S. Schultes, K. Bidle, P. Claquin, and B. Moriceau, Si and C interactions in the world ocean: Importance of ecological processes and implications for the role of diatoms in the biological pump, *Global Biogeochemical Cycles*, *20*, 1–15, 2006.

Rahmstorf, S., Ocean circulation and climate during the past 120,000 years, *Nature*, *419*, 207–214, 2002.

Rhein, M., S. R. Rintoul, S. Aoki, E. Campos, D. Chambers, R. A. Feely, S. Gulev, G. C. Johnson, S. A. Josey, A. Kostianoy, C. Mauritzen, D. Roemmich, L. D. Talley, and F. Wang, Observations: Ocean, in *Climate Change 2013: The Physical Science Basis. Contribution of Working Group I to the Fifth Assessment Report of the Intergovernmental Panel on Climate Change*, edited by T. F. Stocker, D. Qin, G.-K. Plattner, M. Tignor, S. K. Allen, J. Boschung, A. Nauels, Y. Xia, V. Bex, and P. M. Midgley, Cambridge, United Kingdom and New York, NY, USA, Cambridge University Press, 2013.

Riebesell, U., I. Zondervan, B. Rost, P. D. Tortell, R. E. Zeebe, and F. M. M. Morel, Reduced calcification of marine plankton in response to increased atmospheric CO_2, *Nature*, *407*, 364–367, 2000.

Riebesell, U., A. Körtzinger, and A. Oschlies, Sensitivities of marine carbon fluxes to ocean change, *Proceedings of the National Academy of Sciences*, *106*, 20,602–20,609, 2009.

Roemmich, D., W. J. Gould, and J. Gilson, 135 years of global ocean warming between the Challenger expedition and the Argo Programme, *Nature Climate Change*, *2*, 425–428, 2012.

Rogerson, M., E. J. Rohling, P. P. E. Weaver, and J. W. Murray, The Azores Front since the Last Glacial Maximum, *Earth and Planetary Science Latters*, *22*, 779–789, 2004.

Rommets, J., R. Dapper, and H. J. W. de Baar, JGOFS North Atlantic R.V. Tyro Leg 1 of the cruise in 1989, Upper Ocean Processes. Netherlands Institute for Sea Research (NIOZ), *Tech. rep.*, 1991a.

Rommets, J., R. Dapper, and H. G. Fransz, JGOFS North Atlantic R.V. Tyro Leg 3 of the cruise in 1990, Upper Ocean Processes. Netherlands Institute for Sea Research (NIOZ), *Tech. rep.*, 1991b.

Rykaczewski, R. R., and J. P. Dunne, A measured look at ocean chlorophyll trends, *Nature*, *472*, E5–E6, 2011.

Sabine, C. L., R. A. Feely, N. Gruber, R. M. Key, K. Lee, J. L. Bullister, R. Wanninkhof, C. S. Wong, D. W. R. Wallace, B. Tilbrook, F. J. Millero, T.-H. Peng, A. Kozyr, T. Ono, and A. F. Rios, The Oceanic Sink for Anthropogenic CO_2, *Science*, *305*, 367–371, 2004.

Sarmiento, J. L., R. Slater, R. Barber, L. Bopp, S. C. Doney, A. C. Hirst, J. Kelypas, R. Matear, U. Mikolajewicz, P. Monfray, V. Soldatov, S. A. Spall, and R. Stouffer, Response of ocean ecosystems to climate warming, *Global Biogeochemical Cycles*, *18*, 1–23, 2004.

Sathyendranath, S., T. Platt, E. P. W. Horne, W. Harrison, O. Ulloa, R. Outerbridge, and N. Hoepffner, Estimation of new production in the ocean by compound remote sensing, *Nature*, *353*, 129–133, 1991.

Schiebel, R., J. Waniek, A. Zeltner, and M. Alves, Impact of the Azores Front on the distribution of planktic foraminifers, shelled gastropods, and coccolithophorids, *Deep Sea Research Part II: Topical Studies in Oceanography*, *49*, 4035–4050, 2002.

Schlesinger, M. E., and N. Ramankutty, An oscillation in the global climate system of period 65–75 years, *Nature*, *367*, 723–726, 1994.

Schwab, C., H. Kinkel, M. Weinelt, and J. Repschläger, Coccolithophore paleoproductivity and ecology response to deglacial and Holocene changes in the Azores Current System, *Paleoceanography*, *27*, 1–18, 2012.

Siedler, G., J. A. Church, and W. J. e. Gould, *Ocean circulation and climate: observing and modelling the global ocean* , International geophysics series, Volume 77, Academic Press, San Diego, 2001.

Siedler, G., L. Armi, and T. J. Müller, Meddies and decadal changes at the Azores Front from 1980 to 2000, *Deep Sea Research Part II: Topical Studies in Oceanography*, *52*, 583–604, 2005.

Sigman, D. M., and E. A. Boyle, Glacial/interglacial variations in atmospheric carbon dioxide, *Nature*, *407*, 859–869, 2000.

Steinacher, M., F. Joos, T. L. Frölicher, L. Bopp, P. Cadule, V. Cocco, S. C. Doney, M. Gehlen, K. Lindsay, J. K. Moore, B. Schneider, and J. Segschneider, Projected 21st century decrease in marine productivity: a multi-model analysis, *Biogeosciences*, *7*, 979–1005, 2010.

Stewart, R. H., *Introduction to Physical Oceanography*, http://oceanworld.tamu.edu/resources/ocng_textbook/PDF_files/book_pdf_files.html., 2008.

Storch, H. v., and F. W. Zwiers, *Statistical analysis in climate research*, Cambridge University Press, Cambridge, 2003.

Stramma, L., Geostrophic transport in the Warm Water Sphere of the eastern subtropical North Atlantic, *Journal of Marine Research*, *42*, 537–558, 1984.

Stramma, L., and G. Siedler, Seasonal Changes in the North Atlantic Subtropical Gyre, *Journal of Geophysical Research*, *93*, 8111–8118, 1988.

Taylor, A. H., and J. A. Stephens, The North Atlantic Oscillation and the latitude of the Gulf Stream, *Tellus*, *50A*, 134–142, 1998.

Taylor, A. H., M. B. Jordan, and J. A. Stephens, Gulf Stream shifts following ENSO events, *Nature*, *393*, 638, 1998.

Teira, E., B. Mouriño, E. Marañón, V. Pérez, M. J. Pazó, P. Serret, D. de Armas, J. Escánez, E. M. S. Woodward, and E. Fernández, Variability of chlorophyll and primary production in the Eastern North Atlantic Subtropical Gyre: potential factors affecting phytoplankton activity, *Deep Sea Research Part I: Oceanographic Research Papers*, *52*, 569–588, 2005.

Thompson, D. W. J., and J. M. Wallace, The arctic oscillation signature in the wintertime geopotential height and temperature fields, *Geophysical Research Letters*, *25*, 1297–1300, 1998.

Thompson, D. W. J., and J. M. Wallace, Annular modes in the extratropical circulation. Part I: Month-to-month variability, *Journal of Climate*, *13*, 1000–1016, 2000.

Tomczak, M., and G. J. Stuart, *Regional Oceanography: An Introduction*, Pergamon, Oxford, 1994.

Torrence, C., Interdecadal Changes in the ENSO-Monsoon System, *Journal of Climate*, *12*, 1999.

Torrence, C., and G. P. Compo, A Practical Guide to Wavelet Analysis, *Bulletin of the American Meteorological Society*, *79*, 61–78, 1998.

Trenberth, K. E., and J. W. Hurrell, Decadal atmospheric ocean variations in the Pacific, *Climate Dynamics*, *9*, 303–319, 1994.

Uitz, J., H. Claustre, A. Morel, and S. B. Hooker, Vertical distribution of phytoplankton communities in open ocean: An assessment based on surface chlorophyll, *Journal of Geophysical Research*, *111*, 1–23, 2006.

Vellinga, M., and R. A. Wood, Global climatic impacts of a collapse of the Atlantic thermohaline circulation, *Climatic Change*, *54*, 251–267, 2002.

Visbeck, M., E. P. Chassignet, R. Curry, T. Delworth, B. Dickson, and G. Krahmann, The Ocean's Response to North Atlantic Oscillation Variability, in *The North Atlantic Oscillation*, edited by J. Hurrell, Y. Kushnir, G. Ottersen, and M. Visbeck, American Geophysical Union, 2003.

Volk, T., and M. I. Hoffert, Ocean Carbon Pumps: Analysis of Relative Strengths and Efficiencies in Ocean Driven Atmospheric CO_2 Changes, *Geophysical Monograph Series*, *32*, 99–110, 1985.

Volkov, D. L., and L. L. Fu, Interannual variability of the Azores Current strength and eddy energy in relation to atmospheric forcing, *Journal of Geophysical Research*, *116*, 12, 2011.

Wallace, J. M., and D. S. Gutzler, Teleconnections in the Geopotential Height Field during the Northern Hemisphere Winter, *Monthly Weather Review*, *109*, 784–812, 1981.

Waniek, J., W. Koeve, and R. D. Prien, Trajectories of sinking particles and the catchment areas above sediment traps in the northeast Atlantic, *Journal of Marine Research*, *58*, 983–1006, 2000.

Waniek, J. J., D. E. Schulz-Bull, T. Blanz, R. D. Prien, A. Oschlies, and T. J. Müller, Interannual variability of deep water particle flux in relation to production and lateral sources in the northeast Atlantic, *Deep Sea Research Part I: Oceanographic Research Papers*, *52*, 33–50, 2005a.

Waniek, J. J., D. E. Schulz-Bull, J. Kuss, and T. Blanz, Long time series of deep water particle flux in three biogeochemical provinces of the northeast Atlantic, *Journal of Marine Systems*, *56*, 391–415, 2005b.

Ward, B. A., and J. J. Waniek, Phytoplankton growth conditions during autumn and winter in the Irminger Sea, North Atlantic, *Marine Ecology - Progress Series*, *334*, 47–61, 2007.

Wild, M., Global dimming and brightening: Review, *Journal of Geophysical Research*, *114*, 1–31, 2009.

Wild, M., H. Gilgen, A. Roesch, A. Ohmura, C. N. Long, E. G. Dutton, B. Forgan, A. Kallis, V. Russak, and A. Tsvetkov, From Dimming to Brightening: Decadal Changes in Solar Radiation at Earth's Surface, *Science*, *308*, 847–850, 2005.

Worthington, L. V., *On the North Atlantic circulation*, The Johns Hopkins oceanographic studies, Volume 6, Johns Hopkins Univ. Press, Baltimore, 1976.

Yasunaka, S., and K. Hanawa, Regime Shifts Found in the Northern Hemisphere SST Field, *Journal of the Meteorological Society of Japan*, *88*, 119–135, 2002.

Zeitzschel, B., J. Lenz, H. Thiel, R. Boje, U. Passow, and A. Stuhr, Expedition Plankton 89 -Benthos 89, Reise Nr. 10, *Tech. rep.*, Institut für Meereskunde an der Universität Hamburg, 1990.

List of Figures

List of Tables

List of Abbreviations

AMM	Atlantic Meridional Mode
AMO	Atlantic Multidecadal Oscillation
AO	Arctic Oscillation
CTD	Conductivity Temperature Depth
DCM	Deep Chlorophyll Maximum
EAP	East Atlantic Pattern
ECMWF	European Centre for Medium - Range Weather Forecasts
ENAW	Eastern North Atlantic Water
ENSO	El Niño / Southern Oscillation
EOF	Empirical Orthogonal Function
ERA	European Reanalysis
GIOVANNI	Goddard Earth Sciences Data and Information Services Center Interactive Online Visualization ANd aNalysis Infrastructure
GSNW	Gulf Stream Northern Wall
MLD	Mixed Layer Depth
NAO	North Atlantic Oscillation
NAST	North Atlantic Subtropical Gyral Province
NCEP	National Centers for Environmental Prediction
NOAA-CIRES	National Oceanic and Atmospheric Administration – Cooperative Institute for Research in Environmental Sciences
PDO	Pacific Decadal Oscillation
QuickSCAT	Quick Scatterometer

SeaWiFS	SEA-viewing Wide Field of-view Sensor
SODA POP	Simple Ocean Data Assimilation Parallel Ocean Program
SST	Sea Surface Temperature
WNAW	Western North Atlantic Water

Specific contributions to the manuscripts

The contributions of the authors to the manuscripts are indicated in the following:

Fründt, B., and Waniek, J. J.: Impact of the Azores Front Propagation on Deep Ocean Particle Flux, *Central European Journal of Geosciences*, 4(4), 531-544.

Specific Contribution: B. F. made the analysis of the data, prepared the concept of the paper and did the writing. J. J. W. provided sediment trap material and made contributions to the manuscript. J. J. W. is the project holder.

Fründt, B., Dippner, J. W., and Waniek, J. J.: Chlorophyll *a* reconstruction from *in-situ* measurements, Part I: Method description, *Journal of Geophysical Research: Biogeosciences*, 120, 237-245.

Specific Contribution: J. J. W. is the project holder, initiated the work and gave the basic idea. B. F. developed the method, prepared the concept and did most of the writing. *In-situ* measurements of the Poseidon cruises were provided by J. J. W. Contributions to the manuscript were done by J. W. D. and J. J. W.

Fründt, B., Dippner, J. W., Schulz-Bull, D. E., and Waniek, J. J.: Chlorophyll *a* reconstruction from *in-situ* measurements, Part II: Marked carbon uptake decrease in the last century, *Journal of Geophysical Research: Biogeosciences*, 120, 246-253.

Specific Contribution: B. F. made data analysis and interpretation, prepared the concept of the paper and did the writing. J. W. D., D. E. S.-B. and J. J. W. made contributions to the manuscript. J. J. W. is the project holder.

Danksagung

Zuerst möchte ich mich bei meiner Doktor-Mutter Dr. habil. Joanna J. Waniek für die Vergabe der Doktorarbeit sowie die intensive wissenschaftliche Betreuung und Unterstützung bedanken. Ich danke ihr, dass sie mir die Möglichkeit gab, insbesondere interdisziplinär zu arbeiten und an mehreren wissenschaftlichen Exkursionen teilzunehmen. Desweiteren gilt mein Dank meinem Thesis Komitee, Dr. habil. Joanna J. Waniek, Prof. Dr. Detlef E. Schulz-Bull, Dr. habil. Joachim W. Dippner und Prof. Dr. Harry L. Bryden für die guten wisschenschaftlichen Diskussionen und bereitwilliger Hilfe, wenn es nötig war. Prof. Bryden danke ich insbesondere für die Betreuung während meines Aufenthaltes in Southampton und Dr. Dippner, dass seine Bürotür für mich immer offen war.

In diesem Rahmen möchte ich auch den Kapitänen sowie den Besatzungsmitgliedern der RV Poseidon und der RV Maria S. Merian für ihre technische Unterstützung und die schöne Zeit an Bord bedanken.

Für wissenschaftliche und weitere Unterstützung am IOW danke ich Ines Hand, Birgit Sadkowiak, Dr. Ralf Prien, Hildegard Kubsch, Ina Topp, Annika Fiskal, Andrea Tschakste, Astrid Lerz, Dr. Rolf Schneider, Irina Goldschmidt, Dr. David Meyer, Janne Hähnel, Annika Schmidt, Dr. Kerstin Perner und allen weiteren Mitarbeitern der Sektion Meereschemie.

Mein ganz besonderer Dank gilt hier meinen Büromitstreitern Dr. Andrea Bauer, Dr. Juliane Brust-Möbius, Dr. David Kaiser und Johann Götte für biologische Hilfestellungen, Matlab-Diskussionen, die vielen Gespräche und einfach die nette Zeit, die wir zusammen verbringen konnten.

Schließlich gilt mein größter Dank meiner Familie und Freunden für ihre ständige Unterstützung, Hilfe und Geduld in allen Phasen während der Doktorarbeit.

Eidesstattliche Erklärung

Ich versichere hiermit an Eides statt, dass ich die vorliegende Arbeit selbstständig angefertigt und ohne fremde Hilfe verfasst habe, keine außer den von mir angegebenen Hilfsmitteln und Quellen dazu verwendet habe und die den benutzten Werken inhaltlich und wörtlich entnommenen Stellen als solche kenntlich gemacht habe.

Birte Fründt

Rostock, den 27.06.2014